



SYNTHESIS AND CHARACTERIZATION OF CLAY/POLYMER NANOCOMPOSITE MATERIALS AND THEIR APPLICATION FOR LITHIUM BATTERIES

Tesi di Laurea Magistrale in Ingegneria Chimica e dei Processi Sostenibili

PRESENTATA DA:

Maria Florencia Caballero

RELATORI:

Prof.ssa Silvia Bodoardo

Dr.ssa Martina Gamba

Abstract

Since the acceptance of global warming as a scientific fact, increased worry about CO₂ emissions has led to active research and innovation in alternative clean, renewable energy sources to replace fossil fuels that have been used as the main energy source since the industrial revolution. Although the easiest and most efficient way to generate thermal or electrical energy is still nowadays based on coal, oil, and natural gas, these constitute a finite source and in consequence another way of generating power will be needed in the future. One of the drawbacks of renewable power sources such as wind or solar energy, is that they depend on the environmental conditions and therefore they might not be generated during periods of peak energy demand.

Batteries are essential components of most electrical devices. They are used as the power source in cars, laptops, smartphones, and other electronic appliances storing and generating electricity. Batteries take importance as a storage solution to fulfil the previously mentioned challenging requirements and store energy generated by the wind or the sun until required, as well as in the implementation of electrical vehicles to reduce carbon dioxide emissions.

Continuous effort and research take place in order to improve commercial batteries making them more efficient and affordable. The main priority of research projects and battery technology development has been, in the past recent years, to increase the energy density of lithium batteries. The goal is to meet the growing demand for mobile devices, which increasingly need more energy, and to increase the autonomy of second-generation electric vehicles, which demand higher capacity and more efficient batteries.

On the one hand, although using metallic lithium anodes for next generation batteries would increase up to ten times the capacity obtained from actual batteries, lithium reactivity and dendrite formation and growth represent one of the main obstacles. One of the main focuses of research in post lithium-ion batteries are strategies to protect the metallic lithium anode. On the other hand, LiNi_{0.5}Mn_{1.5}O₄ is a high voltage cathode material for lithium ion batteries and represents a promising alternative to the most common ones used in the market because of some properties like eco-friendliness, high-power capability and low cost. However, one of its main drawbacks is fast capacity fade due to manganese dissolution, migration and deposition on the anode material. In addition, commercial polyolefin separators used in lithium batteries have poor affinity towards carbonate-based electrolytes and low thermal stability.

These mentioned problems concerning lithium batteries were faced in this thesis work. Firstly, a clay/polymer nanocomposite material was synthesized from polyaniline and an Argentinian montmorillonite with the aim of obtaining a synergistic combination of properties. Some chemical characterization techniques including: XRD, FTIR, TGA, XPS, and zeta potential measurements, were performed in order to study, analyse and verify that the composite obtained was in line with the synthesis purpose.

Secondly, the obtained nanocomposite was applied as a coated membrane on to a commercial separator (Celgard®2500) commonly used in batteries in order to improve its properties, and it was electrochemically tested to study its stability and compatibility towards lithium plating and stripping as well as the performance as a metallic lithium protection strategy. The coated separator was then used in half and complete cells using a high voltage cathode ($\text{LiNi}_{0.5}\text{Mn}_{1.5}\text{O}_4$) with the aim of working as a barrier in order to impede migration of manganese ions towards the graphite anode and therefore, increase the battery performance.

*“Si para recobrar lo recobrado
debí perder primero lo perdido,
si para conseguir lo conseguido
tuve que soportar lo soportado,*

*si para estar ahora enamorado
fue menester haber estado herido,
tengo por bien sufrido lo sufrido,
tengo por bien llorado lo llorado.*

*Porque después de todo he comprobado
que no se goza bien de lo gozado
sino después de haberlo padecido.*

*Porque después de todo he comprendido
que lo que el árbol tiene de florido
vive de lo que tiene sepultado.”*

Francisco Luis Bernárdez

Table of Contents

Chapter 1: Introduction	7
1.1 FUNDAMENTALS OF ELECTROCHEMISTRY	7
1.2 BASIC CONCEPTS IN BATTERIES.....	9
1.2.1 BATTERY PARAMETERS.....	10
1.3 LITHIUM CHARACTERISTICS.....	12
1.4 LITHIUM ION BATTERIES	14
1.4.1 CATHODE MATERIALS FOR LITHIUM ION BATTERIES.....	16
1.4.2 HIGH VOLTAGE CATHODE MATERIALS (LNMO)	17
1.5 METALLIC LITHIUM BATTERIES.....	19
1.6 AIM OF THE THESIS WORK	25
Chapter 2: Physicochemical properties of Polyaniline and Montmorillonites	27
2.1 CONDUCTIVE POLYMERS.....	27
2.2 POLYANILINE	29
2.2.1 POLYANILINE SYNTHESIS	30
2.2.2 POLYANILINE STRUCTURE AND CRYSTALLINITY	32
2.2.3 CHARGE CARRIERS AND CONDUCTIVITY IN POLYANILINE	34
2.3 MONTMORILLONITES: CRYSTALLINE STRUCTURE	35
2.3.1 CATION EXCHANGE CAPACITY IN MONTMORILLONITES	37
2.3.2 ACTIVE SITES IN MONTMORILLONITES	38
2.4 ORGANO-MONTMORILLONITES.....	39
2.4.1 GELATION IN ORGANO-MONTMORILLONITE.....	41
Chapter 3: Synthesis and characterization of clay/polymer nanocomposites	43
3.1 SYNTHESIS OF CLAY/POLYMER NANOCOMPOSITE MATERIALS.....	43
3.2 CHARACTERIZATION TECHNIQUES AND RESULTS.....	48
3.2.1 POWDER X-RAY DIFFRACTION (XRD).....	48
3.2.1.1 RESULTS	50
3.2.2 X-RAY PHOTOELECTRON SPECTROSCOPY (XPS)	51

3.2.2.1 RESULTS	53
3.2.3 FOURIER TRANSFORM INFRARED SPECTROSCOPY (FTIR)	57
3.2.3.1 RESULTS	59
3.2.4 THERMOGRAVIMETRIC ANALYSIS (TGA)	62
3.2.4.1 RESULTS	63
3.2.5 ZETA POTENTIAL MEASUREMENT	67
3.2.5.1 RESULTS	68
Chapter 4: Electrochemical application of synthesized clay/polymer nanocomposites	71
4.1 COATING STRATEGY	71
4.2 CONDUCTIVITY MEASURES	72
4.3 ELECTROLYTE UPTAKE AND RETENTION	74
4.4 CELLS ASSEMBLING	76
4.5 ELECTROCHEMICAL TESTING.....	76
4.5.1 Li PLATING AND STRIPPING	77
4.5.1.1 RESULTS	78
4.5.2 CYCLING PERFORMANCE USING A HIGH VOLTAGE CATHODE (LNMO)	89
4.5.2.1 RESULTS	90
4.6 FURTHER CHEMICAL CHARACTERIZATION	97
4.6.1 XPS RESULTS.....	97
4.6.2 FTIR RESULTS.....	99
APPENDIX A	103
APPENDIX B.....	105
CONCLUSIONS.....	107
Bibliography.....	109

Chapter 1: Introduction

1.1 FUNDAMENTALS OF ELECTROCHEMISTRY

Electrochemistry studies the interrelation between electrical energy and chemical energy. Processes and factors that affect the transport of charge and mass through the interface between different domains of an electrochemical system are of interest, for example, between an electronic conductor (electrode) and an ionic conductor (electrolyte) when a certain potential is applied to the system. Two types of processes occur at the electrodes during an electrochemical reaction: faradaic processes and non-faradaic processes. The faradaic processes are those where the transfer of electrons through the electrode/electrolyte interface involves a change in the oxidation state of certain species, meaning that there is a proportionality between the current that passes through the system and the quantity of active material that reacts on the electrode (Faraday's law). On the other hand, non-faradaic processes involve changes in the structure of the electrode/electrolyte interface or electric double layer when the applied potential varies, due mainly to adsorption and desorption of electrochemical species [1]. The electric double layer (Figure 1.1) is a structure that appears on the surface of the electrode when it is exposed to an electrolyte, composed of two parallel layers of charge around the electrode. The layer closest to the electrode is formed by ions (positive or negative) that are adsorbed on the surface because of interactions between the electrode and the species in the electrolyte, while the second layer comprises ions attracted to the surface charge of the first layer due to electrostatic forces, but which are not adhered to the electrode. In correspondence to this effect, there is a variation of potential with the distance from the bare surface of the electrode.

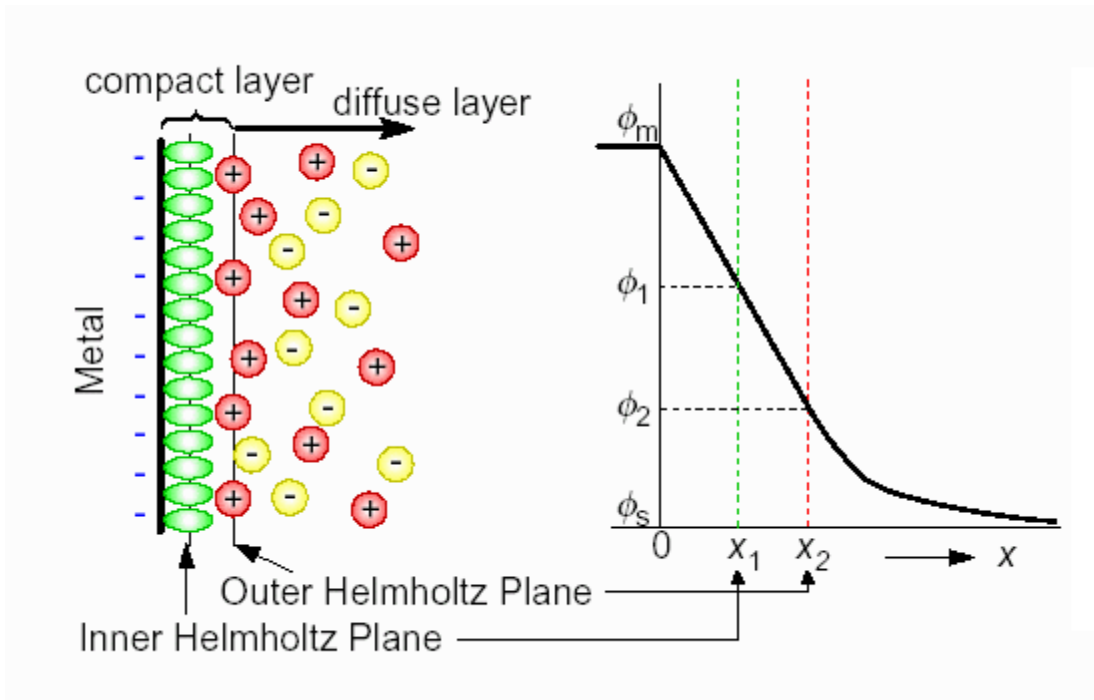
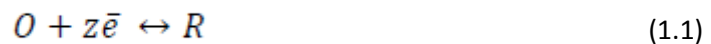


Figure 1.1 Electric double layer and potential variation in the Electrode-Electrolyte interface.

The thermodynamic and kinetic aspects associated with faradaic processes can be analysed considering the general semi-reaction:



where O is the oxidized state of a certain species that accepts z electrons, and R, is the reduced state or the electron donor. In equilibrium, when there is no external current flow, the Nernst equation describes the potential of the semi-reaction as a function of the concentration of the electroactive species. [2]

$$E_{O/R} = E_{O/R}^{\circ} + \frac{RT}{zF} \ln \left(\frac{a_O}{a_R} \right) \quad (1.2)$$

In this equation, $E_{O/R}$ and $E_{O/R}^{\circ}$ are the equilibrium and the standard potential of the semi-reaction respectively. T , the absolute temperature, F , the Faraday constant (96486 C/mol) and R , the ideal gas constant (8.314 J/mol.K). a_O and a_R correspond to the activities of the acceptor and the electron donor, respectively. When there is no equilibrium, the overpotential of the half-reaction must be

considered, and corresponds to the potential difference between the potential in which the electrochemical reaction (E) occurs and the equilibrium potential. [2]

$$\eta = E - E_{O/R} \quad (1.3)$$

1.2 BASIC CONCEPTS IN BATTERIES

A battery is an electrochemical cell, or a set of them, that is used as a source of direct electric current. In batteries, electrical energy is obtained as a result of spontaneous electrochemical reactions in the cell (discharge process of the battery), or energy can be stored in them by forcing a non-spontaneous electrochemical reaction to occur as a response to an external electric current applied to the system (charging process, when connecting the device to the electrical network). During the discharge, an oxidation reaction occurs at the anode and a reduction reaction at the cathode [2].

Batteries are usually classified into two large groups [2]:

- Primary batteries (non-rechargeable): are characterized by very slow and inefficient recharging kinetics so, their useful life corresponds only to the discharge process. In other words, once discharged, they cannot be reused. Among these devices alkaline batteries are the most popular.
- Secondary (rechargeable) batteries: the transformation of chemical energy into electrical energy is reversible in these batteries, meaning they can be charged and discharged successively for many cycles. Examples of this type of devices are Li-ion batteries and nickel-metal hydride (NiMH) batteries.

In general, a battery needs 5 essential elements to produce electricity:

I) Cathode

The cathode is an electrode that is connected to the positive terminal of a battery. Without applying external electric current, a reduction reaction occurs taking the electrons that are generated from the oxidation at the anode.

II) Anode

The anode is connected to the negative terminal of the battery. In absence of external electric current, an oxidation reaction takes place between the material of which the anode is constituted and its interaction with ions from the electrolyte.

III) Electrolyte

The electrolyte is composed of free ions (usually organic salts dissolved in an aqueous solvent), which function as charge carriers in the battery.

IV) Separator

The main function of the porous separator is to avoid physical contact between the electrodes, allowing the transport of ions inside the cell. Commercial separators have a thickness between 25 and 30 μm , although there are ones that are thinner, 10 μm . Ideally, a separator should be as thin as possible to reduce the resistance inside the battery, but this compromises its mechanical strength and safety. [2]

V) Collectors

Collectors are conductive materials that carry the generated current and direct it to the external circuit that is connected to the battery. There are collectors connected to both electrodes.

1.2.1 BATTERY PARAMETERS

Some technical concepts used to characterize and study a battery performance, will be presented below to facilitate the monitoring of this project. [3]

I) Open-Circuit-Voltage (OCV)

The open circuit potential difference of the cell is the voltage (expressed in Volts, V) that is established at the poles of the cell in open circuit conditions (in the absence of external electric current) and represents the maximum voltage available for the discharge, or the minimum value to be reached to carry out the charge of the cell. The value of this parameter in standard reference conditions can be obtained from the variation of Gibbs free energy in standard conditions due to the reactions occurring in the negative and positive electrode respectively (Equation 1.4).

$$OCV\ cell = E_{anode}^0 - E_{cathode}^0 = \Delta E^0 = -\frac{\Delta G^0}{n \cdot F} \quad (1.4)$$

II) Overvoltage

The over potential (η) is defined, during the discharge phase, as the difference between the OCV and the cell potential, while during the charge phase as the difference between the cell potential and its OCV. The over potential has three contributions due to the following polarization phenomena:

- activation polarization, which drives the electrochemical reaction at the electrode surface.
- concentration polarization, which arises from the concentration differences at the electrode surface and in the bulk as a result of mass transfer.
- ohmic polarization, which represents the voltage drop during operation caused by the internal impedance of the cell.

III) Current Density

The current density (j) is defined as the ratio of the total current (I) which flows through the electrode, and the normal surface of the electrode (A). Its units are normally in A/m^2 .

$$j(t) = \frac{I(t)}{A} \quad (1.5)$$

IV) Cell Capacity

The capacity Q , measured in Coulomb [C] or [Ah], represents the quantity of electrical charge accumulated during the charging phase, or available during the discharging phase. The capacity of the cell accumulated / discharged in a time range [t1; t2] can be defined by Equation 1.6 which, in conditions of constant applied current, can be rewritten as in Equation 1.7.

$$Q = \int_{t_1}^{t_2} I(t) dt \quad (1.6)$$

$$Q = I \cdot t \quad (1.7)$$

The theoretical capacity Q_t , equal to the maximum cumulative / dischargeable electric charge from the cell, can be obtained based on the amount of active material present inside the cell through Equation 1.8, where x represents the number of moles of active material present inside the electrode, n the number of equivalent electrons involved in electrochemical reactions and F is the Faraday constant.

$$Q_t = x \cdot n \cdot F \quad (1.8)$$

The specific capacity of an electrochemical cell is the amount of charge that a battery can accumulate / deliver expressed per unit of mass (Ah/g) or volume (Ah/cm³).

VI) C – Rate

A C-rate is a measure of the rate at which a battery is charged (or discharged) relative to its maximum capacity. This parameter can be associated with the time required for the cell to charge / discharge completely. A charge at C/5 and 2C mean, for example, that the charging current is such as to determine a necessary time to completely charge the cell equal to 5 and 0.5 hours, respectively.

VII) Coulombic Efficiency

The coulombic efficiency, Y , is the ratio between the capacity provided during the cell discharge phase ($Q_{\text{discharge}}$) and the capacity accumulated during the previous charge phase (Q_{charge}):

$$Y = \frac{Q_{\text{discharge}}}{Q_{\text{charge}}} \quad (1.9)$$

1.3 LITHIUM CHARACTERISTICS

Lithium is the first of the alkalis in the periodic table. In nature it's found like a mixture of the isotopes Li_6 and Li_7 . It's the lightest solid metal, it's soft, silvery-white, with a low melting point and high reactivity. [4]

Some of the most significant properties of lithium are its high specific heat (calorific capacity), the huge temperature interval in the liquid state, high thermic conductivity, low viscosity and very low density. Metallic lithium is soluble in short chain aliphatic amines, like ethylamine. It's insoluble in hydrocarbons. [4] Its main physical and chemical properties are shown in Figure 1.2.

Atomic number	3
Atomic mass	6.941 g.mol ⁻¹
Electronegativity according to Pauling	1.0
Density	0.53 g.cm ⁻³ at 20 °C
Melting point	180.5 °C
Boiling point	1342 °C
Vanderwaals radius	0.145 nm
Ionic radius	0.06 nm
Isotopes	2
Electronic shell	1s ² 2s ¹ or [He] 2s ¹
Energy of first ionisation	520.1 kJ.mol ⁻¹
Standard potential	-3.04 V

Figure 1.2. Main physical and chemical properties of Lithium. [4]

In Earth's crust it is present with a concentration around 65 ppm, making it a moderately abundant chemical element. Among its most common minerals are spodumene ($\text{AlLi}(\text{SiO}_3)_2$), amblygonite ($(\text{FAl})\text{LiPO}_4$) and lepidolite ($(\text{KLi}_2\text{Al}(\text{Al,Si})_3\text{O}_{10}(\text{F,OH})_2$)), which is a hydrated fluorosilicate complex. Lithium is found in natural brines, brines associated with oil wells and geothermal fields, in clays and in seawater [2].

Within the last decade, lithium has gone from being an industrial mineral used principally in ceramics and glass applications to a technology metal vital to the development of alternatively fuelled vehicles. [5]

Reserves of lithium can be classified into two large groups: continental brines and mineralized rocks. Brines are formed in places where the water that has leached lithium from the rocks evaporates, giving rise to concentrated salts. In mines, lithium is contained within mineralized rocks, in which

the content of this metal is variable. Argentina, Chile and Bolivia constitute the so called 'Lithium Triangle' which represent over 60% of the global reserve of lithium (Figure 1.3). Production of lithium is, with around a 50:50 ratio, divided between brine and hard rock operations. However, brine deposits have generally lower operating costs, since lithium is already isolated and in solution within the deposit. Figure 1.3 shows the lithium reserves by country, as well as the global lithium production and the predictions for the future.

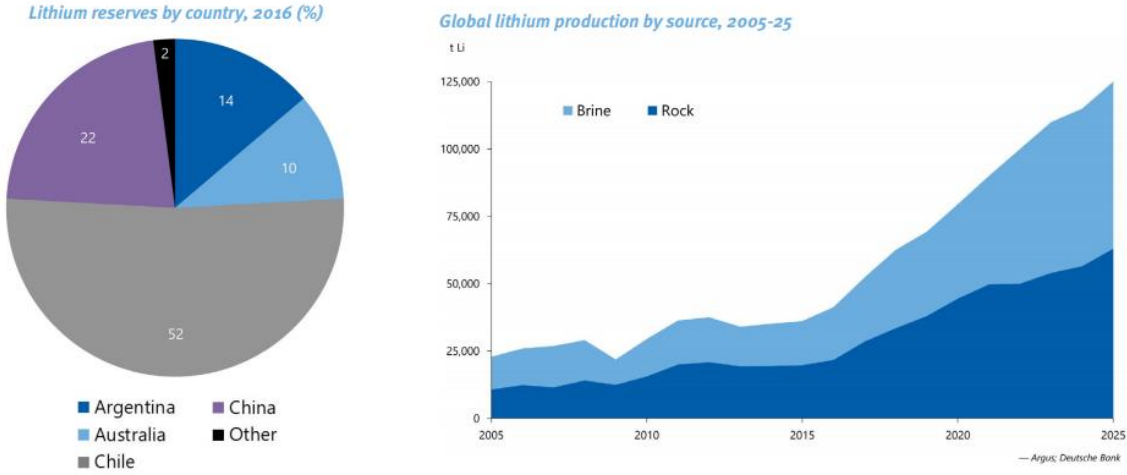


Figure 1.3. Global lithium reserves by country and production by source. [5]

Lithium consumption is driven by the rise in the lithium-ion battery market that is expected to reach more than 223 GWh by 2025. The strongest demand growth for lithium is expected to come from Li-ion batteries used in electric vehicles, including electronic bikes and energy storage applications. It is also believed that growth will be supported in the next years by lower cost of batteries and by global efforts to reduce carbon emissions. [5] Figure 1.4 shows the calculated tendency for lithium demand growth in the next years.

On the other hand, the need to reduce the massive use of fossil fuels in transportation systems, which produce approximately 23% of the CO₂ emitted globally, has driven the research and development of hybrid or electric cars powered by less polluting media, such as metallic lithium batteries. Metallic lithium batteries satisfy, theoretically, the requirements of these vehicles, since they are light, occupy a low volume and have a large energy storage capacity. Such characteristics are possible because lithium has a high standard potential of reduction (negative) and is the metal with the lowest density of the periodic table. In addition, these batteries do not have the so-called "memory effect", which is an undesirable phenomenon that generates a loss in the storage capacity when repeated charging cycles are performed without having completely discharged the batteries [2].

Global demand for lithium-ion batteries, 2005-25 (mn cells)

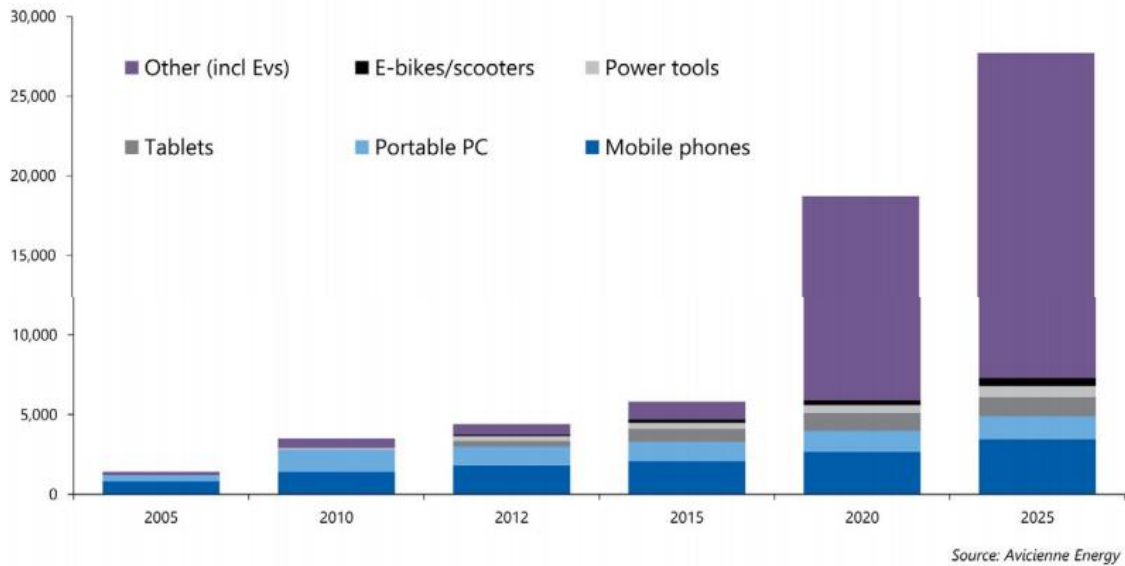


Figure 1.4. Global demand for lithium-ion batteries and its tendency for the future. [4]

1.4 LITHIUM ION BATTERIES

Li-ion batteries, in their most common version, are composed of graphite anodes, cobalt lithium oxide cathodes (LiCoO_2) and liquid electrolytes based on a lithium alkyl salt (usually LiPF_6) dissolved in a mixture of carbonates such as ethylene carbonate (EC), dimethyl carbonate (DMC), diethylene carbonate (DEC) or ethyl-methyl carbonate (EMC). Other lithium salts can also be used, such as LiBF_4 , LiAsF_6 and LiClO_4 . Both the graphite anodes and the lithium-cobalt oxide cathodes are molecularly structured in layers, a feature that allows intercalating ions (Li^+) between them in a reversible way. During the processes of charging and discharging of the battery, lithium ions are inserted or removed from the interstitial space between atomic layers within these electrodes. [2]

Figure 1.5 shows a typical diagram of a Li-ion battery, where its main constituents can be observed.

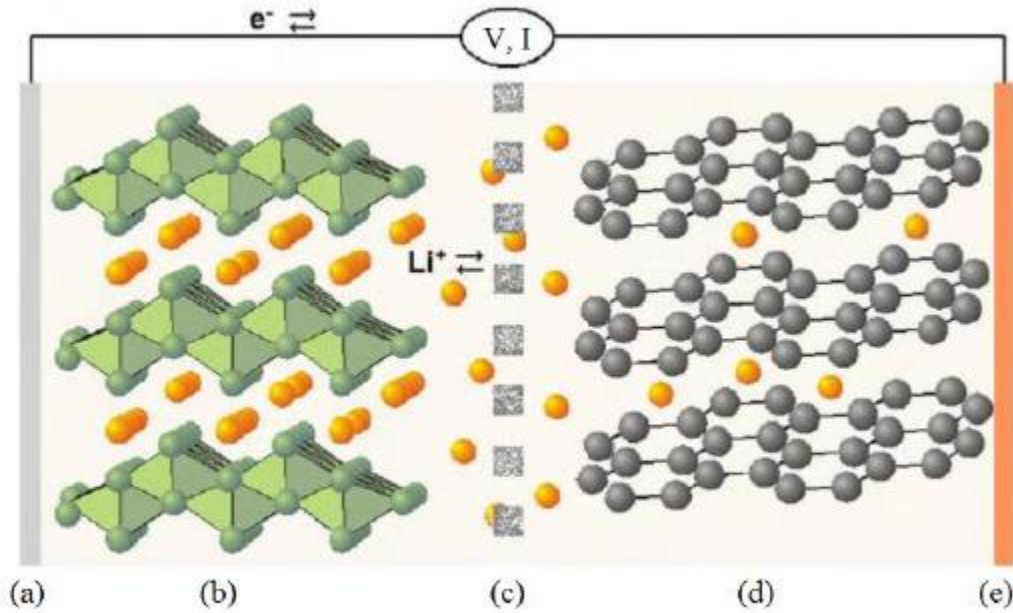
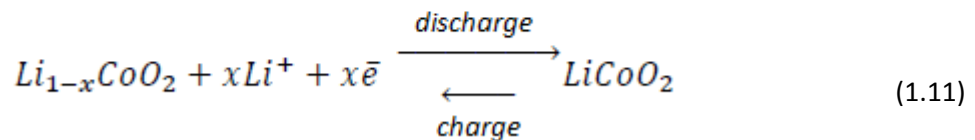
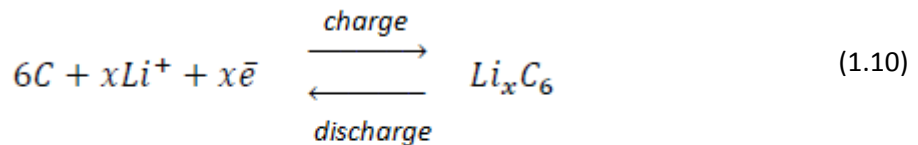


Figure 1.5. Main components of a Li-ion battery, a) Aluminium current collector, b) LiCoO₂ cathode, c) porous separator soaked with liquid electrolyte, d) graphite anode, e) copper current collector. The Li⁺ ions (orange spheres) flow through the electrolyte and are intercalated between the layers of the electrodes. The electrons flow through the external circuit [2].

The electrochemical reactions that occur during the charging and discharging processes of a Li-ion battery are presented below, where the first reaction occurs at the graphite anode and the second at the LiCoO₂ cathode. The number of electrons exchanged is denoted by the letter "x". Theoretically, the maximum lithium content that can be intercalated between the graphite sheets is one Li⁺ every six carbon atoms (LiC₆). [2]



1.4.1 CATHODE MATERIALS FOR LITHIUM ION BATTERIES

Among the most common cathode materials for Lithium ion batteries are layered LiCoO_2 (LCO), $\text{LiNi}_y\text{Mn}_y\text{Co}_{1-2y}\text{O}_2$ (NMC), spinel LiMn_2O_4 (LMO), $\text{LiMn}_{1.5}\text{O}_4$ (LMN) and olivine LiFePO_4 (LFP). Table 1 summarizes the electrochemical properties of the three classes of insertion compounds. [6]

Table 1.

Framework	Compound	Specific capacity* (mAh/g)	Average potential (V vs. Li^0/Li^+)
Layered	LiCoO_2	272 (140)	4.2
	$\text{LiNi}_{1/3}\text{Mn}_{1/3}\text{Co}_{1/3}\text{O}_2$	272 (200)	4.0
Spinel	LiMn_2O_4	148 (120)	4.1
	$\text{LiMn}_{1.5}\text{Ni}_{0.5}\text{O}_4$	148 (120)	4.7
Olivine	LiFePO_4	170 (160)	3.45
	$\text{LiFe}_{0.5}\text{Mn}_{0.5}\text{PO}_4$	170 (160)	3.4/4.1

*Value in parenthesis indicates the practical specific capacity of electrode.

With respect to the crystalline structure (Figure 1.6), these compounds are classified, in correspondence to the ion diffusion pathways and activation energy that govern Li-ion transport within the electrode material, into two dimensional $\text{Li}[\text{M}]\text{O}_2$ with $\text{M} = \text{Co}, \text{Ni}, (\text{Ni}_x\text{Co}_{1-x})$ or $(\text{Ni}_x\text{Mn}_y\text{Co}_z)$, the three-dimensional $\text{Li}[\text{X}]_2\text{O}_4$ with $\text{X} = \text{Mn}, (\text{Mn}_{1-y/2}\text{Li}_{y/2})$ or $(\text{Mn}_{3/4}\text{Ni}_{1/4})$ and uni-dimensional $\text{Li}[\text{M}]\text{PO}_4$ where $\text{M} = \text{Fe}, \text{Mn}, \text{Ni}, \text{Co}$ or $(\text{Fe}_y\text{Mn}_{1-y})$. [6]

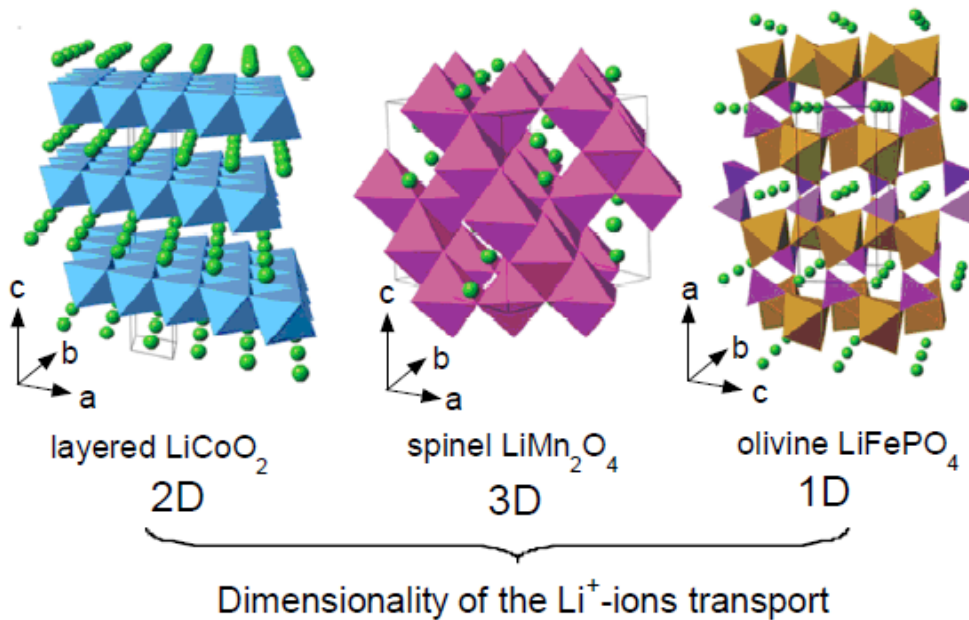


Figure 1.6. Crystalline structure of layered, spinel and olivine cathode materials and their dimensionality of the Li^+ ions transport. [6]

The very good cycling performance and low self-discharge make the layered oxide LiCoO_2 the most widely used cathode material in the electronic market. However, the high costs due to the low cobalt availability, low thermal stability, and fast capacity fading at high currents have led the research towards other cathode materials. The development of $\text{LiNi}_{1/3}\text{Co}_{1/3}\text{Mn}_{1/3}\text{O}_2$ (NMC) and $\text{LiNi}_{0.8}\text{Co}_{0.15}\text{Al}_{0.05}\text{O}_2$ (NCA) with their appealing properties, such as low-cost, high-capacity and good rate capability made these materials particularly attractive for automotive applications.

Properties like environmental friendliness, good safety characteristics, and high-power capability have introduced spinel crystal structure materials, pioneered by LiMn_2O_4 (LMO), as promising cathode materials for lithium ion batteries. Still, the mayor disadvantage of LMO is the huge capacity fading due to the structural transition from spinel to tetragonal structure caused by disproportion of Mn^{+3} ions and dissolution of Mn^{+2} into the electrolyte. This behaviour has effectively been proved to improve by replacing part of the Mn with other metal ions, being the high voltage $\text{LiNi}_{0.5}\text{Mn}_{1.5}\text{O}_4$ the most promising material of this class.

Lithium-transition metal phosphates are olivine structured promising cathode materials, since they are environmentally friendly and display high thermal and chemical stability (the strong covalent bond between oxygen and phosphorous ions makes difficult the removal of oxygen atoms from the lattice) and low cost. Nevertheless, the most important drawback of these cathodes is the intrinsically low ionic and electronic conductivity. [7]

In this thesis, only high voltage cathode materials (LNMO) will be discussed further, since a LNMO cathode was used in the electrochemical experiments.

1.4.2 HIGH VOLTAGE CATHODE MATERIALS (LNMO)

The spinel $\text{LiNi}_x\text{Mn}_{2-x}\text{O}_4$ ($0 < x < 0.5$) is a promising high-voltage cathode material for the development of high-energy Li-ion batteries. Reversible oxidation of $\text{Ni}^{+2}/\text{Ni}^{+3}$ and $\text{Ni}^{+3}/\text{Ni}^{+4}$ that occurs at 4.70 and 4.75 V vs Li^0/Li^+ , leads to a high nominal operating voltage as well as a high theoretical specific capacity (146.7 mAh/g). [7]

LNMO is also promising as a competitive material considering the battery costs, since this cathode material is the cheapest among LIBs. [7]

$\text{LiNi}_{0.5}\text{Mn}_{1.5}\text{O}_4$ can crystallize in two crystallographic structures depending on the synthesis conditions, the face-centred spinel ($Fd-3m$) named as 'disordered spinel' and the simple cubic phase ($P4_332$) named as 'ordered spinel'. In the first one, Ni and Mn atoms are randomly distributed in 16d sites where Li and oxygen atoms occupy 8a and 32e sites respectively. In the ordered spinel phase, the atoms are regularly distributed as follows: Ni on 4a sites, Mn on 12d sites, Li atoms on 8c sites, and O on 8c and 24e sites. In LNMO, 1/5 of the material capacity is provided by the oxidation of Mn^{+3} whereas the other 4/5 is provided by the oxidation of Ni^{+2} . An order-disorder phase transition can occur associated with oxygen loss, where part of the Mn^{+4} ions are reduced to Mn^{+3} to keep the electric neutrality. This affects the electrode performance since Mn^{+3} has a larger ionic radius expanding the lattice, which benefits Li^+ diffusion. However, a disproportionation reaction may occur, where Mn^{+3} forms Mn^{+2} which is dissolved into the electrolyte. These manganese ions migrate and deposit on the graphite anode where they catalyse decomposition reactions of the electrolyte and increase Li^+ retention in the solid electrolyte interphase (SEI). For this reason, a gradual capacity fade takes place in Li ion batteries. This effect represents the major drawback of the material, and

different techniques and researches are implemented to develop a material with suitable structure and enhanced electrochemical performance. [6], [7], [8], [9]

Some strategies to improve the interface stability in LNMO electrodes include:

I) Electrolyte additives

The most common electrolyte solution for LIBs is a mixture of aprotic organic solvents, such as ethylene carbonate (EC) with dimethyl carbonate (DMC) and/or diethyl carbonate (DEC), and LiPF₆ salt. Research studies about incorporating additives like lithium bis(oxalate)borate (LiBOB), tris(hexafluoro-iso-propyl)phosphate, glutaric anhydride, succinic anhydride or 1,3-propane sultone have proved to improve the electrochemical performance of high voltage cathode materials by forming a protective layer on the cathode surface that prevents electrolyte decomposition reactions and inhibits manganese dissolution from the cathode, thus stabilizing the cathode/electrolyte interface upon high-operating voltages.

II) Particle size

In the synthesis of LNMO cathode materials, a proper combination of particle size and shape can improve the cycling performance and rate capability. Matching of micro-sized particles in disordered phase with nano-sized ones in ordered phase, appears to be the best combination.

III) Surface modification

Electrodes surface modification by coating nanoparticles like ZnO, SiO₂, V₂O₅, TiO₂ or Al₂O₃ has been demonstrated to greatly improve the electrochemical performance and increase the structural stability of LNMO materials, by protecting the cathode surface against HF attack and preventing Mn dissolution.

IV) Improving the separator

The separator in LIBs is an important component for cell energy, power densities and cycle life, and crucial for cell safety. Being able to provide a good interface between both electrodes and the electrolyte, requires it to be chemically and electrochemically stable, specially under strong oxidative and reductive environments when the battery is fully charged, or in presence of high-voltage cathode materials. Mechanical strength and a proper porosity are also properties that the separator should display in order to withstand the tensions during the battery assembly and to guarantee a good electrolyte absorption and retention, necessary to achieve a good ionic conductivity between the electrodes. However, separators add electrical resistance to the cell adversely affecting the battery performance. [10]

An appropriate tortuous structure, which strictly depends on the pore size, is desirable to retain lithium dendrites whereas a homogeneous distribution of pores is crucial to provide a uniform current distribution and avoid capacity losses. Besides, porosity and pore size strongly affect the ionic conductivity of the electrolyte and the electrochemical performance of the battery. [10]

Considering their structure and composition, separators can be mainly classified into microporous polymer membranes, non-woven fabric mats and inorganic composite membranes. The most commonly used ones that are available on the market are single or multilayer sheets based on microporous polyethylene (PE) or polypropylene (PP). [10] The most important disadvantages of this current commercial separators are their relatively low melting temperature, 130 °C for PE and 160 °C for PP, which could cause direct contact between electrodes and even lead to explosion of batteries when overheating or short circuit occurs, and the hydrophobic character and low porosity of stretch film that affect the electrolyte uptake and severely impede the ionic conductivity in the battery. [11]

The extremely low wettability with liquid electrolytes as well as the weak thermal stability, have limited the further use of these kind of separators in energy storage systems, especially in hybrid electric vehicles (HEVs). Different techniques have been taken to reduce these defects, such as polymers' surface grafting modification of separators, ceramic coatings on them, and their replacement with nonwoven membranes or polymer electrolytes.

Coatings on polyolefin separators with different inorganic materials such as SiO₂, Al₂O₃, ZrO₂, zeolite, Mg(OH)₂, Al(OH)₃ have been proven not only to improve their thermal stability, but also enhance the electrolyte wettability for polar organic electrolytes based on carbonates like dimethyl carbonate (DMC), ethylene carbonate (EC), or diethyl carbonate (DEC). [12]

Being thin, mechanically robust, highly porous, and stable at potentials higher than 4.5 V vs. Li⁺/Li⁰, are highly demanded properties of a suitable separator for high power energy densities lithium-ion batteries and therefore, optimizing all the separator's properties is of great importance.

1.5 METALLIC LITHIUM BATTERIES

Although batteries with metallic lithium anodes have a theoretical capacity equal to 3860 mAh/g (approximately ten times higher than that expected for Li-ion batteries), the application of these anodes in batteries is limited because of the formation and growth of dendrites on the surface. Such formation causes loss of reversibility in chemical reactions and, eventually, short circuits and safety problems in the battery. [2]

In this type of batteries, the following electrochemical reaction takes place at the anode during the charge / discharge process:



The surface of metallic lithium highly reacts with water, with atmospheric gases, with polar aprotic solvents such as alkyl carbonates and with most anions of salts used in the electrolyte. This reactivity generates a passivation film of multiple structure and different chemical composition, known as Solid Electrolyte Interphase (SEI), that covers the lithium surface. The products of the chemical reactions between the metallic lithium and its superficial film with the electrolyte, form superficial

layers that passivates the anode preventing chemical reactions to happen when the film has a sufficient thickness to restrict the transfer of electrons through it. This passivation film is formed even before there is current flow between the electrodes, and its composition depends strongly on the electrolyte used. In addition, it has variable thickness and composition with the passage of electric current. [2]

When the lithium anode is introduced into a polar aprotic solvent, many processes occur in parallel, such as the dissolution of part of the surface species present at the beginning and their redeposition, nucleophilic substitution reactions between the metal oxide and the hydroxide with electrophilic solvents (like alkyl esters and carbonates), formation of insoluble salts by reactions between the anions with the metal cations and the diffusion of solvent molecules towards the interface between the lithium and the initial layers, that are then reduced by the active metal. Insoluble salts and other products precipitate on the electrode and form a surface layer due to which, a further reduction of the species in solution requires the transport of electrons through this film. With this, the reduction processes become every time more selective. The composition of the SEI comprises multilayered surface films (from metal/film interface to film/solution interface). In proximity to the metallic lithium, layers may contain oxides and halides, while in further regions are constituted mainly by carbonates and organic salts, such as ROLi , ROCO_2Li , RCOOLi and polymeric species, where R corresponds to an organic group from the solvents used [13].

When the surface films become sufficiently thick, they block the transfer of electrons. However, in places of high local conductivity, electrons manage to pass through the surface films and, therefore, the reduction of species in solution continues. Some species in solution precipitate on the electrode and secondary reactions may occur between the surface species and those present in the electrolyte (for example, water reactions with ROCO_2Li and lithium salts with acidic species). There is evidence that the inner part of the surface films is in nature more inorganic, composed of species with low oxidation state (due to the highly reductive environment close to the surface of the metal), while the external parts of the surface films on lithium mainly comprise organic lithium salts. The surface layer near the solution is porous, while the inner part, close to the active metal, is compact [13].

Figure 1.7 schematizes the surface layers that are formed on the surface of metallic lithium. Before applying current, lithium is already covered by films composed of Li_2O , LiOH and Li_2CO_3 .

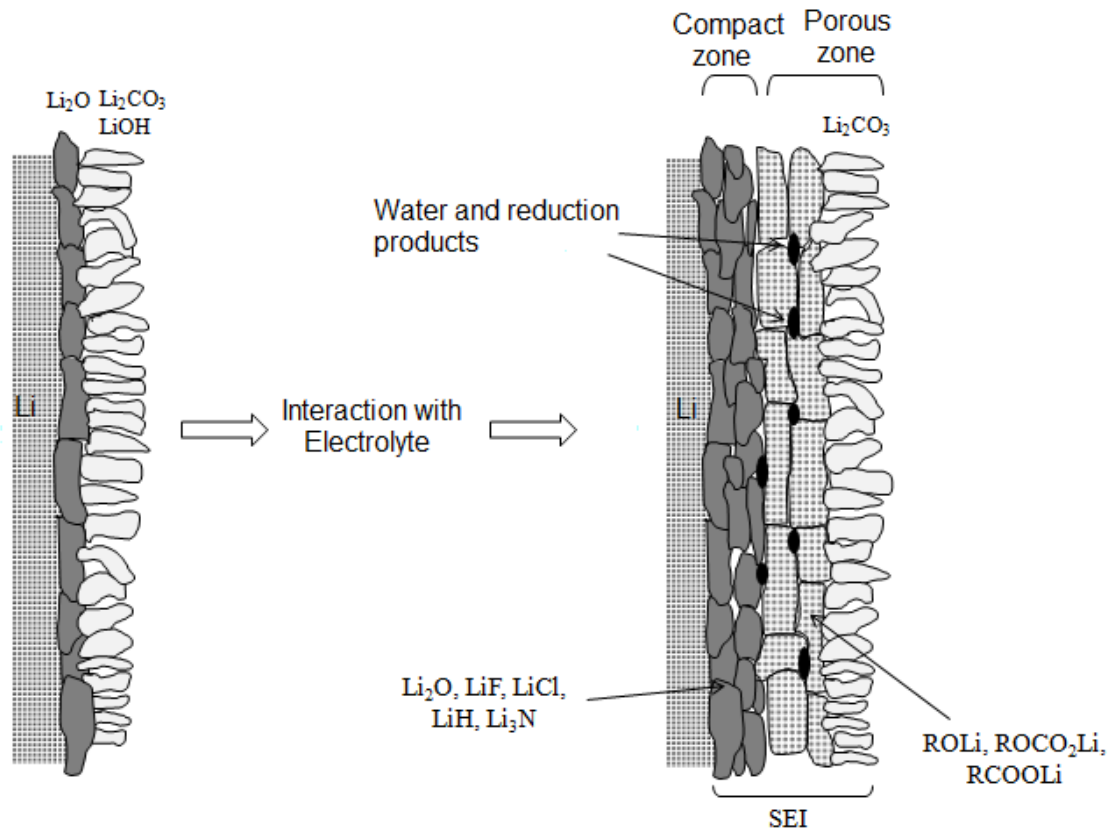


Figure 1.7. Diagram of surface layers on metallic lithium anode after its contact with the electrolyte. Initially, lithium anode is covered by films composed of Li_2O , LiOH and Li_2CO_3 [2].

The following electrochemical reactions exemplify the wide variety of reactions that occur between the metallic lithium anode and the components in the electrolyte (Figure 1.8). These reactions correspond to a battery that uses a 1 M LiPF_6 electrolyte in a mixture of organic solvents of ethylene carbonate and dimethyl carbonate (EC-DMC) [14]. Because of the composition of this solution, the presence of HF in traces is unavoidable (around 50 ppm in high purity electrolytes [15], [16], [17]). As described before, SEI layer has a non-uniform multi-layer, mosaic-like structure at the microscopic level [17]. These non-uniformities detected in surface films induce an inhomogeneous current distribution over the lithium anode, during the processes of metal plating and stripping.

Because these layers are composed of lithium salts, their cohesion and flexibility are limited, for which they cannot effectively accommodate the morphological changes of the active material during cycling performance. This causes ruptures in certain sectors of the superficial layers, where metallic lithium is directly exposed to the electrolyte and these places become preferential sites for the electrochemical processes (due to the lower electrical resistance). [2]

The formation of dendritic lithium (as shown in Figure 1.9) is attributed to this effect that is observed at relatively high current densities ($i \geq 1 \text{ mA/cm}^2$). When forming dendrites, the exposed metallic lithium reacts with electrolyte species to repair the passivation layer. This produces a loss of active lithium and compounds present in the solution which are no longer able to participate in the cycling, shortening the useful life of the battery. [18]

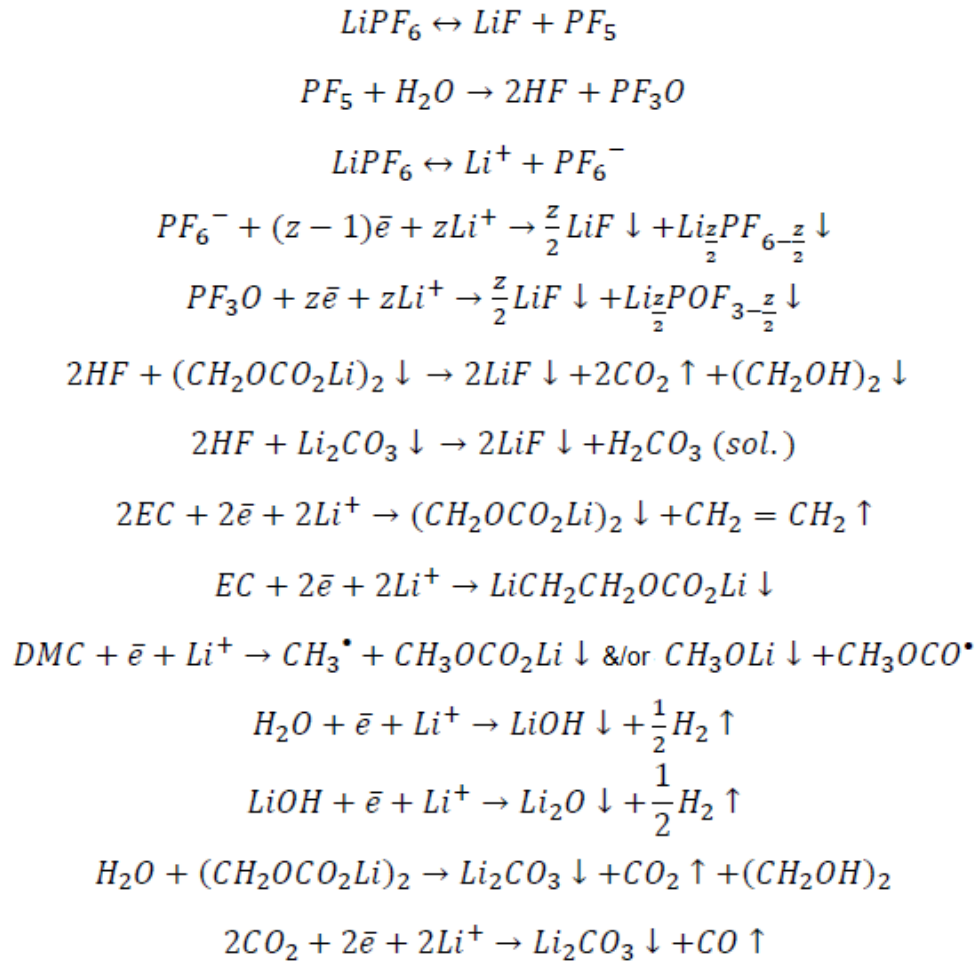
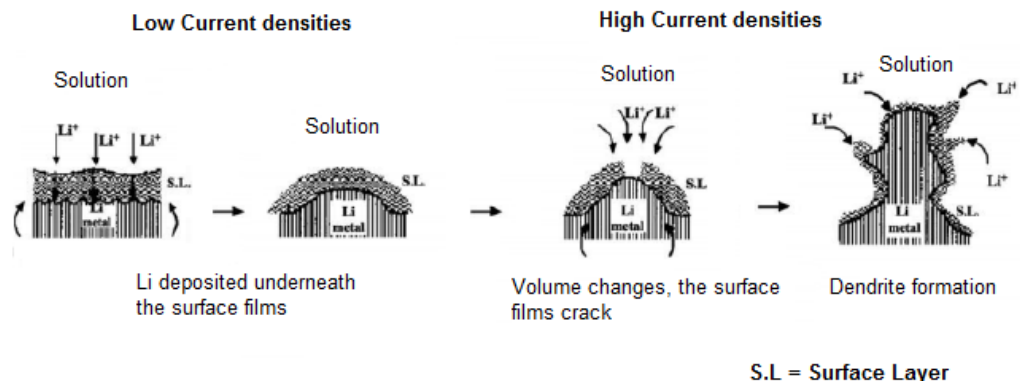


Figure 1.8 Electrochemical reactions between metallic lithium anode and LiPF₆ electrolyte in EC-DMC. [2]

Li Deposition



Li Dissolution

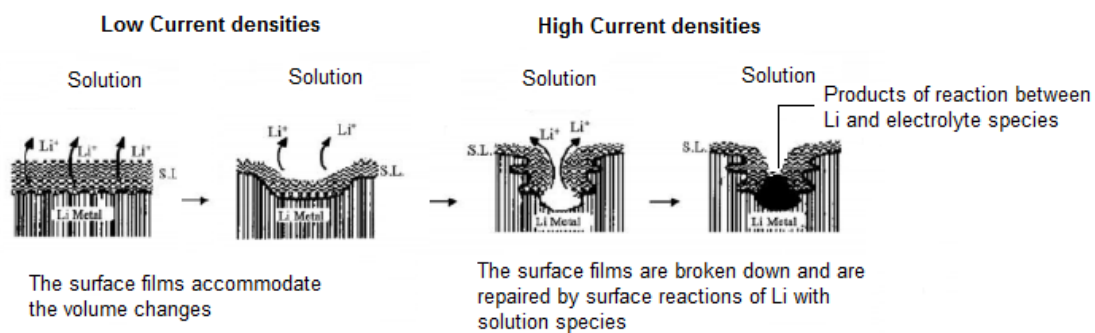


Figure 1.9. Dendrite formation and non-uniform Li dissolution accompanied by breakdown and repair of the surface films. [18]

Some alternatives to improve the performance of metallic lithium anodes include: [19]

I) Structure design

The effective current density on lithium surface during discharge/charge process has a significant influence on the Li dendrite formation and growth. Low current, in general, leads to relatively uniform deposition and stable cycling performance while dendritic deposition becomes significant at high current density. For compact lithium foil, structure design via Li-alloy or confinement into matrix would be effective to guide uniform Li deposition. Various 3D current collectors with high specific surface have been developed to decrease the effective current density and offer more sites for Li nucleation.

II) Microstructure operational control of the SEI layer

A lot of research has been carried out with the aim to control the microstructure of the SEI layer using additives such as HF and CO₂, which have generated improvements in the morphology of lithium deposits and in the cycling efficiency of the anode. The use of vinylene carbonate (VC) as an additive in the electrolyte allows an improvement in the cycling efficiency and in the morphology of the anodes when they are pressurized and at elevated temperatures (around 50 °C).

Another alternative to promote a reversible behaviour of the lithium anodes is the formation of flexible surface films, which allow to better accommodate the morphological changes during the processes of metal deposition and dissolution. It has been found that the use of cyclic ether solvents such as 1-3 dioxolane (DN) allows the formation of a more flexible SEI layer on the lithium anode, in a LiAsF₆ electrolyte with a tributylamine additive (TBA) as a basic stabilizer. The reduction of this solvent and / or the presence of ROLi species on the surface lead to the partial anionic polymerization of this, forming species of the type LiO (CH₂CH₂OCH₂O)_n. These species are elastomers and allow the surface layers to be sufficiently flexible to maintain the passivation of the active metal. When this electrolyte is used, the cycling efficiency of the anodes is very high, and the morphology of the deposits is very smooth. However, batteries that use this electrolyte can only be charged at very low rates (1 C / 10-12 h), otherwise the number of available cycles is very low because at high load rates, the speed of the surface reactions between the electrodeposited lithium and the components in solution increase considerably, so that the electrolyte is consumed very fast.

III) Separator modification

Some studies on the separator improvement towards suppressing dendrites, like polydopamine (PDA) or hybrid polydopamine/octaammonium (PDA/POSS) coatings, have proved to improve the ionic conductivity as well as the Li⁺ transference number contributing to better Li deposition. Comparing with surface treatment of the metallic anode, separator modifications are much easier and more feasible. For example, simple carbon coating onto the separator not only impedes dendrite penetration by covering most of the pores, but also enhance its conductivity and reduce impedance.

IV) Alternative electrolytes

Several researchers have studied the use of solid polymers as an alternative electrolyte of rechargeable batteries with metallic lithium anodes. These polymers are compounds based mainly on polyethylene oxide (PEO), polyacrylonitrile (PAN) or polyvinylidene fluoride copolymerized with hexafluoro propylene (PVDF / HFP). The low ionic conductivities ($\approx 10^{-8}$ - 10^{-4} S / cm) of this solid electrolyte compared to the liquid electrolytes frequently used in batteries ($\approx 10^{-3}$ S / cm), have led to study mixtures of them with liquid solvents (gels) with the objective of approaching conductivities of the typical electrolytes. These gels are produced by addition of low molecular weight plasticizers/organic liquid electrolyte in PEO.

Ionic liquids (ILs) have also been studied as possible candidates for electrolytes, which typically consist of salts in the liquid state which contain larger asymmetric organic cations compared to their inorganic counterparts. These electrolytes have a negligible volatility and practically no flammability, which confers greater safety in the operation of the battery. However, they show higher viscosities and lower ionic conductivities than commercial electrolytes for batteries, which makes the mass transport difficult during operation. Among the most commonly used ionic liquids are those based on bis (trifluoromethanesulfonyl) imide (TFSI) and bis (fluorosulfonyl) imide (FSI) anions, to which organic diluents can be added at low concentrations to reduce the viscosity.

1.6 AIM OF THE THESIS WORK

The first aim of this thesis work was to synthesise a nanocomposite based on polyaniline and an Argentinian montmorillonite in order to achieve a synergistic combination of properties that could not be obtained by the materials alone. Chapter 2 details the physical and chemical properties of both polyaniline and clay (montmorillonite) and the advantageous characteristics of each one. Chapter 3 explains the synthesis procedures as well as the results of the characterization techniques used to study the obtained nanocomposites.

Secondly, featuring the mentioned problems concerning high voltage cathode materials in lithium ion batteries and metallic lithium anode in next generation batteries, it was decided to study an electrochemical application of the synthesized clay/polymer nanocomposites. The strategy faced was to coat a slurry of the composite materials onto a commercial separator used in batteries, to improve the properties of the separator. The modified separator was then electrochemically tested as:

- A strategy to protect metallic lithium, by reducing dendrites formation and growth.
- A strategy to increase cycling performance of high voltage cathode materials ($\text{LiNi}_{1.5}\text{Mn}_{0.5}\text{O}_4$), by impeding manganese transference to the anode.

In chapter 4, these electrochemical applications and the characterization results are developed.

Chapter 2: Physicochemical properties of Polyaniline and Montmorillonites

2.1 CONDUCTIVE POLYMERS

Conductive polymers (CP) are a group of polymers that share the property of being able to behave as electrical conductors, unlike the 'classical' polymers that behave as electrical insulators.

The electrical behaviour of CPs is closer to that of semiconductor materials than to metals, because they only present high values of electrical conductivity (metallic conductivity) in certain oxidation states. The conductivity is generated from a reorganization of the electronic structure that generates charge carriers in the macromolecule. Conjugation provides the orbital system that allows charge carriers to move because of continuous overlapping of pi-orbitals along the backbone. Charge carriers can be introduced by partial oxidation (p-doping) of the polymer chain with electron acceptors or by partial reduction (n-doping) with electron donors. Such doping processes mostly introduce charged defects along the polymer backbone. [20] In other words, the doping of a polymer involves the appearance of electric charges in its main chain, which modifies the electrical properties of the polymer and involves the introduction of ionic species of opposite charge (counterions). The so-called "conjugated polymers" have the structure that best adapts to this type of transport mechanism, since they are constituted by a continuous succession of π conjugated bonds along its main chain, which facilitates the mobility of the charge carriers.

These kinds of polymers have been utilized in a wide range of applications because they possess both the electronic properties of semiconductors and the processability of conventional polymers.

Among several ways to introduce charge carriers or to dope the conjugated polymer to become conductive, the most widely used ones are electrochemical and chemical oxidation/reduction.

Examples of conductive polymers are polyacetylene (PA), polyparaphenylene (PPP), polyaniline (PANI), polypyrrole (PPy) and polythiophene (PT), whose monomeric structures and electrical conductivity are shown in Table 2.1.

Within the group of conductive polymers, polyaniline has a series of characteristics that differentiate it from most CPs, among which are:

- Its main chain does not present an uninterrupted succession of π -conjugated C-C bonds, but an alternation of aromatic rings and nitrogen atoms between them.
- Because of the presence of nitrogen atoms in the main chain, PANI presents a special type of chemical doping by protonation, which means it can be doped with protic acids and undoped by bases.
- The doped state of greater electrical conductivity (called emeraldine salt) is highly stable under normal environmental conditions (in the presence of air, humidity, CO₂, etc.) unlike what happens with the doped states of most CPs.

- The conventional PANI synthesis is comparatively cheaper and simpler than the rest of the conductive polymers, which is an advantage considering the practical application of this CP.

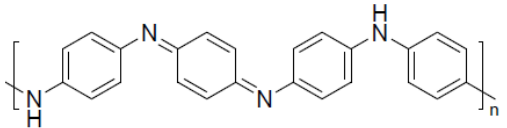
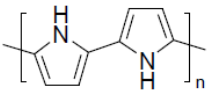
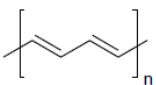
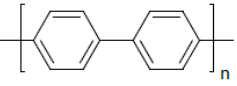
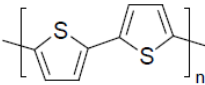
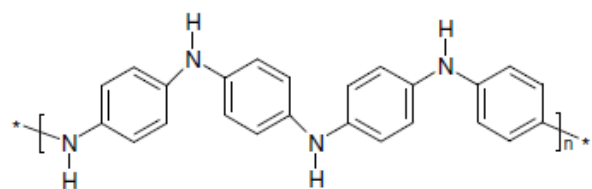
POLYMER	CONDUCTIVITY (S/cm)
 <p data-bbox="418 638 667 674">Polyaniline (PANI)</p>	$10 - 10^2$
 <p data-bbox="461 852 695 888">Polypyrrole (PPy)</p>	10^2
 <p data-bbox="440 1073 695 1108">Polyacetylene (PA)</p>	$10^3 - 10^5$
 <p data-bbox="402 1304 743 1339">Polyparaphenylene (PPP)</p>	10^3
 <p data-bbox="444 1520 711 1556">Polythiophene (PT)</p>	10^2

Table 2.1. Monomeric structure and electric conductivity (standard conditions) of most common conductive polymers

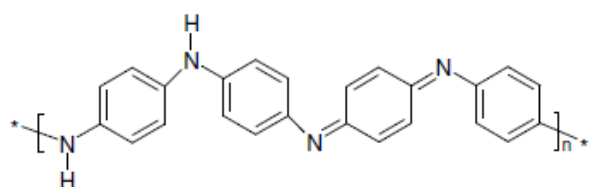
2.2 POLYANILINE

Polyaniline is the polymer derived from the oxidative polymerization of aniline. Different structures of the polymer chain can be obtained depending on the oxidation degree and the degree of protonation of the macromolecule.

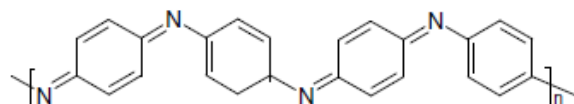
Considering the degree of oxidation, there are three states that are used as a reference. The first one, known as leucoemeraldine, corresponds to the completely reduced state of the polymer and consists of benzene units bonded through amino groups. The second one, is called emeraldine and is a semi-oxidation state obtained by converting half of the amine groups into imine. The third one corresponds to the completely oxidized state of the polymer, which consists of quinoid groups linked to nitrogen atoms through double bonds and is called pernigraniline. Figure 2.1 shows the three structures in their base form in which the nitrogenous groups are not protonated. The pernigraniline form is not stable in an acidic medium and the oxidation of the emeraldine form leads to degradation of the polymer.



Leucoemeraldine base



Emeraldine base



Pernigraniline base

Figure 2.1. Polyaniline structures with different oxidation states in their base form [21]

The amine and imine groups of the polymer can also bind protons through acid-base equilibria. This conduces to different species of the polymer depending on the degree of protonation that the macromolecule has. The protonated forms of the completely reduced and semi-oxidized polymer

are called leucoemeraldine salt and emeraldine salt respectively. Of all the species mentioned, the emeraldine salt is the only conductive form of PANI.

In the case of protonated polyanilines, the transition from emeraldine base (EB) to emeraldine salt (ES) implies two types of nitrogen that can be protonated: the "amine" type nitrogens or the "imine" type. Figure 2.2 shows both possibilities. The structure B, in which imine-type nitrogens are protonated, explains the high electrical conductivity of protonated emeraldine. This configuration has several forms of resonance in which the positive charge can be located in any of the nitrogens, which explains the energy stabilization of this form and the delocalisation of positive charges along the chain that favours the mobility of charges.

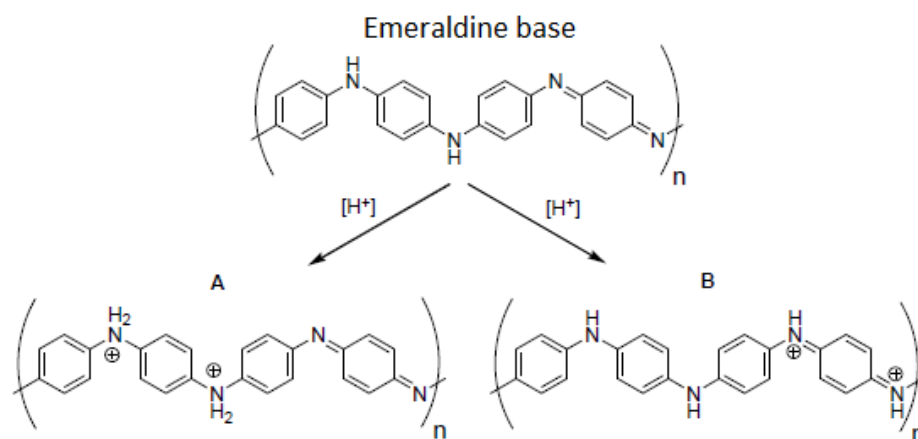


Figure 2.2. Different possibilities of protonated emeraldine in PANI [22]

The structure with 'polaronic' radicals (Figure 2.3) is the one most commonly represented, since it explains various experimental observations such as the existence of unpaired electrons [23] or the electronic absorption spectrum [24], [25] in the PANI in the emeraldine salt state.

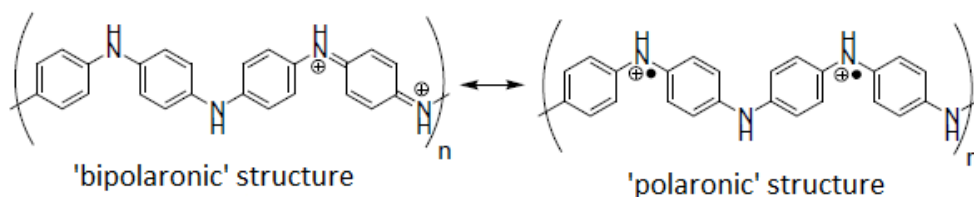


Figure 2.3. Bipolaronic and polaronic structures of protonated PANI in ES form [22]

2.2.1 POLYANILINE SYNTHESIS

Polyaniline is synthesized almost exclusively from aniline or some anilinium salt by means of an oxidative polymerization chain reaction. [22] In general two methods are distinguished depending

on the type of oxidation carried out: the electrochemical polymerization, in which the aniline is oxidized in the anode of an electrochemical cell as consequence of the applied electric current, and the chemical polymerization, in which the aniline is oxidized by some oxidizing compound present in sufficient quantity.

The oxidation of aniline, in the aniline form or anilinium salt, to give polyaniline can be represented according to this electrochemical semi reaction (Figure 2.4).

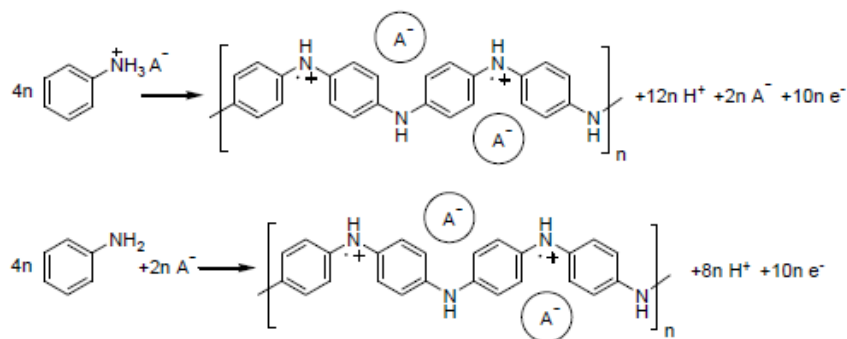


Figure 2.4. Oxidation semi-reaction of aniline or of an anilinium salt to PANI (ES) [22]. A^- is the counter-anion of the acidic dopant, present to balance the electrical charge in the system.

As seen, the reaction product is PANI in the emeraldine salt state, and the exact number of moles of electrons involved per mole of aniline would be 2.5 moles, accepted by a chemical oxidant or by the anode in an electrochemical cell. Some peculiarities of this reaction are: [22]

- The polymerization reaction is favoured by polar solvents, especially water.
- The polymerization reaction is effective at acidic pHs, at basic pHs aniline oligomers are produced, which react producing various condensed heterocycles.
- The most common oxidant used is ammonium peroxydisulfate $(NH_4)_2S_2O_8$ (APS), for its relative chemical stability and low cost.
- The type (s) of protic acids present in the reaction medium, which appear in the final polymer as counterions, do not influence in principle the kinetics and performance of the reaction (although they do influence the morphology and properties of the polymer).
- From a kinetic point of view, the reaction has two main steps: an initial period (induction), endothermic and slow in which no polymerization occurs, and an exothermic period of fast polymerization conducting to polyaniline in the form of emeraldine salt.
- The pH of the reaction medium decreases as the polymerization progresses, because H^+ is produced during aniline oxidation.
- The reaction is effective (produces PANI of high purity as a majority product) in general at temperatures not higher than $40^\circ C$ (in water) and proceeds correctly at low temperatures, even below the freezing point of the reaction mixture. In general, the lower the temperature,

the greater the average molecular weight, crystallinity and conductivity of the obtained polymer.

- Although being a relatively fast reaction, in the main chain of PANI only head-tail type couplings are observed, meaning that in the final structure nitrogens are disposed in 'para', and no couplings in 'ortho' or formation of carbon-carbon or nitrogen-nitrogen bonds are observed, which could be expected from a fast reaction which is supposed to take place with radical intermediaries and in absence of catalysts.

One of the major advantages of PANI over other conductive polymers lies in its comparatively much simpler and cheaper synthesis. Both the starting products (aniline and oxidant) and the solvent (water, with a certain amount of acid) have affordable prices. Furthermore, the reaction usually does not require special procedures since the product is obtained with high purity, and the separation is carried out simply by filtration and washing. The oxidative synthesis of PANI also exhibits great versatility, not only allowing a wide variety of oxidizing agents (chemical or electrochemical), but also allowing wide variations in the reaction conditions (temperature, concentrations), and the addition of various elements to the reaction medium (substrates to be coated, other polymers, nanoparticles and other species to synthesize composite materials).

2.2.2 POLYANILINE STRUCTURE AND CRYSTALLINITY

Polyaniline synthesized by oxidative polymerization in acidic medium presents a surprisingly high structural regularity for a radical reaction without specific catalyst. This is due to the complex self-assembly mechanism that promotes the regular growth of the polymer chain. At first there are no appreciable amounts of branches, or couplings that are not "head-tail", and it can be said that the polymer has a homogeneous structure along the chain.

Focusing on the "primary structure" of polyaniline, that is, the structure and conformation of the isolated macromolecules, most of the structural information of PANI that is presented in the literature, is based on computational calculations and is corroborated by the concordance with experimental data. Polyaniline chain, in every oxidation state, can be modelled as a sequence of repetitive units each with six carbons, one nitrogen and the corresponding hydrogen atoms (Figure 2.5). The geometry of the chain is determined essentially by the values of three types of angles, θ , φ and Ψ for each repetitive unit, which are outlined in Figure 2.5. The first is the angle θ that forms the sequence of bonds C-N-C, which is usually close to 120° corresponding to a sp^2 hybridization of nitrogen. The second is the dihedral angle of torsion φ , between the plane formed by the aromatic ring and the plane formed by the sequence of links C-N-C (C1-N1-C2 in the figure). The third is the dihedral angle Ψ that forms two consecutive C-N-C planes of the chain (C1-N1-C2 and C3-N2-C4 in the figure). [22]

Polyaniline is classified as a "semi-rigid rod" polymer, which means that the general arrangement of the macromolecules is straight but not totally rigid. In the CPs that stiffness is given by the rotation restriction of bonds, particularly the π bonds that predominate in the conductive polymers. In the special case of PANI, the presence of heteroatoms (nitrogen) in the main chain of the polymer gives a certain freedom of rotation to the structure that manifests in the mentioned dihedral angles. [22]

The angle Ψ has a clear influence on the total length and straightness of the macromolecule, the greater elongation of the chain would correspond to a zigzag type structure in which all the angles

$\Psi = 180^\circ$. A PANI chain in which the angles Ψ are always less than 180° , or always greater than 180° form a helix (dextrorotatory for $\Psi < 180^\circ$ and laevorotatory for $\Psi > 180^\circ$). This coil conformation will be more compact for Ψ values further from 180° , and more extended for values closer to 180° . This chirality or "Helicity" has been observed for polyanilines containing chiral counterions, the prototypical case is camphor sulfonic acid (CSA) which appears in a multitude of publications as "chiral dopant" of PANI. PANI synthesized in absence of any chirality inducer does not present any preferential helicity, which means, angles Ψ greater than or equal to 180° would be indistinctly present and these values will determine the conformation of the macromolecule and will depend mainly on the environment surrounding it (solvent, counterions, other PANI chains or other matrices). In fact, some authors talk about "secondary doping" of polyaniline, a phenomenon by which a solvent or another substance that surrounds the PANI (in this case PANI in ES form already protonated or with "primary doping") induces a conformational change in the chain, going from a compact helix to an expanded or extended one, which results mainly in changes in electrical conductivity and in the UV-Vis absorbance spectrum. [22]-[30]

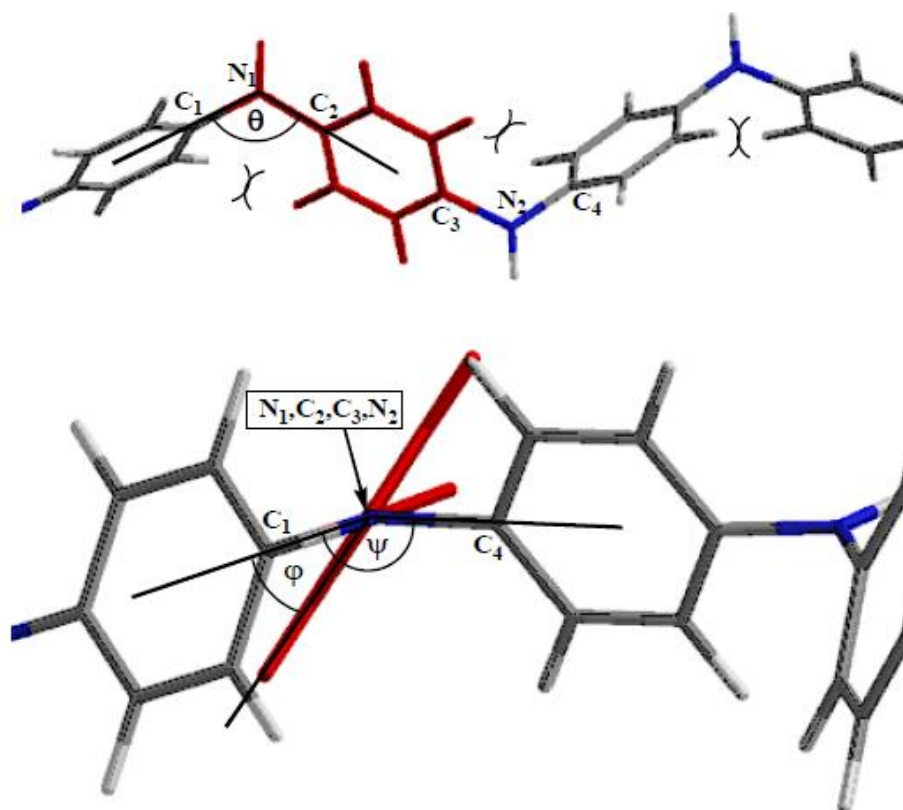


Figure 2.5. Representation of the characteristic angles of a repetitive unit of PANI (primary structure). [22]

Because of its well-defined chemical structure and strong chain interactions, including π - π stacking interactions, hydrogen bridges, Van der Waals and London dispersion forces, and coulombic interactions in the case of emeraldine salt state, PANI would be expected to have a high degree of

crystallinity in the solid state. However, X-ray diffraction studies reveal that polyaniline is a semi crystalline polymer, characteristic reflections are usually observed but with low intensity and wide width that indicate that PANI is a polymer not completely amorphous but very little crystalline, being the state with greater ordering of all the ES state. [30]

2.2.3 CHARGE CARRIERS AND CONDUCTIVITY IN POLYANILINE

Of all the states of polyaniline, only the emeraldine salt state exhibits a high electrical conductivity and is therefore considered as the doped state of PANI. The rest of states (leucoemeraldine, emeraldine base, pernegranylne base and salt) are electrical insulators. The electrical conductivity of PANI-ES is due to the high mobility of charge carriers, of positive nature, in the polymer chain.

Two types of doping can conduce to PANI-ES: classical doping by oxidation from leucoemeraldine or doping by protonation from emeraldine base. In the first case the positive charges appear by direct abstraction of electrons from the polymer chain in a redox process. In the second case PANI is in a semi-oxidized neutral state and the protonation of the imine nitrogen groups creates the positive charges, which leads directly to the formation of bipolarons (positive paired charges). In ES, however, it has been demonstrated the presence of isolated polarons (radical cations), which would originate by electronic reorganization (Figure 2.6). These two species (polarons and bipolarons) are in thermodynamic equilibrium

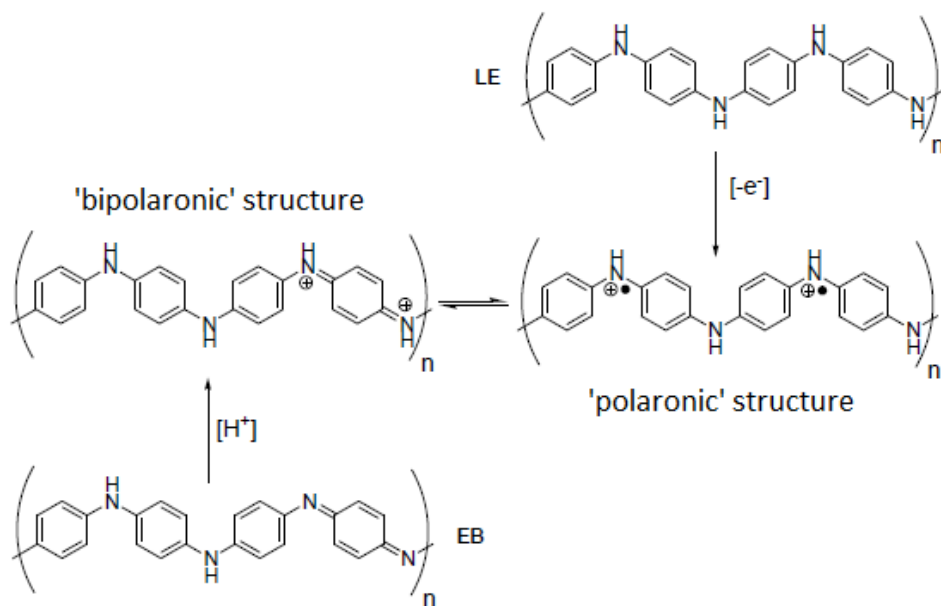


Figure 2.6. Protic and oxidative doping processes that lead to PANI-ES state. [22]

Published values of electrical conductivity for PANI in the ES state vary from $1-10^2$ S/cm, typical of semiconductor materials, to over 1000 S/cm, values more typical of metallic conductors. This disparity of results is due to factors such as the morphology, the nature of the dopant counter ion and the degree of crystallinity. In the PANI-ES there is a great resistance to electric current passage in the contact surfaces between particles. For this reason, the material has an intrinsic resistance that depends on the particulate dimensions, which means that in a material composed of smaller

particles the electric current will have to cross a greater number of highly resistive particle-particle contacts. Thus, in general, the lowest values in the mentioned conductivities range correspond to nanostructured PANI-ES, the intermediate values (around 1-20 S/cm) correspond to PANI-ES with the "classic" granular morphology and the highest values usually come from samples subjected to a homogeneous dissolution process and subsequent evaporation of the solvent, with which non-particulate materials are obtained (this is the case of solutions of PANI-ES doped with camphor sulfonic acid in m-cresol).[22], [31], [32], [33], [34]

Because of non-covalent interactions and possible steric impediments between the counterion and the polymer chain, the dopant counterion can alter the conformation of the ring sequence in the polymer chain. Several authors propose that an extended conformation of the PANI chain (with dihedral angles closer to 180 °) results in an increase in the mobility of the charge carriers and therefore in a higher conductivity. On the other hand, the effect of the crystallinity degree on the conductivity of PANI-ES is positive, since a better packing of the chains in the material would favour the charge transport between chains. [29]

2.3 MONTMORILLONITES: CRYSTALLINE STRUCTURE

Clay minerals are natural components of the soil. They are classified as phyllosilicates since they have laminar structure.

The phyllosilicates in general, have a structure based on tetrahedral groups $(\text{SiO}_4)^{-4}$ that are coupled with other tetrahedral groups by sharing three of their four oxygens forming layers of infinite extension and formula $(\text{Si}_2\text{O}_5)^{-2}$ that constitute the fundamental unit of the phyllosilicates. In these layers, the tetrahedrons are distributed forming hexagons and bind to octahedral aluminum oxide $(\text{Al}_2\text{O}_6)^{-6}$ groups that are present in another layer. The plane of union between both layers is formed by the oxygen atoms of the tetrahedra that are not shared with other tetrahedra (apical oxygens) and by OH groups of the octahedral layer so that, in this plane, an OH^- group remains in the center of each hexagon formed by 6 apical oxygens. [35]

A similar union may occur on the opposite surface of the octahedral layer. Thus, the phyllosilicates can be formed by two layers (one octahedral and one tetrahedral) and are called bilaminar, 1:1 or T:O; or three layers (one octahedral and two tetrahedral) called trilaminar, 2:1 or T:O: T. The unit formed by the union of an octahedral layer plus one or two tetrahedral ones, is called lamella. [35]

Smectites are phyllosilicates 2:1. Normally Si^{+4} , Al^{+3} and Fe^{+3} are placed in the tetrahedral sites. The substitution of a Si^{+4} by a R^{+3} cation in the tetrahedral site, creates an excess of negative charge in both basal and apical oxygens. This affects both the total (basal and on the edge) charge, as well as the local negative charge (on the surface or base) of the sheet 2:1. The octahedral sites can be occupied by trivalent cations (R^{+3}), usually by Al^{+3} or Fe^{+3} , in two octahedral sites and by a vacancy in the third site $[(\text{R}^{+3})_2(\text{OH})_6]$, or either by divalent cations (R^{+2}), normally Fe^{+2} , Mg^{+2} or Mn^{+2} , in all octahedral sites $[(\text{R}^{+2})_3(\text{OH})_6]$. When most of the cations in the octahedral layer are R^{+3} , they are called dioctahedral smectites. The substitution of R^{+3} or R^{+2} by cations of lower oxidation state and the presence of vacancies in the octahedral layer generate an excess of negative charge in the sheets. [35]

These isomorphic substitutions in the tetrahedral and octahedral layers of smectites occur naturally by geological processes, originating permanent charges that are balanced by the presence of inorganic cations in the interlaminar space (space between two consecutive sheets). The chemical nature of these cations determines in part the physical-chemical properties of the clay mineral. A common characteristic of these cations is their hydration enthalpy, which values are in the range of -300 to -1500 kJ / mol. As a result, these cations always present a full or partial hydration sphere which contributes to the hydrophilicity of these minerals.

Montmorillonite is a dioctahedral smectite and its most frequent interlaminar cations are alkaline (Na^+ and K^+) or alkaline earth (Mg^{+2} and Ca^{+2}). [35] Figure 2.7 shows the crystalline structure of montmorillonite and its general composition.

With an x-ray diffraction (XRD) analysis, the distance between sheets (basal spacing) can be measured. The peak d_{001} corresponds, in montmorillonites, to the basal spacing, which is the distance between two sheets T: O: T and is equal to the sum of the thickness of a T: O: T sheet plus the interlaminar space. Thus, this technique allows to measure the degree of expansion or swelling, which in the case of smectites is a function of the interlaminar cation. In this type of minerals, the minimum distance between sheets is 0.96 nm and is determined in dehydrated montmorillonite in ambient conditions. This value varies depending on the interlaminar cation and its degree of hydration. In addition, the incorporation of organic cations in the interlayer (depending on the concentration and its molecular volume) causes a basal spacing expansion that results in shifts of the peak d_{001} towards lower angles. [35]

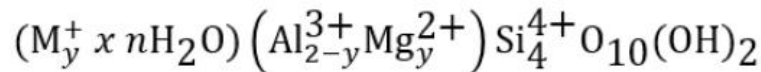
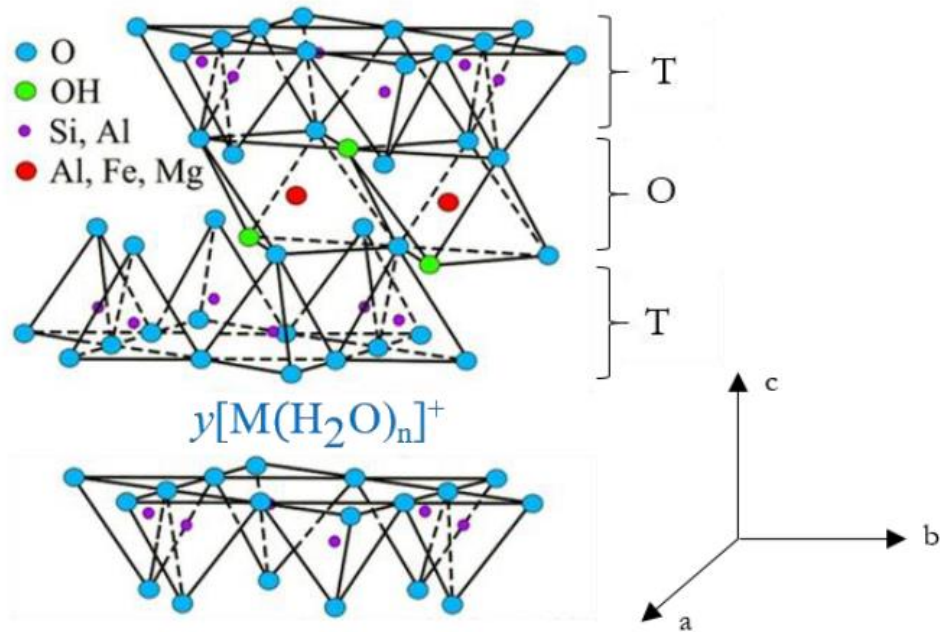


Figure 2.7. Crystalline structure and chemical composition of montmorillonite. T: tetrahedral layer, O: octahedral layer. [35]

2.3.1 CATION EXCHANGE CAPACITY IN MONTMORILLONITES

The cation exchange capacity is the magnitude that quantifies the tendency of montmorillonites to sorb cationic species from a solution and is related to the layer charge.

This value is expressed as positive charge equivalents per mass unit of clay, for example in [mmol / g]. In general, the exchange between cations to compensate the negative charge of the sheets is: reversible; limited by the diffusion step; stoichiometric; and in most cases prevails the selectivity of one cation over another. In practice, to determine it experimentally, it is necessary to completely replace all the inorganic exchangeable cations with reference cations that are not present in the mineral sample. [35]

The selectivity towards some cations with respect to others, is due to several factors such as the hydration spheres of cations on the surface and in the solution, electrostatic interactions cation-surface and cation-cation, interactions between water molecules and the surface, polarizability character of the cations, entropic factors, etc. In general, for montmorillonites, divalent cations are preferred over monovalent cations, and organic cations are preferred over inorganic ones.

2.3.2 ACTIVE SITES IN MONTMORILLONITES

Montmorillonites can participate in a very wide variety of reactions with organic compounds: the water molecules in their interlaminar space can be displaced by polar organic molecules; the interlaminar cations can form complexes with neutral organic ligands or be exchanged by various types of organic cations (alkylammonium ions, for example). In each of these processes, the driving force is the development of interactions (van der Waals forces, hydrogen bonds, ion-dipole interactions, coordination couplings) between the molecules and some specific sites on the surface of the mineral, called active sites.

In montmorillonite it is possible to distinguish the following active sites:[35]

I) Siloxane surface

In absence of isomorphic substitutions and defects in the sheets, the siloxane surface of a clay mineral is composed of oxygen atoms involved in covalent bonds Si-O. Under these conditions, the surface is neutral and hydrophobic, and therefore it is not able to form hydrogen bonds with water molecules, but it can undergo van der Waals interactions with little or non-polar organic molecules. Thus, in the organo-montmorillonites where interlaminar inorganic cations have been exchanged for organic cations, there is a double contribution to the hydrophobic character: one given by the presence of organic cations between the sheets and the other, given by the siloxane surface.

II) Sites of permanent charge

These sites originate because of the isomorphic substitutions that occur naturally in both the tetrahedral and the octahedral layers of montmorillonites. Isomorphic substitutions polarize the oxygen atoms of the surface and promote their interaction via hydrogen bonds with water molecules, and electrostatically with cations or polar organic molecules.

The negative charges in the sheet are distributed differently if the substitution occurs either in the octahedral or in the tetrahedral layer. In the case of substitutions in the octahedral layers, such as Al^{+3} by Mg^{+2} , the charge distribution is delocalized over a region close to the plane of the oxygen atoms. If the replacement is in the tetrahedral layer (Si^{+4} by Al^{+3}), the charge distribution is rather localized on the three oxygen atoms.

The fact that organic cations such as quaternary amines have higher energies of electrostatic interaction than inorganic cations, makes possible the intercalation of organic molecules in the structure of the montmorillonites by cation exchange reactions.

III) Sites of variable charge

These sites originate in the defects (broken edges, folds or holes) that naturally occur in the sheets T: O: T (ideally infinite), leaving the Si-OH and Al-OH groups exposed, that contribute to the hydrophilicity of montmorillonites. At pH values lower than the $\text{pH}^1_{\text{PZC, edge}}$, positively charged groups prevail at the edges which favours their interaction with organic acids or oxyanions. At pH greater than the $\text{pH}_{\text{PZC, edge}}$, neutral and negative charges prevail, with which the interaction

¹ $\text{pH}_{\text{PZC, edge}}$ is the pH at which the net charge of the edges is neutral.

will be favoured with neutral and cationic species. However, the total contribution of these sites to the overall reactivity of montmorillonites is not of great importance since they represent only 1% of the total surface area.

IV) Interlaminar metal cations and their hydration spheres

The metal cations present in the sites of permanent charge of montmorillonite can act as active sites, binding to organic compounds directly or through hydrogen bonds of their hydration spheres. The type of union is determined mainly by the hardness or softness of the cations. For example, it was observed that aliphatic and aromatic amines coordinate directly with soft cations such as Zn^{+2} , Cd^{+2} , Cu^{+2} and Ag^{+} , while forming hydrogen bridges with hard cations (alkali, alkaline-earth and Al^{+3} ions) in the interlayer, although these last are not stable complexes in solution. In addition, the development of electrostatic interactions between the interlaminar cation and a polar organic molecule is possible.

2.4 ORGANO-MONTMORILLONITE

An organo-montmorillonite is a modified montmorillonite in which the interlaminar inorganic cations (with their hydration spheres) have been replaced by organic cations, made possible because of the cation exchange capacity that this kind of materials present. Different types of organic compounds have been investigated in the production of organo-clays: non-ionic surfactants such as linear ethoxylated alcohols, crown ethers, aromatic systems such as imidazole and quinolines salts, alkyl phosphonic salts, aniline salts, etc., but the salts of quaternary alkylammonium are undoubtedly the most used. These compounds are cationic surfactants that are synthesized by the alkylation of amines.

Among all clay minerals, smectites and especially montmorillonites have been extensively researched in the preparation of organo-clays due to their excellent properties such as large surface area, cation exchange capacity and swelling. Depending on the charge of the layers in montmorillonites (density of interlaminar cations and consequent packing of the alkylammonium cations), the length of the alkyl chains of the surfactant, and their percentage exchanged, the hydrocarbon chains adopt different arrangements between the sheets. These are conformations in which the chains are located parallel to the sheets, either forming mono- or bilayers; or tilted with respect to these, forming pseudo-trilayer or paraffinic structures. In particular, the pseudo-trilayer conformation is energetically unstable due to the electrostatic repulsion between the charged heads and that is why the chains adopt paraffin type arrangements. In addition, the paraffin-type arrangement allows the ammonium groups to better adjust to sites of permanent charge. [35]

Figure 2.8 shows the different possible configurations.

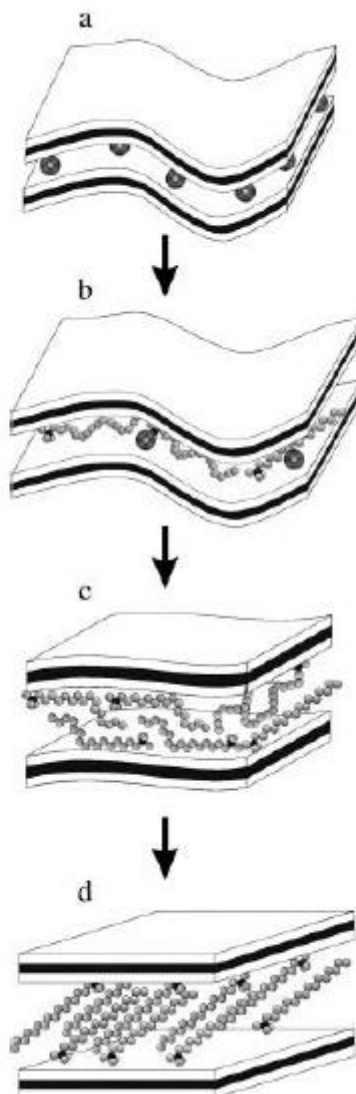


Figure 2.8. Scheme of curved sheets of montmorillonites transforming into flat sheets with the addition of surfactant and packing of the alkyl chains in the interlayer: (a) Na-montmorillonite, (b) monolayer arrangement, (c) pseudo-trilayer (d) paraffin arrangement.[35]

The adsorption of organic molecules on the surface of montmorillonite generates the appearance of new hydrophobic active sites in the clay, which makes them more likely to present a subsequent adsorption of non-polar organic molecules. In particular, the incorporation of organic compounds and their arrangement in the interlayer can be inferred by XRD from the position of the d_{001} peak in the diffractograms; the union of organic cations on the external surface and edges of the clay can be known by zeta potential curves as a function of pH; the interaction of organic matter with the active sites of montmorillonite, as well as the organic content in the sample, can be estimated from thermal analysis techniques. [35]

2.4.1 GELATION IN ORGANO-MONTMORILLONITE

Organophilicity and the ability for swelling and thixotropic gel formation in organic media are properties of great importance of organo-montmorillonites (OM) with long alkyl chains, in particular those with alkylammonium ions. [36]

Typically, organophilic clays are easily wetted by most organic solvents showing widely differing gelling ability depending on the nature of the organic solvent (polar, non-polar, protic or aprotic). Several studies have shown that polar activators such as MeOH, EtOH, Me₂CO or propylene carbonate can enter the interlayer, adsorb on the silicate surfaces and begin the expansion process. Polar activators also contribute to the gel structure by linking the dispersed clay particles edge-to-edge in a hydrogen-bonding matrix. [37] Numerous investigations have been carried out to study the mechanism for swelling and gel-formation of organic modified clays, in organic media.

For example, Burba & McAtee (1981) have shown that glycol can lift the aliphatic chain and increase the basal spacing in certain clays. It is commonly observed that the gelling ability of an organophilic clay is very sensitive to the amine/clay ratio. Figure 2.9 displays the apparent viscosity of a hydrocarbon gel in function of this ratio.

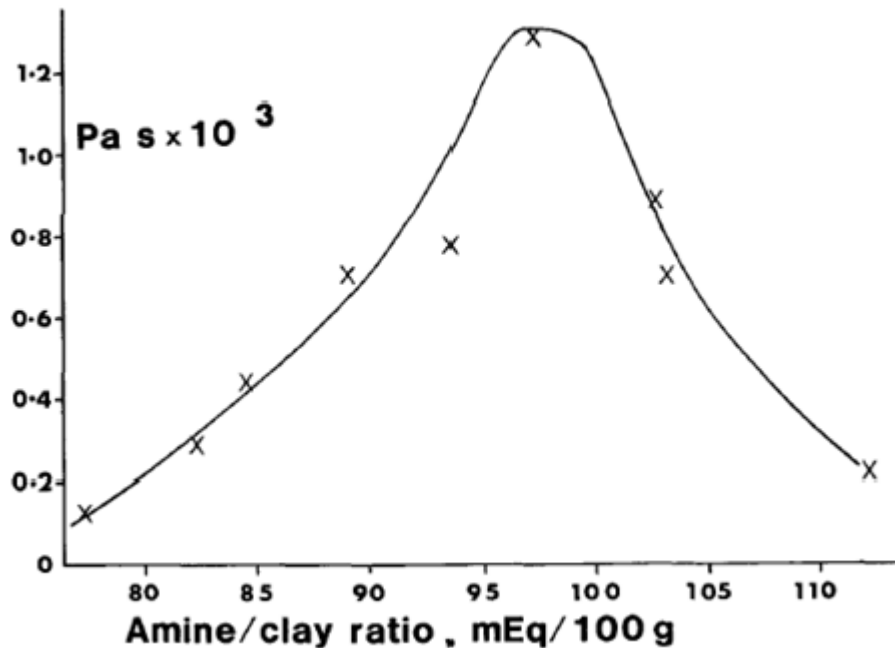


Figure 2.9. Effect of amine/clay ratio on the viscosity of organophilic clay dispersions in light mineral oil (93.33 wt% light mineral oil, 1.67 wt% propylene carbonate, 5 wt% organophilic clay). [37]

Some experimental studies have shown that optimal gel strength of octadecyl benzyldimethylammonium montmorillonite (OBDM) in organic media is obtained at complete saturation of the exchange sites by alkylammonium ions, being gel formation more effective with increasing basal spacing in montmorillonite. Gel formation is also stronger when the alkyl chains contain double bonds or aromatic groups and depends on the Physico-chemical properties of the solvents. The increase of polarity of the solvent conduces to increasing liquid-solid interaction and electrostatic repulsion between particles, which favour peptization. [36]

Chapter 3: Synthesis and characterization of clay/polymer nanocomposites

3.1 SYNTHESIS OF CLAY/POLYMER NANOCOMPOSITE MATERIALS

Nanocomposite materials prepared by intercalation and insertion of organic guests into inorganic hosts, result in organic/inorganic components combined at a nanoscale which display novel properties that are not possible from either component separately. A variety of insertion and polymerization methods have been used to synthesize different lamellar nanocomposites where different kinds of polymers (e.g., polypyrrol, polyaniline and polyethylene oxide), are intercalated in between the layers of the host material (e.g., V_2O_5 , MoO_3 , chlorides, oxychlorides, phosphates and clays). The slabs of the inorganic host serve as a template where an in-situ polymerization occurs in the confined environment in between the layers, conducting to the formation of a relatively ordered polymer chain structure. [38]

Polyaniline (PANI) is a unique conductive polymer because of its low density, high conductivity, easy preparation and physical/chemical properties. However, PANI prepared in the absence of a support is not always easy to process because of its amorphous or poor crystalline nature and its insolubility in common solvents, which hinders a uniform casting. PANI could be grown inside a structurally organized host, obtaining oriented polymer chains, by means of an in-situ chemical oxidation.

In this thesis work, an Argentinian montmorillonite (MMT) was used as a layered host to in-situ polymerize aniline in the lamellar space obtaining polyaniline-montmorillonite nanocomposites. MMT was used as the inorganic matrix because of the following main features:

- large surface area due to its colloidal size (nanometres) that allows hosting a great number of chemical species.
- its permanent negative charge which can stabilize positively charged interlamellar species, making it an ideal host for PANI in the emeraldine state (protonated).
- its great cation exchange capacity (80-100 mmol/100g) which allows a surface modification of the material by incorporating specific functional groups, facilitates the cations uptake by selective cation exchange reactions, and promotes hydrophobicity in the mineral surface.
- a variable and flexible interlayer spacing, which allows the interlamellar incorporation of bulky molecules with different modes of aggregation.
- the presence of multiple active sites that can participate in a wide variety of reactions with organic compounds.
- good mechanical and thermal properties.
- its wettability and permeability to polar solvents.

The proposed polymerization mechanism found in the literature is shown in Figure 3.1 and described as [38]:

- First, a bilayer of aniline monomers is inserted in between the layers of the montmorillonite host.
- Because of the limited space in the interlamellar environment, the chemical oxidant cannot effectively enter and diffuse into the interlayers. In consequence, only a few radicals are produced at the edge of the monomer/clay composite particles and the polymerization initiates from the outer to the inner of the interlamellar in the monomer composites.
- Aniline reacts with the chemical oxidant and the polymerization starts with the formation of an anilinium cation radical (electrophilic) which reacts with another nucleophilic monomer to form a dimer radical.
- The chain growth reaction continues within the interlayers until a high molecular weight polymer is obtained.
- Reorientation and/or extrusion of aniline oligomers during the chain growth, conduces to a deintercalation of a portion of aniline which results in a single layer of PANI chains within the interlamellar space. The deintercalated monomers can be oxidized in the solution forming soluble oligomers or anilinium ions.
- A small portion of this monomers participate in the polymerization between adjacent nanocomposite particles, creating chain bridges and aggregation of nanocomposite microcrystals which enhance the electrochemical properties.

Depending on the monomer/clay ratio, different kinds of structural configurations may be obtained. Two extreme possibilities are: intercalated nanocomposites where the polymer chains are in between the tactoids layers with a regular repeating distance (Figure 3.2 (1)) and exfoliated nanocomposites where clay crystallites are delaminated constituting individual layers dispersed in a polymer matrix (Figure 3.2 (4)). In the middle, intermediate configurations are possible (Figure 3.2 (2) and (3)). [39]

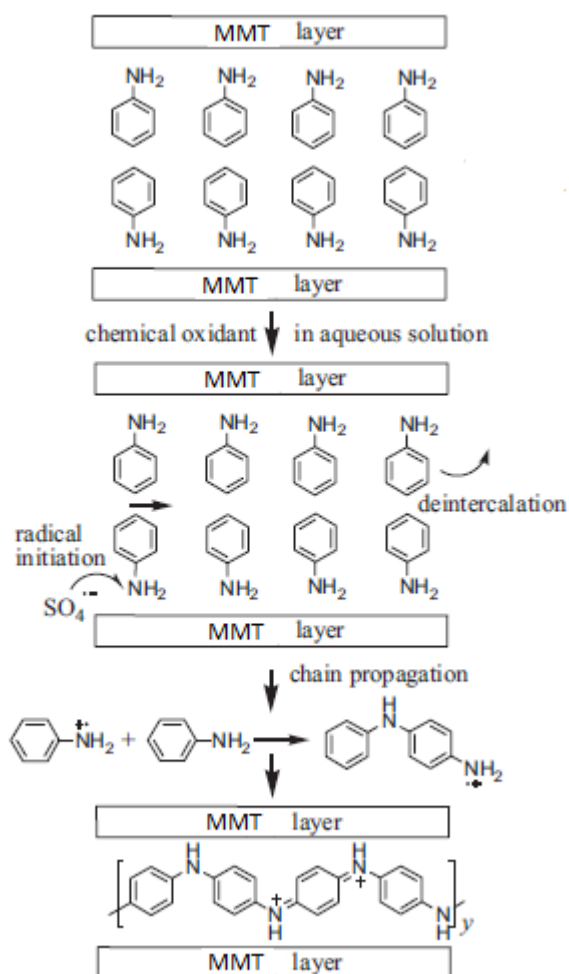


Figure 3.1. Proposed mechanism for the polymerization of aniline between the layered host. [38]

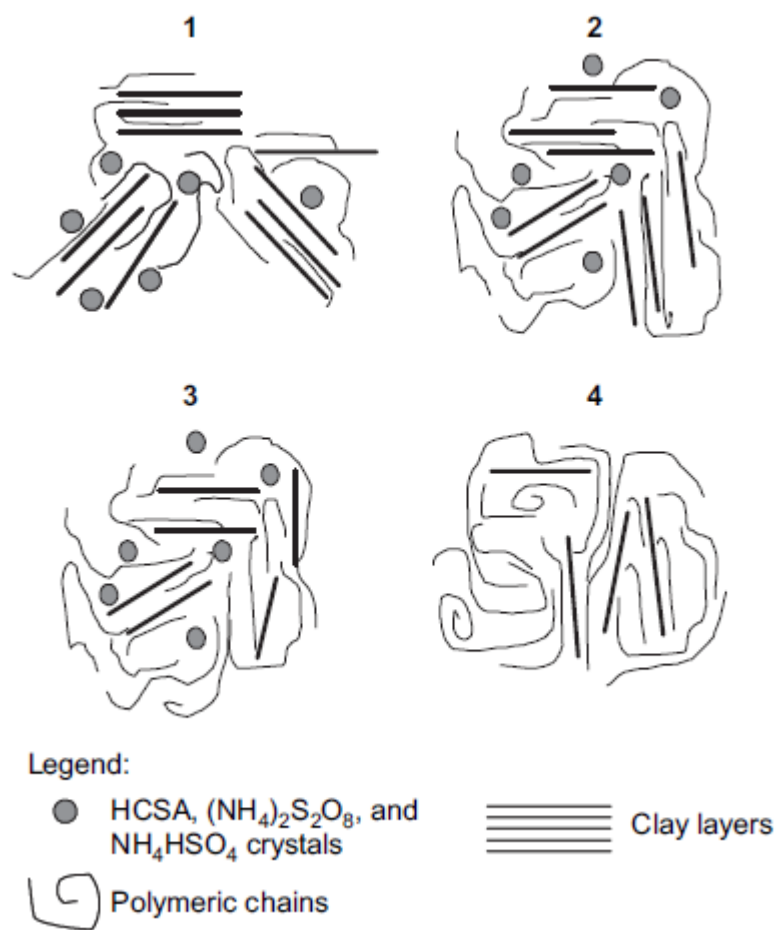
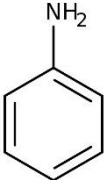


Figure 3.2. Schematic representation of possible domains of PANI/MMT composites based on SEM, XRD, and Silicon K-edge XANES data. [39]

In this work, two samples were prepared with the objective of obtaining both intercalated and exfoliated PANI/MMT nanocomposites. One sample with a higher percentage of polyaniline corresponding to configuration 4 in figure 3.2, and another with a higher percentage of MMT corresponding to configuration 1 or 2 in figure 3.2. The materials used are displayed in Table 3.1.

Table 3.1.

Materials	Chemical structure and/or formula	Observations
Aniline		aniline 99.5% used as purchased from SIGMA-ALDRICH®
Montmorillonite	$(M_y^+ \times nH_2O) (Al_{2-y}^{3+}, Mg_y^{2+}) Si_4^{4+} O_{10}(OH)_2$	brought from Argentina
Sulfuric Acid	H_2SO_4	sulfuric acid 95-97% used as purchased from SIGMA-ALDRICH®
Ammonium peroxydisulfate	$(NH_4)_2S_2O_8$	prepared solution

The synthesis procedure was the following:

- A monomer solution was prepared: [Aniline] = 0,2 M; [H₂SO₄] = 0,5 M.
- A suspension of montmorillonite was prepared and kept 0,5 hours under sonication to favour the delamination
- The monomer solution was slowly added to the montmorillonite suspension keeping constant stirring.
- The obtained suspension was sonicated for 0,5 h, since the formed organoclay was agglomerated, and then stirred for another 4 h.
- The monomer composites were chemically treated with (NH₄)₂S₂O₈ (PSA) 1M, which was added drop by drop, until the colour of the samples turned to dark green. The reaction was kept overnight stirring.
- The obtained precipitates were filtered, washed with distilled water several times until neutral pH was achieved, and dried at 60 °C.

The monomer, clay and PSA amount used in each case are shown in Table 3.2 while the obtained samples after filtration and drying can be seen in Figure 3.3.

Table 3.2.

Sample	Monomer amount (mmol)	Clay mass (mg)	PSA amount (mmol)	Final suspension volume (mL)
PANI_MMT_PSA_2-100-1	21	100	21	100
PANI_MMT_PSA_200-1-1	2.1	1000	2.1	250



Figure 3.3.

3.2 CHARACTERIZATION TECHNIQUES AND RESULTS

3.2.1 POWDER X-RAY DIFFRACTION (XRD)

X-ray diffraction is a bulk analytical technique that is used mainly for the quantification of crystalline solids and for the determination of lattice parameters, space group, crystallite size, degree of crystallinity, residual stress, etc. The technique is based on the wave-particle duality of the X-rays, which wavelength is similar to the inter-layer spacing (d spacing) of the atomic layers in crystalline solids. In certain circumstances X-rays are diffracted by the crystal lattices of the material undergoing constructive and destructive interferences that provide information about the arrangement of the atoms in the crystal lattice (Figure 3.4). The equipment is constituted by a

monochromatic source of X-rays (a metallic plate that is bombarded with electrons and emits in a certain wavelength according to the nature of the metal), and a detector (photomultiplier) that catches the diffracted rays. [40]

The diffraction of X-rays by crystalline solids is determined by Bragg's law:

$$2d \sin \theta = n \lambda \quad (3.1)$$

Where d is interplanar spacing, θ is the angle between incident X-ray beam and the plane of atoms, λ is the wavelength of the incident rays, and n is the order of reflectance (the wavelength path difference between consecutive reflecting sheets). The scattered X-rays result in constructive interference only when Bragg's law is satisfied.

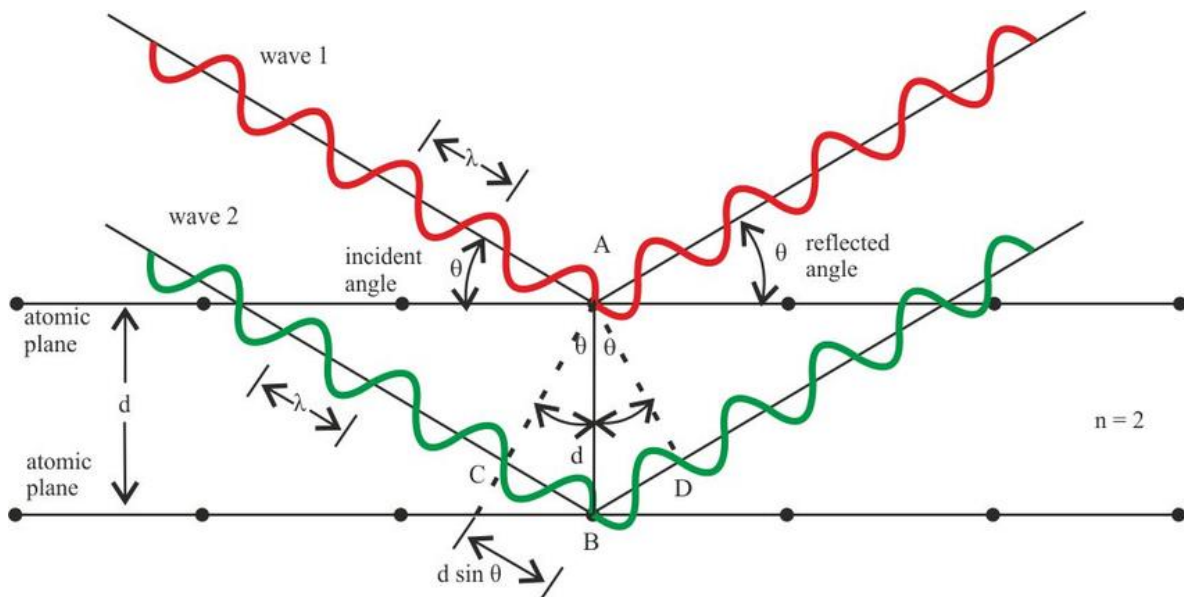


Figure 3.4. X-ray diffraction from crystal lattice.

In a single crystal, X-rays are diffracted in different possible directions depending on the size and shape of the unit cell of the material. The arrangement of atoms and their atomic number, in a particular plane, determine the intensity of the diffracted wave. Most solids, however, are constituted by numerous tiny crystallites randomly arranged so, all possible interatomic planes are met by the beam where a certain number of crystals, for each set of planes, are oriented at an angle that satisfies Bragg's law (Figure 3.5). A detector records the peak positions and intensities of the diffracted beams and the resultant diffraction pattern is presented as a plot of the intensity of diffracted X-rays versus 2θ (degrees). [40]

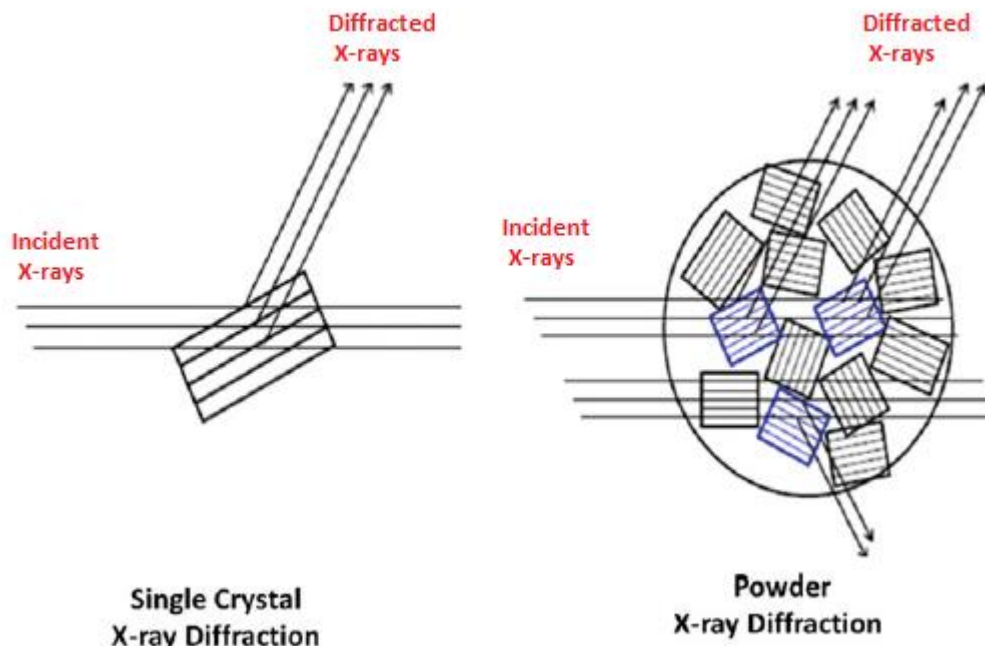


Figure 3.5. X-ray diffraction from a single crystalline sample and a polycrystalline sample.[40]

In a typical diffractogram peak shapes and widths give information about the average size of the crystals (by measuring the width of the peak at mid-height) and the deviations from a perfect crystal. [40]

As it was described in section 2.3, the degree of expansion and swelling of the interlamellar space in montmorillonite can be studied by XRD analysis following the shift of the basal reflection (d001). The interlayer spaces thicknesses of the clay/polymer composites can be determined from the difference between the interlayer distance calculated from Bragg's equation corresponding to the d001 peak and that of dehydrated MMT (9.7 Å).

Powder X-ray diffraction technique was performed at the Department of Applied Science and Technology (DISAT) - Politecnico di Torino, for each sample as well as for bare MMT, to verify the presence of polyaniline in between the MMT sheets.

3.2.1.1 RESULTS

As it can be seen in Figure 3.6, in both composite samples the peak shifted to a lower angle (2θ) with respect to that of raw MMT sample. The calculated interlayer spaces for each composite are 4 and 4.5 Å for PANI_MMT_PSA_2-100-1 and PANI_MMT_PSA_200-1-1, respectively. An increase in the basal spacing of MMT was observed, suggesting that PANI was intercalated in the clay/polymer composites (nevertheless PANI chains should also be outside clay galleries). Following Yang2017 [38], the interlayer distances obtained corresponded to a single layer of PANI chains with the aromatic rings of PANI molecule almost parallel to MMT planes. Peaks d010, d100 and d110 were assigned to polyaniline. As it was described in section 2.2.2, X-ray diffraction studies reveal that polyaniline is a semi crystalline polymer, characteristic reflections are usually observed but with low

intensity and wide width that indicate that PANI is a polymer not completely amorphous but very little crystalline. It can be seen from Figure 3.6 that the presence of polyaniline decreases the crystallinity degree of the composites, especially evident in the composite with the highest amount of PANI.

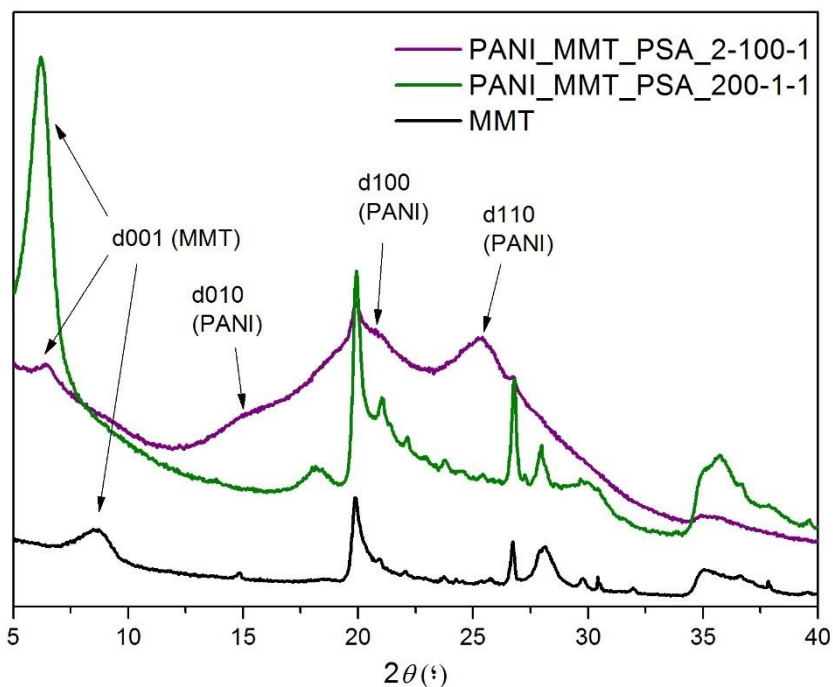


Figure 3.6. XRD Spectra obtained for the clay/polymer nanocomposite samples and pure MMT.

3.2.2 X-RAY PHOTOELECTRON SPECTROSCOPY (XPS)

XPS is a surface analysis technique that provides quantitative and chemical state information of the surface of the material in study. This technique not only allows the identification of the elements on the surface of the material, but also gives information about the chemical state of the elements (oxidation state and chemical surrounding).

In principle, the surface of the sample is excited with mono-energetic Al $K\alpha$ x-rays causing photoelectrons to be emitted from the sample surface. An electron energy analyser is used to measure the energy of the emitted photoelectrons (Figure 3.7). From the binding energy and intensity of a photoelectron peak, the elemental identity, chemical state, and quantity of a detected element can be determined. These rays, however, have such an energy that allows them to penetrate no more than a few atomic layers of the surface permitting, therefore, to derive only the information regarding the very first superficial layers of the sample. As the beam interacts with the

surface atoms, these expel electrons that are collected by a detector which measures their kinetic energy. Through formula 3.2 the binding energy can be derived. [41]

$$E_b = h \nu - E_k \quad (3.2)$$

Where E_b (binding energy) is the minimum energy required to remove a delocalised electron from the surface of the material, ν is the photon frequency, h is Plank's constant (6.626×10^{-34} J.s), and E_k is the kinetic energy measured by the detector.

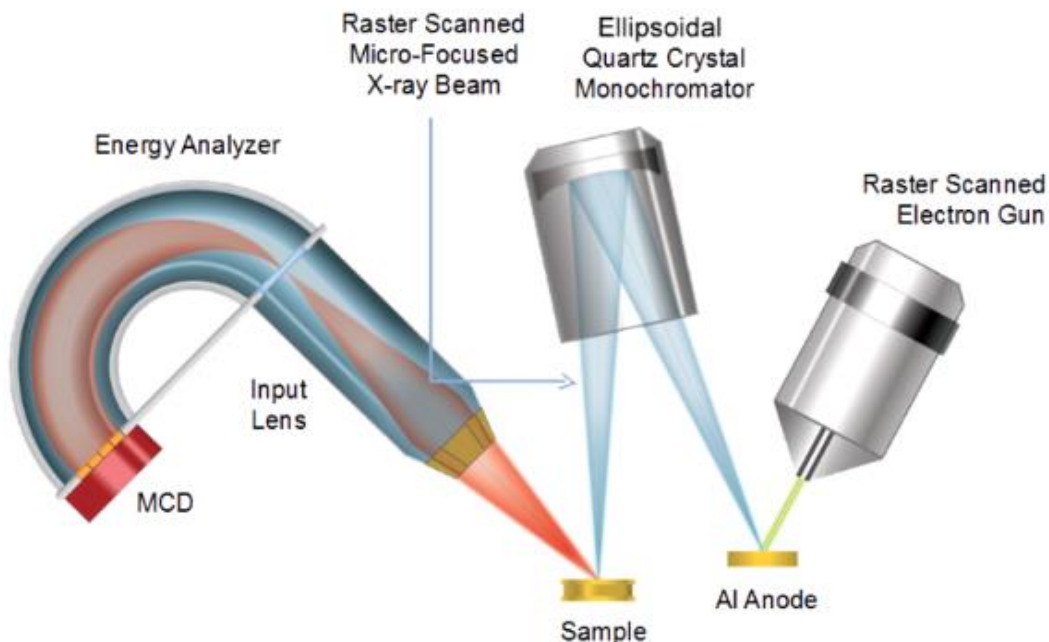


Figure 3.7. XPS instrument. [41]

X-ray photoelectron spectroscopy is a useful tool for determining and quantifying the different redox states of PANI as well as the degree of protonation. As it was explained in detail in section 2.2, the general formula of polyaniline can be written as $[(-B-NH-B-NH-)_y(-B-N=Q=N-)_x]_{1-y}$, where B and Q refer to the C_6H_4 rings in the benzenoid and quinoid forms respectively. The oxidation state of polyaniline can be estimated by: $y = 0$ in the pernigraniline state (fully oxidized), $y = 0.25$ in the nigraniline state ((intermediate oxidation state between the completely oxidized form and the emeraldine conductive form), $y = 0.5$ in the emeraldine state (50% oxidized), $y = 0.75$ in the protoemeraldine form (intermediate oxidation state between the completely reduced form and the emeraldine conductive form), and $y = 1$ in the leucoemeraldine form (fully reduced). [42]

Figure 3.8 shows the XPS spectra of different oxidation states of PANI. In the fully reduced state (leucoemeraldine, LM) the peak at about 399.4 eV evidences the presence of a single nitrogen environment, whereas equal proportions of imine and amine N 1s components can be seen in the emeraldine (EM) state and an imine to amine component ratio of about 3 to 1 in the nigraniline

(NA) form. When the EM base is protonated with H_2SO_4 1M, the peak correspondent to the imine nitrogen atoms disappears, and appears a corresponding amount of positively charged nitrogen atoms. [43] This is consistence with the assumption that imine nitrogen atoms are preferentially protonated with a $\text{pK}_a = 2.5$, in contrast with the amine nitrogen ($\text{pK}_a = 5.5$) which result protonated only in highly acidic solutions. [42]

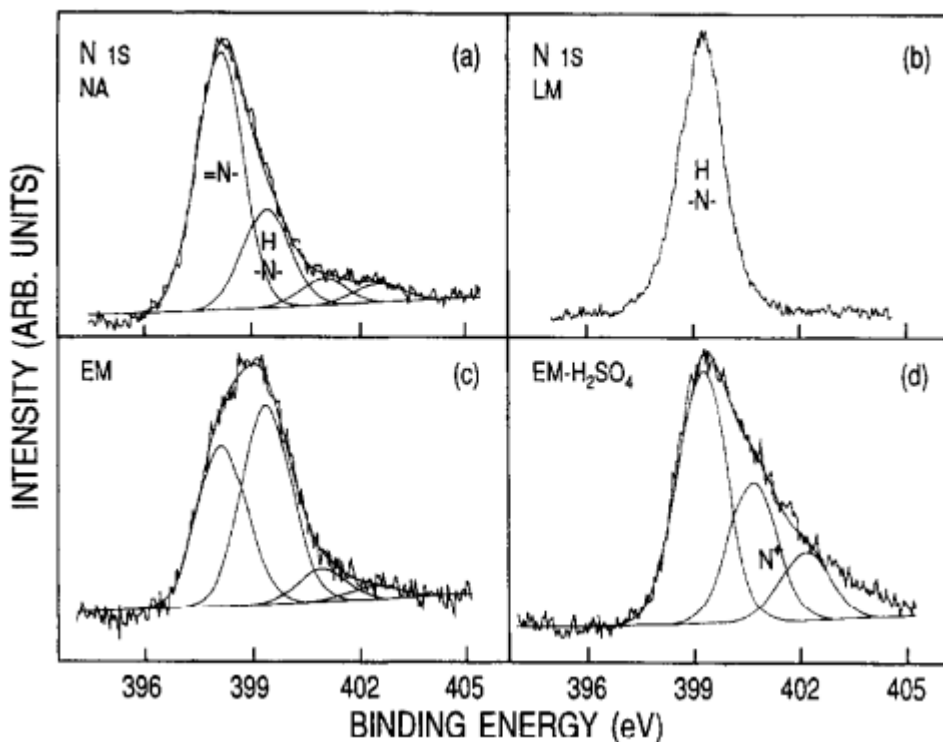


Figure 3.8. N 1s XPS spectra of (a) NA, (b) EM, (c) LM and (d) 1 M H_2SO_4 EM films. [43]

XPS spectra were measured by Y-TEC (YPF TECNOLOGIA) in Argentina, in the frame of the project: 'Escalado del proceso de producción de LiFePO_4/C '. This technique was used to have further information about the oxidation state of the polyaniline present in the composites, as well as the ratio PANI/MMT.

3.2.2.1 RESULTS

The survey spectra of the samples are shown in Figure 3.9. It can be seen that for the samples MMT and PANI_MMT_PSA_200-1-1 the majority surface elements are O, Si, C and in smaller quantities are detected : Al , Na ($\sim 498\text{eV}$, yellow dot in Figure 3.9), and Mg ($\sim 306\text{ eV}$, pink dot in Figure 3.9). For sample PANI_MMT_PSA_2-100-1 the majority surface elements are O, C, N and in smaller amount S (present in PSA, oxidizing agent, and counterion HSO_4^- , doping agent, used in the synthesis). In this last case the typical clay signals (Si, and metals Na, Mg, Al) are not observed.

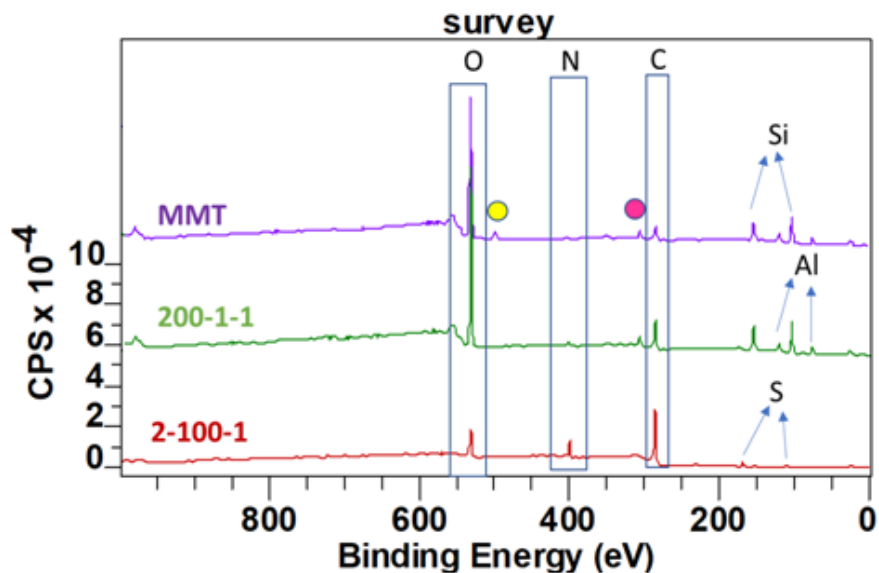


Figure 3.9. Survey spectrum of the samples: bare MMT, PANI_MMT_PSA_200-1-1 and PANI_MMT_PSA_2-100-1.

The Si 2p and N 1s spectra were measured in order to determine the N:Si ratio and identify and quantify the N species present. Figure 3.10 shows the Si 2p and Al 2p spectra measured for the samples and in Figure 3.11 the N1s spectra can be seen. From the relative areas of these signals the N:Si ratios were determined for each sample (Table 3.3). In the case of Figure 3.12 also the deconvolutions corresponding to the nitrogen species present are shown, according to the values of Binding Energy (Eb) with an error of $\pm 0.1\text{eV}$: amine -NH- Eb = 399.5 eV; amine radical and/or protonated -N +, -NH₂ + - Eb = 401.2 eV; imine protonated -NH + = Eb = 402.9 eV. [39]

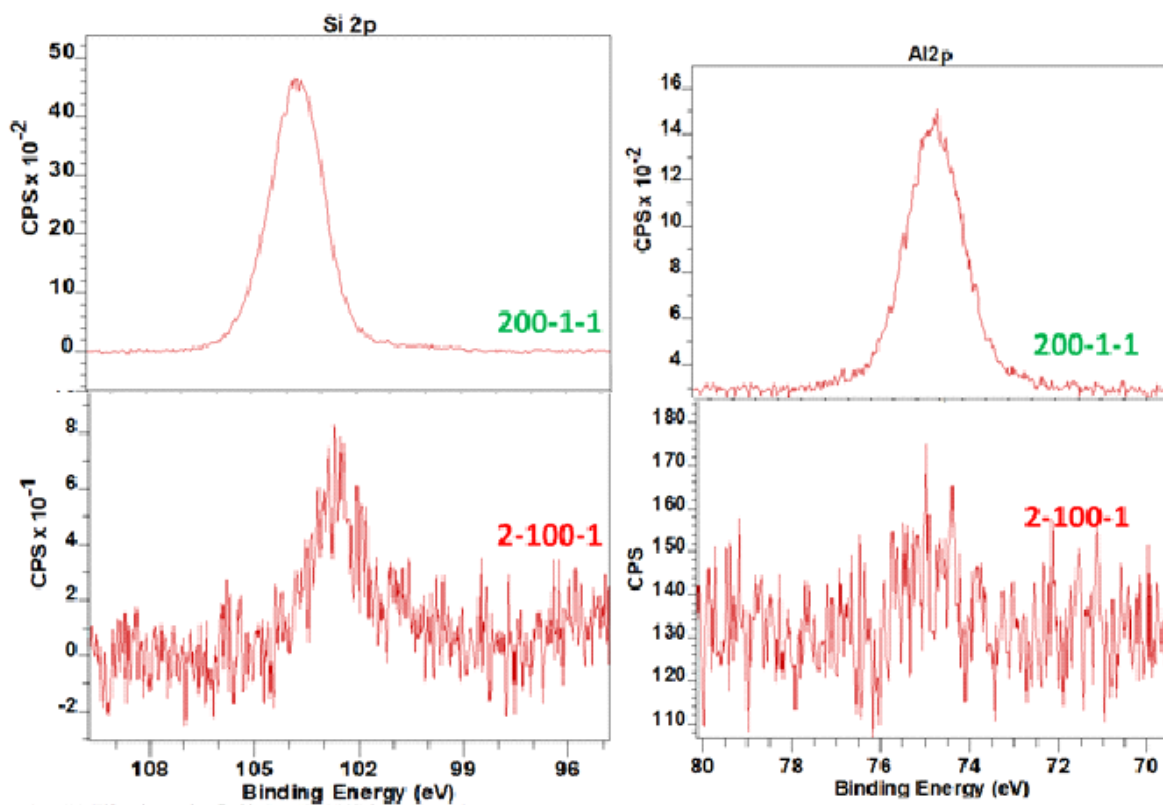


Figure 3.10. XPS Spectra of Si 2p (left) and Al 2p (right) measured for samples PANI_MMT_PSA_200-1-1 and PANI_MMT_PSA_2-100-1.

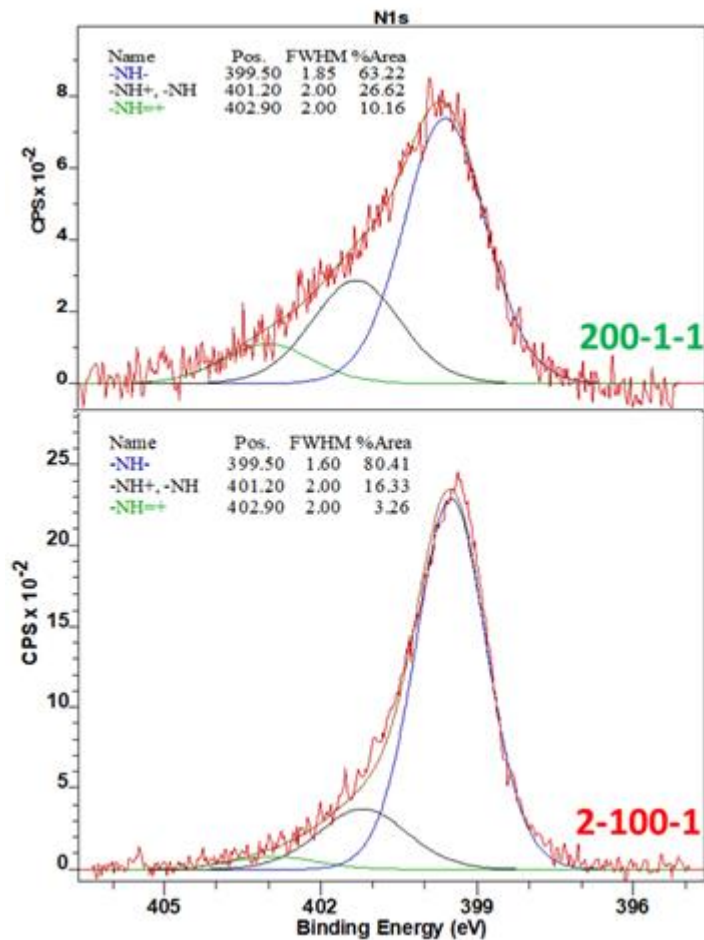


Figure 3.11. N1s XPS spectra measured for samples PANI_MMT_PSA_200-1-1 and PANI_MMT_PSA_2-100-1.

Table 3.3. Relative percentages of N and Si species, and ratio N/Si of samples.

Sample	%N	%Si	N/Si
PANI_MMT_PSA_2-100-1	92.2	7.8	11.82
PANI_MMT_PSA_200-1-1	11.1	88.9	0.125

Since nitrogen atoms come from PANI and Si atoms come from siloxane layers of MMT, the ratio N/Si reflects the ratio PANI/MMT.

Table 3.4 shows the deconvolution results of the N 1s spectra according to the nitrogen species present. Labels "Ra" refer to the relative areas of the species for the signal analysed.

Table 3.4. Relative percentages of N species for samples PANI_MMT_PSA_200-1-1 and PANI_MMT_PSA_2-100-1:

		Samples	
		200-1-1	2-100-1
Eb(eV)	Species	%Ra	%Ra
399.5	-NH-	63.22	80.41
401.2	-N ⁺ =, -NH ₂ ⁺ -	26.62	16.33
402.9	-NH ⁺ =	10.16	3.26
(-B-NH-B-NH-) _y		0.63	0.80
doping level (N ⁺ /N)		36.78	19.59

It is detected that in the sample PANI_MMT_200-1-1 the oxidation state ($y = 0.63$) is close to the one of the emeraldine state ($y = 0.5$) while for the sample with a higher ratio polymer/clay, the oxidation state is closer to the one of the protoemeraldine state ($y = 0.75$) meaning that the oxidation time or the quantity of oxidant (PSA) was not enough to obtain the 50 % oxidation state of the emeraldine form. However, it is known that XPS is a surface technique and most of the information comes from the first three atomic monolayers of the particle, meaning that only polymeric chains on the external surfaces or on the edge of MMT crystal, contribute to the XPS N1s signal of the composites.

3.2.3 FOURIER TRANSFORM INFRARED SPECTROSCOPY (FTIR)

FTIR is an analytical technique that uses infrared light to scan test samples and identify chemical properties. The chemical composition and the bonding arrangement of constituents in the material can be obtained.

FTIR permits to determine components or groups of atoms that absorb in the infrared spectrum at specific frequencies, allowing to identify the molecular structure. The instrument sends infrared radiation through a sample where the absorbed radiation is converted into rotational and/or vibrational energy by the molecules. Infrared radiation is absorbed when a dipole naturally vibrates at the same frequency in the absorber. The resulting signal at the detector presents a pattern of vibrations that is unique for a given molecule or chemical structure, representing a molecular fingerprint of the sample. [45], [46]

The IR spectrum is generated by the spectrometer by Fourier transformation of the signal from an interferometer with a moving mirror that produces an optical transform of the infrared signal. The relation between intensity and frequency, is then obtained by Numerical Fourier analysis. The spectrometer may operate in transmission or reflectance. ATR (Attenuated Total Reflectance) technique involves a phenomenon of internal reflectance to propagate the incident energy (Figure 3.12). IR reflectance is attenuated by absorption within a surface layer, having a penetration depth of a few micrometres.

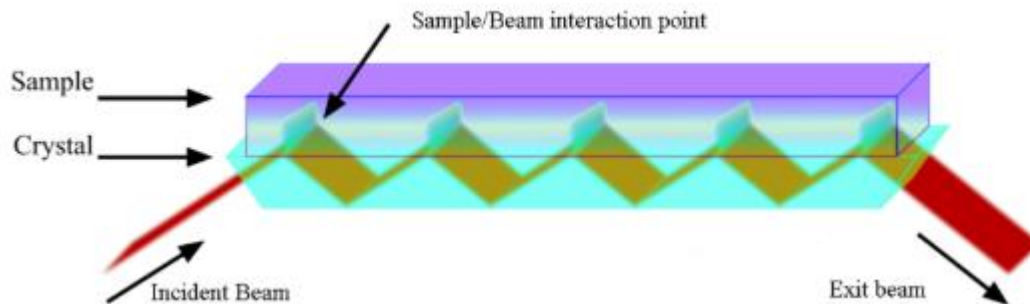


Figure 3.12. Interaction of the infrared beam with the sample when by ATR. [45]

The different states of polyaniline can be distinguished through IR spectroscopy. Although most of the vibrational modes are conserved in all the possible forms of PANI (since the "skeleton" of the main chain is maintained), displacements in the absorption frequencies of these modes are observed due to the different forces, distances and linking angles that each state presents.

In the emeraldine state a phenomenon called the "Fano effect" can be seen in the IR spectra in the asymmetric form of the absorption bands (Figure 3.13). The effect results as a consequence of an overlapping in space and energy of two types of photon absorption: a discrete absorption (centred in a certain frequency, in this case it appears as an IR band) and a continuous absorption (an electronic absorption which covers a longer wavelength interval, in the case of PANI-ES is due to the continuous of electronic states of polaron type and appears as an absorption tail in the UV-Vis spectra towards the NIR-IR). This particularity is represented by a "band interference" that results in a displacement of the maximum of the discrete absorption and on the other hand, in an intensity increase of the discrete band and a localized intensity reduction of the continuous absorption. Therefore, the affected bands of the spectrum have a stepped appearance. The effect is especially pronounced when the PANI-ES has a high conductivity, because it is when the absorption due to the continuum of electronic states is more evident. [22]

Fourier Transform Infrared Spectroscopy (FTIR) was performed at the Department of Applied Science and Technology (DISAT) - Politecnico di Torino, for both composite samples as well as for bare montmorillonite. This technique was carried out in order to verify the presence of polyaniline in its conductive form (emeraldine salt) and to study the molecular interactions.

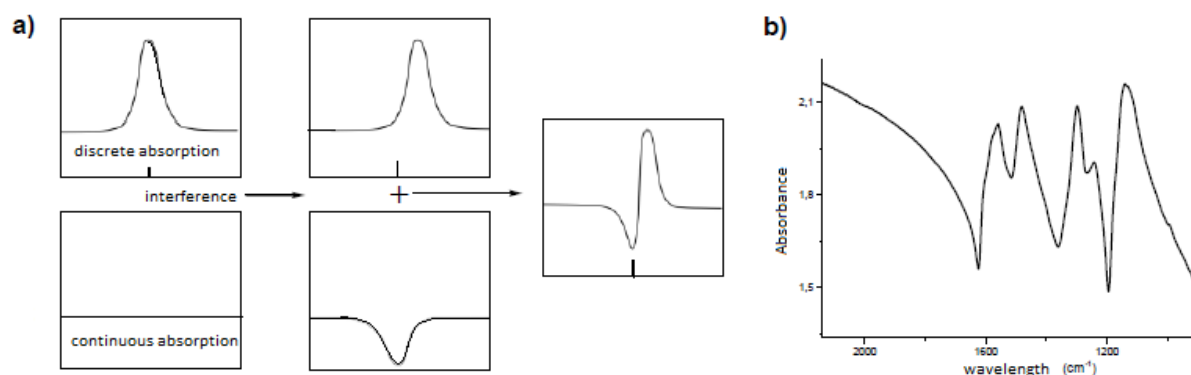


Figure 3.13. (a): Schematic representation of the so-called 'Fano effect' that leads to the appearance of asymmetrical spectral bands. (b): Example of this effect in the IR absorption spectrum of the PANI-ES. [22]

3.2.3.1 RESULTS

Figures 3.14 and 3.15 correspond to the IR spectrum of the samples. The typical 'Fano effect' of PANI can be seen in both composite samples (stronger for the sample with the highest content of polymer), verifying the presence of polyaniline in its conductive form (emeraldine salt). The samples were also compared with the spectrum of pure MMT where for the composite containing the highest amount of clay (PANI_MMT_PSA_200-1-1) also the characteristic peaks of montmorillonite can be identified.

All composite samples present the typical PANI-ES broad absorption band at wavenumbers higher than 2000 cm^{-1} , correspondent to free-charge carrier absorption in the doped polymer. Peaks at $1558 - 1560\text{ cm}^{-1}$ are assigned to quinone-ring stretching deformations, while peaks $1471 - 1488$ correspond to benzene-ring stretching deformations. Bands at $1288 - 1308\text{ cm}^{-1}$ result by p-electron delocalization induced by protonation and bands at $1238 - 1254\text{ cm}^{-1}$ are interpreted as stretching vibration of C-N^+ in the polaron structure. Peaks at $1104 - 1109$ are assigned to vibration mode of the $^+\text{NH}=\text{Q}=\text{NH}^+$ structure formed by protonation. As the content of MMT decreases, the bands associated with water molecules (bounded to inorganic cations) that are in the interlaminar zone in the montmorillonite structure (bands between $3200\text{-}3447\text{ cm}^{-1}$ and $1635\text{-}1613\text{ cm}^{-1}$), diminish their intensity or disappear indicating that the inorganic cations together with their hydration spheres were displaced by the polymer in the space in between sheets. In the sample PANI_MMT_PSA_200-1-1, these peaks appear at 3252 cm^{-1} and 1613 cm^{-1} (as a shoulder) respectively, indicating that possibly not all the inorganic cations have been displaced. [47]

Focusing on the montmorillonite contribution, the main peaks at $988 - 1043\text{ cm}^{-1}$ are attributed to Si-O stretching vibrations. In the sample PANI_MMT_PSA_200-1-1, peaks correspondent to polyaniline are displaced with respect to the other sample. This could be due to the superposition of the polymer spectrum with that of montmorillonite, much more intense in this sample than in the other. In particular, the most important shift is that of the peak at 1109 cm^{-1} to 1156 cm^{-1} in this sample, which indicates the interaction between the N^+ groups in polyaniline and the negative surface of the clay. [48], [49]

The complete assignment of the observed peaks is listed in Table 3.5.

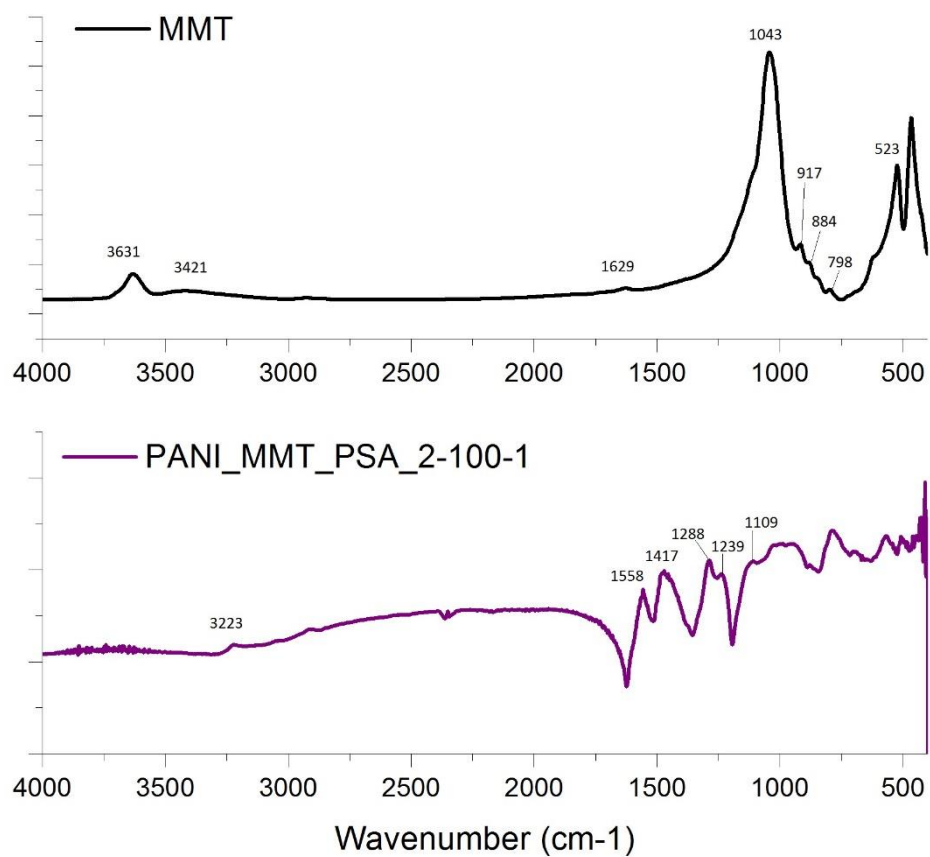


Figure 3.14. IR spectrum of samples PANI_MMT_PSA_2-100-1 and raw MMT.

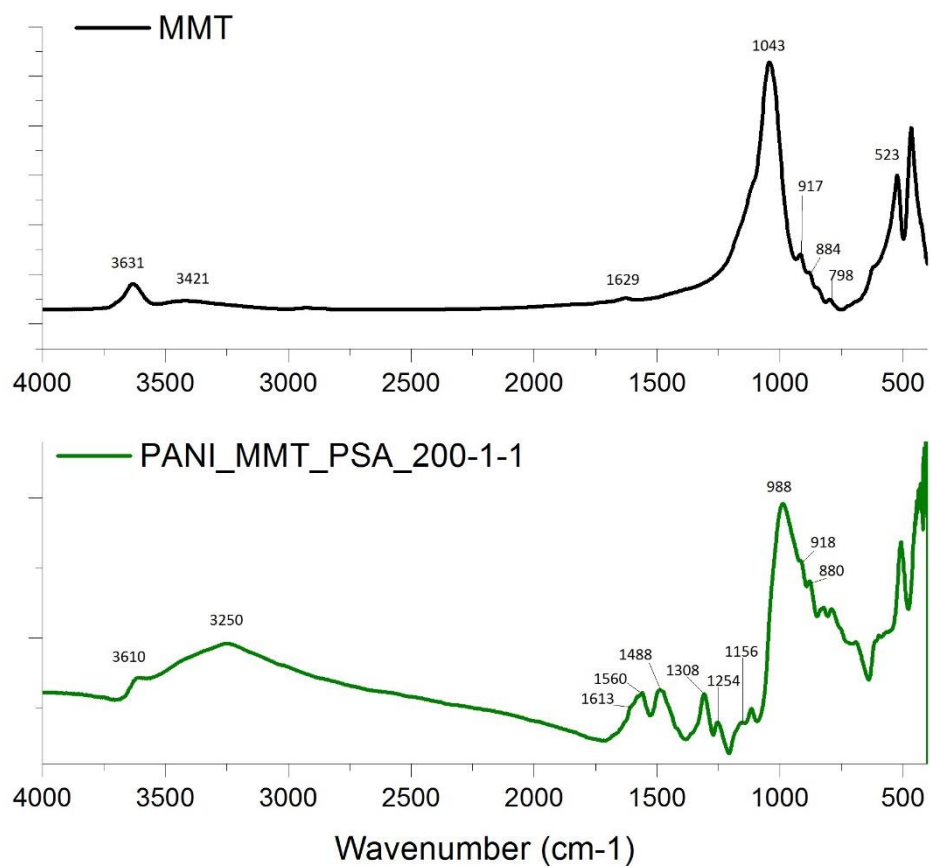


Figure 3.15. IR spectrum of samples PANI_MMT_PSA_200-1-1 and raw MMT.

Table 3.5.

MMT	PANI_MMT_PSA_2-100-1	PANI_MMT_PSA_200-1-1	Assignment
3631		3610	ν (OH) _m
3421	3223	3250	ν (OH) _w
	<2000	<2000	typical PANI-ES broad absorption band
1629		1613 (s)	δ (OH) _w
	1558	1560	ν C=C ar, quinoids
	1471	1488	ν C=C ar, benzenoid
	1288	1308	ν C-N-H
	1239	1254	ν C-N ^{•+} (radical cation)
	1109	1156	⁺ NH=Q=NH ⁺
1043		988	ν Si-O
917		918 (s)	δ AlAlOH
884		880	δ AlFeOH
798			δ Si-O
523			δ Al-O-Si

References: (s) shoulder.

3.2.4 THERMOGRAVIMETRIC ANALYSIS (TGA)

In the TGA analytical technique the mass of the sample is monitored as a function of temperature or time, measuring the variations of weight of the material as a function of increasing temperature or as a function of time (isothermally) in a controlled atmosphere. This technique allows a quantitative composition analysis of the sample, as it determines temperature and weight change of decomposition reactions. It can also be used to determine water content or residual solvents in the material as well as the purity of a mineral, inorganic compound or organic material.

The equipment consists of a sample pan supported by a precision balance inside a furnace with a programmable control of temperature and a purge gas that controls the atmosphere of the sample. The collected data is displayed as a plot of mass, or percentage of initial mass, versus temperature or time. [50]

Thermogravimetric analysis was performed at the Department of Applied Science and Technology (DISAT) - Politecnico di Torino, to determine the proportion in mass of polyaniline and montmorillonite of the clay/polymer nanocomposites.

3.2.4.1 RESULTS

Figures 3.16, 3.17 and 3.18 present the TGA and the first derivative curve (DTGA) obtained in the Thermogravimetric analysis of all the samples. In montmorillonite, the first jump in the TGA curve (between 25 and 200 °C approximately) results from the loss of water molecules that are physically adsorbed and joined to the interlaminar cations. This usually leads to two DTGA peaks: the first, at lower temperatures (88 °C in Figure 3.16) corresponds to the desorption of water molecules weakly bounded to the outer surface or pores of the clay. The second (at 125 °C in Figure 3.16) corresponds to water molecules coordinated to the interlaminar cations, so the temperature at which this process occurs is greater and is conditioned by the chemical nature of the cations. The second stage of mass loss in montmorillonite, theoretically between 400 and 750 °C, corresponds to the loss of structural water, a process called dihydroxylation, which implies the loss of OH groups of structure T: O: T of the clay. [35]

For the composites, additional peaks in the DTGA curves can be seen (schematically between 200 and 550 °C) attributed to the combustion, decomposition, dehydration, vaporization, fusion and / or sublimation of organic matter. It can be noticed that the first peak associated with the desorption of physically adsorbed water moved to lower temperatures in the composites due to the hydrophobicity introduced by the presence of polyaniline. Furthermore, the second small peak (under 200 °C) that was present in the pure MMT sample, disappeared in the composites what confirms the exchange of the hydrated inorganic cations by organic cations (that are not coordinated to water molecules). It is also important to notice that the peak between 200 and 550 °C in DTGA attributed to the decomposition of PANI, appears at a higher temperature for the sample with the highest amount of clay (200-1-1) indicating that the presence of a higher amount of clay increases the thermal stability of the composite.

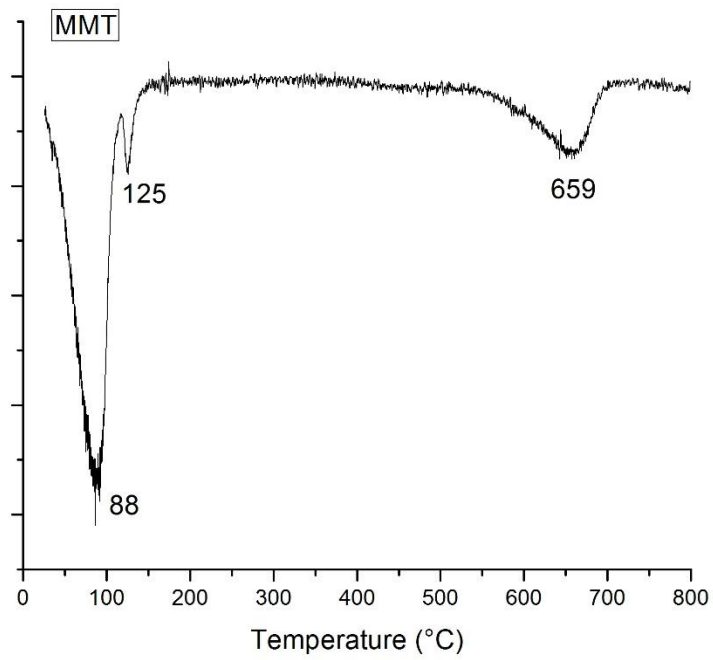
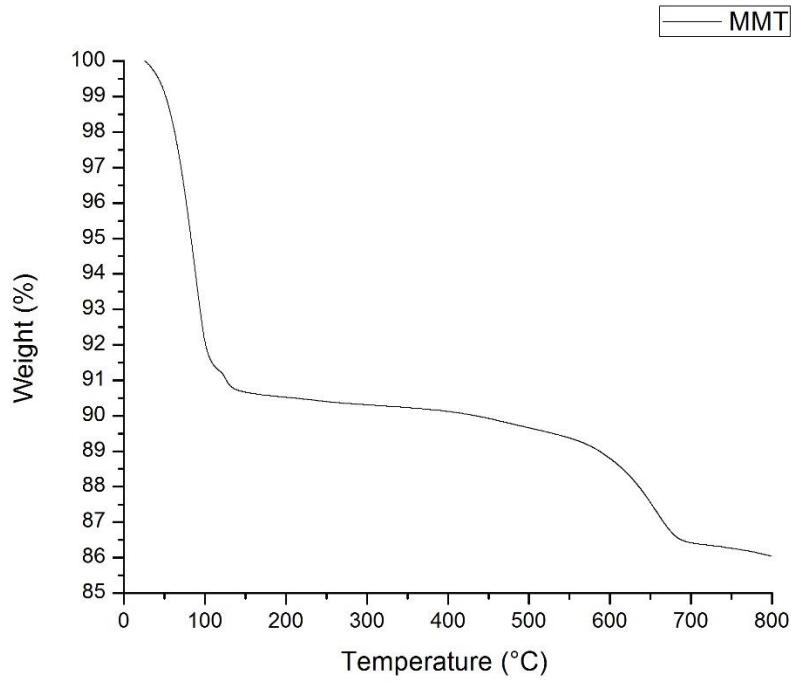


Figure 3.16. TGA and DTGA curves of raw MMT.

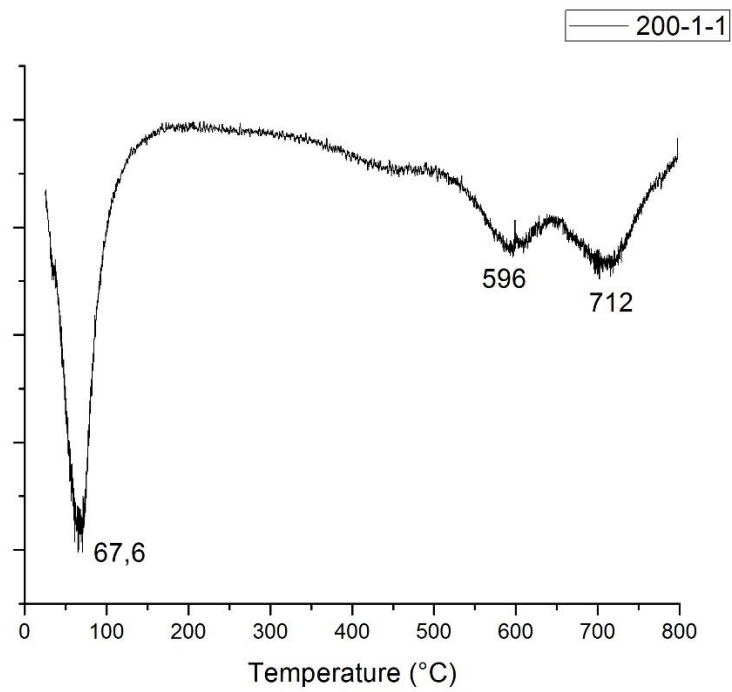
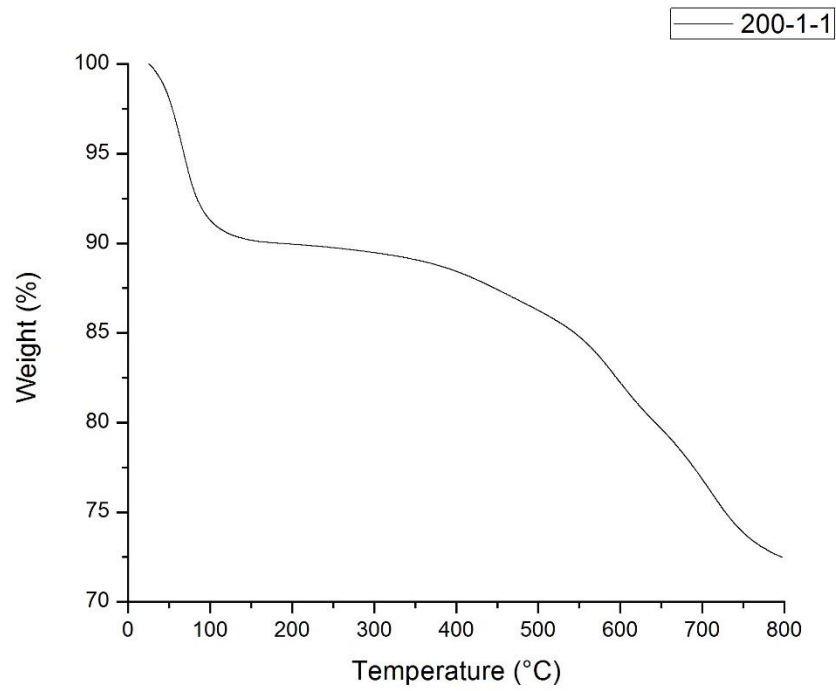


Figure 3.17. TGA and DTGA curves of sample PANI_MMT_PSA_200-1-1.

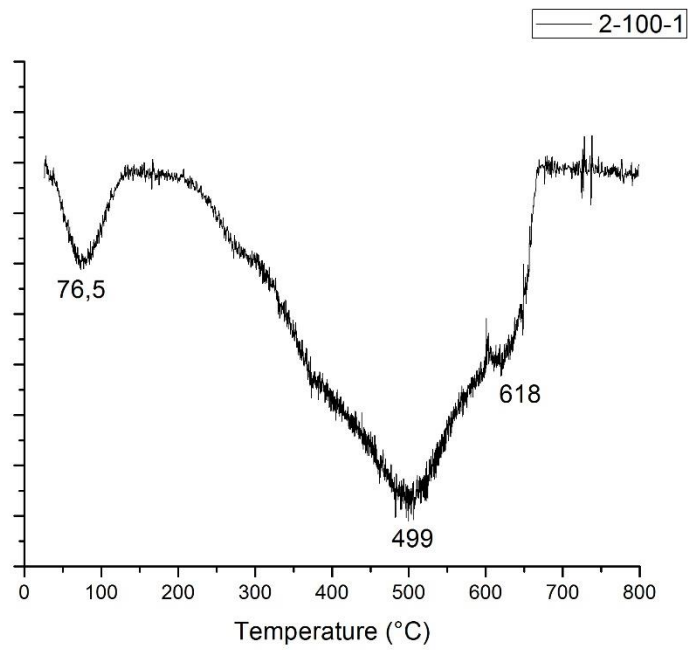
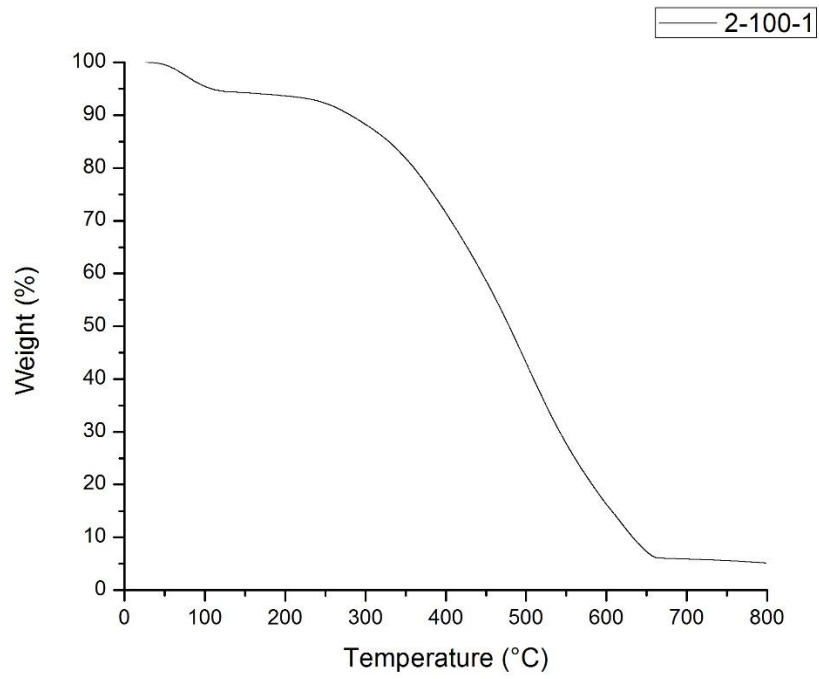


Figure 3.18. TGA and DTGA curves of sample PANI_MMT_PSA_2-100-1.

The polymer/clay ratio was estimated by subtracting the percentage associated to the dihydroxylation of MMT (4%) to the mass lost in the interval 400-800 °C (considering the initial polymer/clay ratio used in the suspension). As can be seen in Table 3.6, for the sample PANI_MMT_PSA_200-1-1 the initial (experimental) PANI/MMT ratio and that obtained from TGA data are in good agreement. On the other hand, sample PANI_MMT_PSA_2-100-1 showed a lower PANI/MMT ratio than that expected based on the experimental setup, suggesting that part of the anilinium ions were not polymerized and consequently were lost in the washing water. The calculated ratios are in agreement with those obtained in the XPS analysis.

Table 3.6.

Sample	PANI/MMT initial (w/w)	PANI/MMT TGA (w/w)
PANI_MMT_PSA_200-1-1	13.2 / 86.7	12.4 / 87.6
PANI_MMT_PSA_2-100-1	93.9 / 6.1	88.4 / 11.5

3.2.5 ZETA POTENTIAL MEASUREMENT

Experimentally, the superficial charge of a particle can be estimated or approximated by measuring the zeta potential of the particle in suspension. When a colloidal particle is in suspension, it develops a network of electric charges on its surface. According to the model of the electric double layer, a layer of counter-ions is formed (ions of opposite charge to that of the particle) called the Stern layer where the electric potential decays linearly with distance; outside this 'fixed' layer, in a nebulous area or diffuse layer, there are different compositions of co-ions (ions of equal charge to that of the particle) and the decay of the electric potential with the distance is exponential (Figure 3.19). The thickness of this double layer depends on the type and concentration of the ions in the solution. The potential in the plane where the diffuse layer and the Stern layer meet is known as zeta potential and is of special importance since it can be measured in a very simple way, by microelectrophoresis, diffusion potential or streaming potential and gives information about the distribution of the ions in the solid / liquid interface, and indirectly, about the superficial charge of the mineral. [35]

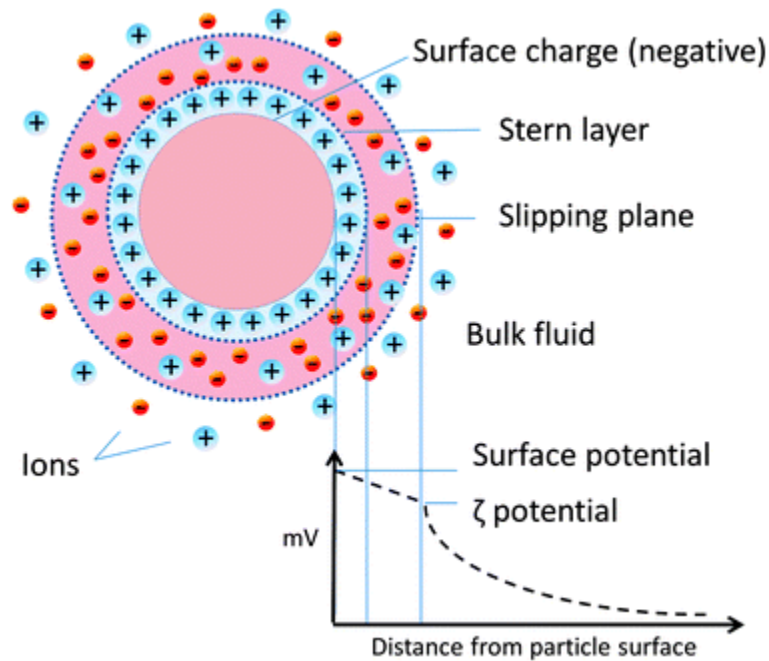


Figure 3.19. Double Layer configuration and zeta potential in a colloidal particle.

The zeta potential measurements based on the microelectrophoresis technique consist of subjecting a colloidal suspension to the action of an external electric field. Consequently, the particles migrate in the field and their movement and direction can be related to their zeta potential. The instrument measures electrophoretic mobility of the particles, which is expressed as microns / second per volts / centimetre. The first term, microns per second, simply represents speed, while the second, volts per centimetre, is an expression of the electrical force of the field. The zeta potential is calculated from the measurements of electrophoretic mobility, however, the relationship between electrophoretic mobility and zeta potential is not simple because of several reasons including the influence of conductivity on the surface, the effect of liquid conductivity on pores in the case of porous materials, non-spherical geometry, etc. In this sense, the calculated zeta potential does not indicate much more than the external charge of the particles and provides a value proportional to the electrophoretic mobility. The equipment directly converts electrophoretic mobility values into zeta potential values (through the Helmholtz-Smoluchowski equation), obtaining zeta potential curves (mV) as a function of pH. [35]

Zeta potential measurements based on microelectrophoresis were performed at Centro de Tecnologia de recursos Minerales y Ceramica (CETMIC), Argentina. This technique was executed in order to estimate the superficial charges of the samples and determine the polymer distribution in the composite structure.

3.2.5.1 RESULTS

Figure 3.20 shows the zeta potential curve vs. pH for all the samples. As it was explained in section 2.3, montmorillonites present two types of surface charges: permanent charged sites (negative interlamellar sites) and pH-dependent charged sites (edges). Since the last represent only 1% of the

total external surface, the zeta potential curve of montmorillonite presents negative values for the entire pH interval.

On one hand, it can be seen for PANI_MMT_PSA_200-1-1, that the behaviour is almost the same as the one of pure MMT indicating that for this composite the polymer was located preferentially in the interlaminar space. On the other hand, for the sample with higher content of polymer the zeta potential displays positive values for acidic pH due to the positive charges present in the doped PANI-ES. In addition, the zeta potential of sample PANI_MMT_PSA_2-100-1 becomes negative at $\text{pH} > 7$, since emeraldine base (EB) species increase in concentration due to de-doping of the emeraldine salt form in basic media ($\text{pK}_a \text{ ES / EB} = 6.5 - 8$). [Ref] This verifies that in this case, the composites consist of exfoliated sheets of MMT immersed in a polymer matrix of polyaniline.

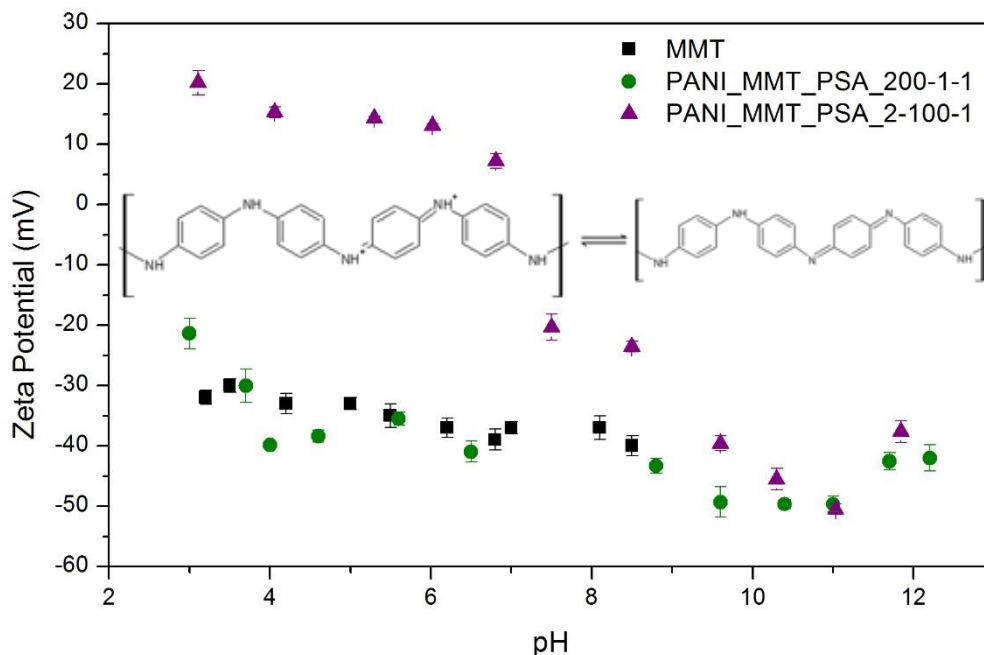


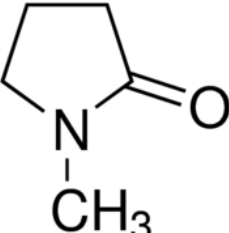
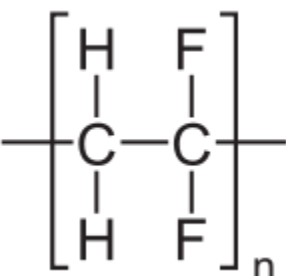
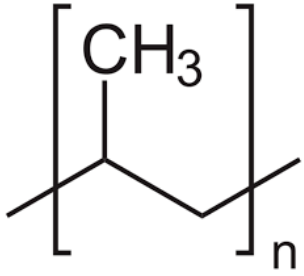
Figure 3.20. Zeta potential measures of samples: pure MMT, PANI_MMT_PSA_200-1-1, and PANI_MMT_PSA_2-100-1.

Chapter 4: Electrochemical application of synthesized clay/polymer nanocomposites

4.1 COATING STRATEGY

Slurries of the synthesized clay/polymer nanocomposites were prepared and coated onto a commercial polypropylene separator. The materials used are listed in Table 4.1.

Table 4.1.

Materials	Chemical structure and/or formula	Observations
N-Methyl-2-Pyrrolidone (NMP)		used as purchased from SIGMA-ALDRICH®
Polyvinylidene fluoride (PVDF)		used as purchased from SIGMA-ALDRICH®
Polypropylene (PP) Separator		Monolayer PP Celgard®2500 Thickness: 25 μm Porosity: 55% Pore Size: 0.064 μm

The followed procedure was:

- Slurries were prepared with the composites, using NMP as solvent and PVDF as binder with a mass ratio composite/binder = 80/20.

- The PVDF pellet (30 mg) was first dissolved in NMP (600 μ L) by ball milling for 10 minutes.
- The corresponding mass of composite was added, and the suspension was mixed for half an hour.
- The formed slurries were blade casted onto commercial Celgard[®]2500 separator film.
- The obtained coated separators where then cut into discs of 20 mm. Figure 4.1 shows the results obtained.

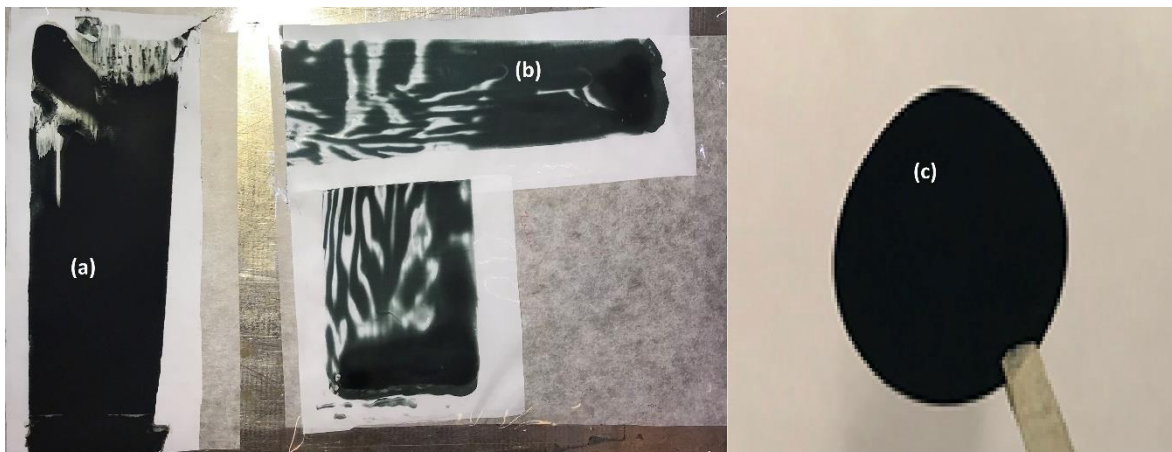


Figure 4.1. Coatings on separator Celgard[®]2500 of samples: (a) PANI_MMT_PSA_2-100-1, (b) PANI_MMT_PSA_200-1-1, and (c) 20 mm disc.

4.2 CONDUCTIVITY MEASURES

I) Ionic Conductivity

Ionic conductivity was measured (following S. Yang et al./ *Enhancement of Thermal Stability and Cycling Performance of Lithium-Ion Battery at High Temperature by Nano-ppy/OMMT-Coated Separator* 10.1155/2017/6948183) by Impedance spectroscopy of separators (coated and not coated) using two stainless steel blocking electrodes. Equation 4.1 was used to calculate the ionic conductivity:

$$\sigma = \frac{L}{R_b \times A} \quad (4.1)$$

L is the coating thickness, R_b the bulk resistance and A the area of the surface area of electrode.

Table 4.2 displays the resulting data. Impedance spectroscopy was performed at OCP (open circuit potential) immediately after assembling the cells, as well as after 24 hours.

Table 4.2

Sample	Bulk Resistance (Ohm)	Thickness (cm)	Area (cm ²)	Conductivity (S/cm)	Bulk Resistance (Ohm) 24 h	Conductivity (S/cm) 24 h
Celgard®2500	1.62E+03	2.50E-04	2.0096	7.69E-08	9.37E+02	1.33E-07
PANI_MMT_2-100-1	6.3	6.48E-04	2.0096	5.12E-05	6.08	5.30E-05
PANI_MMT_200-1-1	1.86	3.88E-04	2.0096	1.04E-04	3.64	5.30E-05

As it can be seen, the ionic conductivity of the separator without coating is much less than the ones obtained for the coated separators. After 24 hours the ionic conductivity of Celgard®2500 increased. For both coated separator of composite samples, ionic conductivity seems to be equivalent.

II) Electronic conductivity

Electronic conductivity was measured (following J.A.Marins et al./*A facile and inexpensive method for preparation of conducting polyaniline-clay composite nanofibers*/Synthetic Metals 162 (2012) 2087-2094) by impedance spectroscopy. The previously described slurry was blade casted on an aluminium foil. The resulting coated aluminium foil was cut into discs of 15 mm diameter and conductivity was calculated from the resistance values measured by impedance. Measurements were carried out for bare aluminium as well as for both coated samples (on aluminium) and the resistance value obtained for aluminium foil was subtracted to the resistance of the coated aluminium samples, so to obtain the bulk resistance of the PANI/MMT membranes.

As can be seen in Table 4.3, all the samples have almost the same loading (mass per unit area), although the coating thicknesses were different.

Table 4.3.

Sample	Resistance (Ohm)	Coated film thickness (m)	Mass per unit area (kg/m ²)	Conductivity (S/cm)
PANI_MMT_PSA_2-100-1	0.9733	4.90E-05	0.0679	2.85E-01
PANI_MMT_PSA_200-1-1	1.9624	1.55E-05	0.0642	4.47E-02

It can be evidenced a conductivity increase with a higher quantity of conducting polymer, which is in correspondence to the values obtained for PANI/MMT composites found in the literature (L. Kulhánková et al. / Thin Solid Films 562 (2014) 319–325). This behaviour can be attributed to alterations in the structure of intra-chain and inter-chain of polymer arrangements produced by the presence of clay. For the sample with a high amount of clay (PANI_MMT_200-1-1) conductive polymeric islands are isolated one from the other, breaking the inter-chain connections. On the

other hand, when the amount of PANI increases a 're-connection' of conducting polymeric islands takes place increasing the bulk conductivity. In addition, MMT layers can also affect the intra-chain PANI arrangements influencing the delocalization and nature of charge carriers in the polymer. [39]

4.3 ELECTROLYTE UPTAKE AND RETENTION

The capacity to uptake (φ) and to retain (ρ) the liquid electrolyte was calculated using the following equations:

$$\varphi = \frac{w1 - w0}{w0} \times 100\% \quad (4.2)$$

$$\rho = \frac{w1 - w0}{w1} \times 100\% \quad (4.3)$$

where w_0 is the weight of dry separator and w_1 is the weight of separator after soaking in electrolyte and removing excess electrolyte on the surface. The electrolyte used was a commercial² 1 M LiPF₆ in ethylene carbonate (EC) and dimethyl carbonate (DMC), (1:1 v/v). Discs of the separators with and without coating were soaked into the electrolyte and both the electrolyte uptake and the electrolyte retention were measured after 3, 24 and 72 hours for each sample. As it can be seen from Table 4.4, the coated separators show a huge improvement of both properties with respect to the bare separator. This can be explained by the fact that, as it was developed in section 2.1.4, when exchanged with organic ions (particularly alkylammonium ions) the resultant organo-montmorillonite has the ability for swelling and thixotropic gel formation with polar organic solvents. Gel formation is especially stronger when the alkyl chains contain double bonds or aromatic groups (which is the case of polyaniline). It is also notable that for the sample PANI_MMT_2-100-1 the predominant content of polyaniline adds organophilic affinity between the composite and the polar organic electrolyte explaining why the separator with this coating shows the best performance. Furthermore, PANI present in the external surface of MMT constitutes a hydrogen-bonding matrix contributing to the interaction with the polar organic solvent. In fact, as shown in Figure 4.2 the coating also increases the wettability towards the electrolyte. It can be clearly seen for the bare separator that the electrolyte forms a drop while for the coated samples it completely wets the separator immediately after touching the surface.

² purchased from SOLVIONIC®

Table 4.4

Sample	w0 (mg)	w1 3hs (mg)	ϕ (%) 3hs	ρ (%) 3hs	w1 24hs (mg)	ϕ (%) 24hs	ρ (%) 24hs	w1 72hs (mg)	ϕ (%) 72hs	ρ (%) 72hs
SEP	3.3	3.3	0.0	0.0	5.2	57.6	36.5	5.8	75.8	43.1
PANI_MMT_2-100-1	6.3	21.3	238.1	70.4	39.5	527.0	84.1	36.1	473.0	82.5
PANI_MMT_200-1-1	5.5	15.3	178.2	64.1	16.2	194.5	66.0	16.5	200.0	66.7

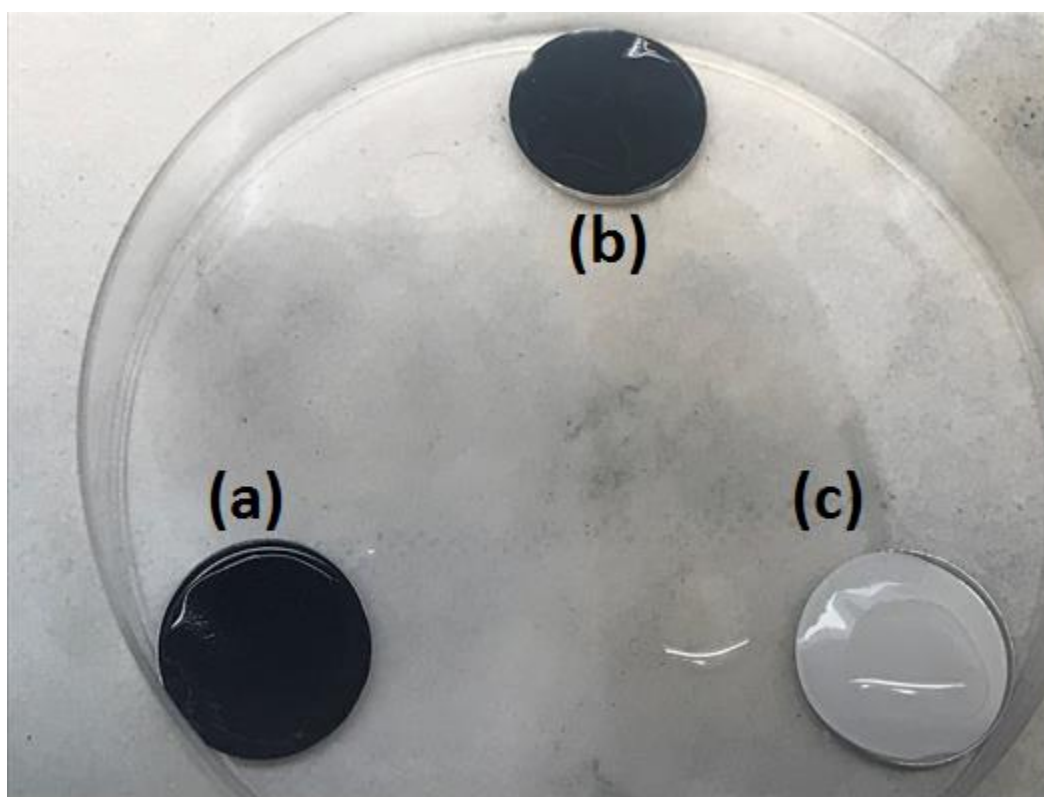


Figure 4.2. Wetted separators of samples: (a) PANI_MMT_2-100-1, (b) PANI_MMT_200-1-1 and (c) bare Celgard® 2500.

4.4 CELLS ASSEMBLING

Electrochemical properties of the different samples of the modified separator were studied by preparing coin cells type 2032 (20 mm diameter and 3.2 mm height). The coated separator films were cut into 20 mm discs. Coin cells were assembled in an Argon filled glove box with water and oxygen levels maintained below 1ppm. The electrolyte used was a commercial 1 M LiPF₆ in ethylene carbonate (EC) and dimethyl carbonate (DMC), (1:1 v/v). Figure 4.3 represents a schematic representation of the coin cell assembly, where the cathode is placed in the bottom cup (stainless steel) of the coin cell and electrolyte is added to wet the electrode. Then the separator is placed above the cathode and again electrolyte is added to wet the separator. In the following step, the anode is placed as well as the top cap welded with a wave spring (stainless steel). Finally, the coin cell is sealed by crimping in a mechanical hand press.

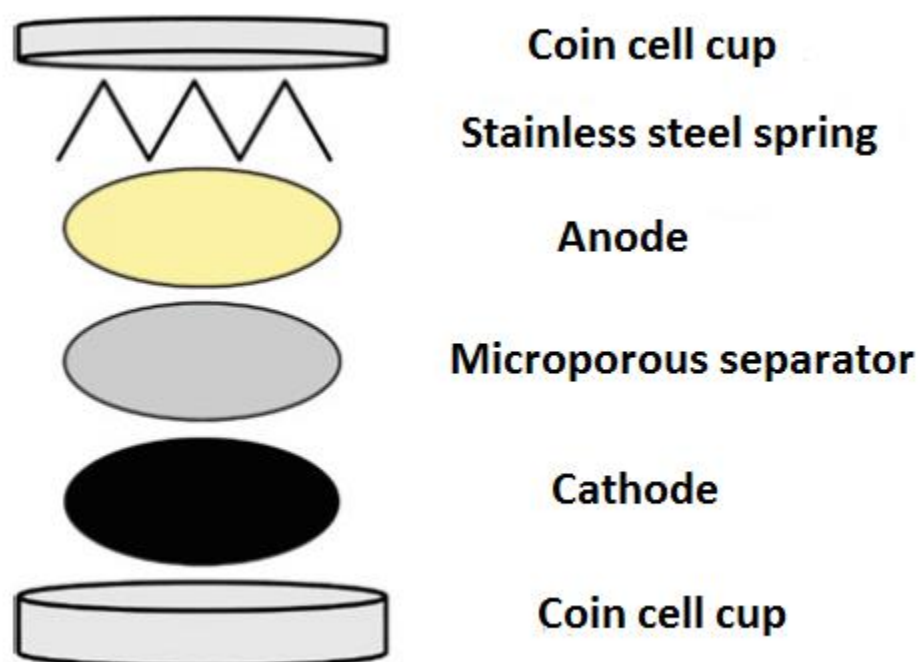


Figure 4.3. Schematic representation of coin cell assembly

4.5 ELECTROCHEMICAL TESTING

Li storage and cycling behaviour of an electrode material can be examined by galvanostatic cycling or constant current cycling technique. During galvanostatic cycling, a constant current (I) is applied to the cell and the potential (V) is monitored as a function of time or number of cycles. Good reversibility in lithium cycling of an electrode material is often described by the capacity retention over many cycles and is usually represented as a plot of specific capacity versus cycle number. All the electrochemical tests were carried out using a multichannel galvanostat BR-2000 (Arbin

Instrument) at the electrochemistry laboratories of the Department of Applied Science and Technology (DISAT) at Politecnico di Torino.

4.5.1 Li PLATING AND STRIPPING

Figure 4.4 shows the mechanism proposed in the literature for the insertion/de-insertion of lithium in nanocomposites of polyaniline and layered inorganic hosts. After several charge/discharge cycles, lithium ions play a significant role doping the interlayered PANI molecules and balancing the charges of the negative slabs of the inorganic host. During the charge cycle, Li^+ are de-doped and move to the electrolyte while the negative slabs lose electrons to balance the layer charge. During the discharge cycle, lithium ions are inserted into the interlayers and doped with polyaniline molecules while the slabs accept electrons to balance the superficial charges. [38]

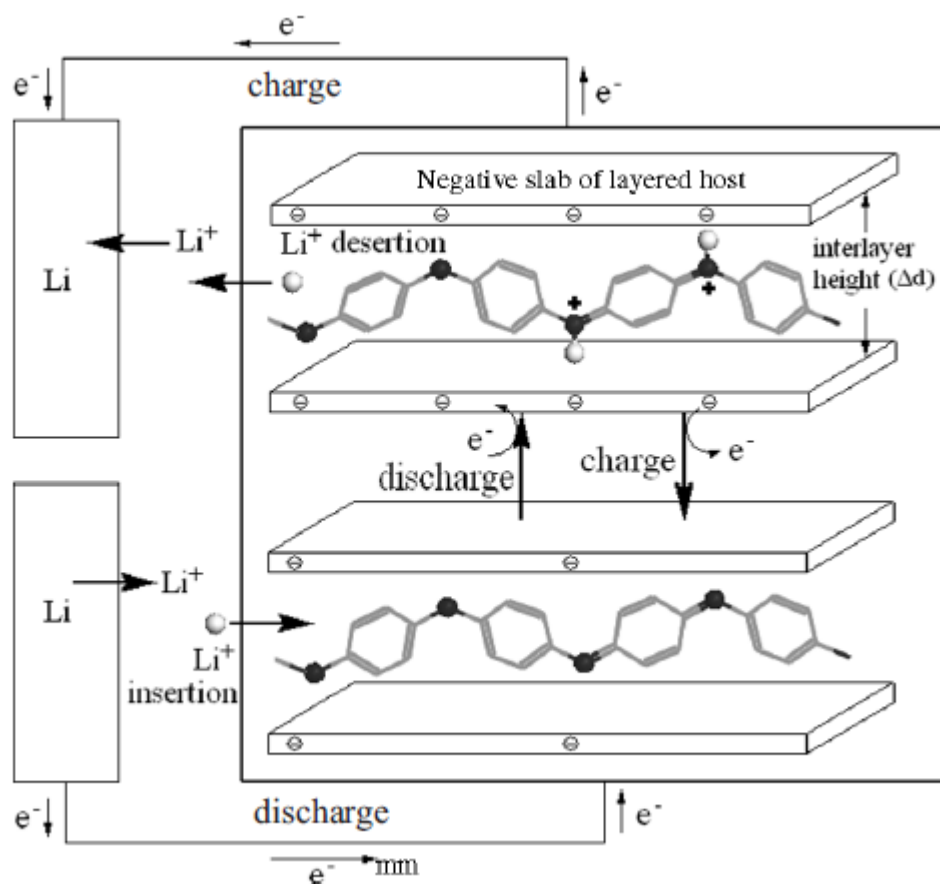


Figure 4.4. Lithium insertion/desorption mechanism for a Li/nanocomposite cell. [38]

Li/Li symmetric coin cells were prepared using metallic lithium as both cathode and anode in order to perform lithium plating and stripping galvanostatic cycles, and to study the lithium conduction of

the samples. Evaluating the ability of the clay/polymer coatings to protect metallic lithium anode was also desired. In the first test, 250 charge/discharge cycles at a current density of 5mA/cm² were performed for all the samples. In the second test, 250 charge/discharge cycles were performed for the samples at a higher current density (10mA/cm²). Both tests were carried out at ambient temperature.

It was decided to perform the tests at high current densities in order to see results in a reasonable period, since lithium plating and stripping tests generally require a lot of time.

4.5.1.1 RESULTS

Figures 4.5 to 4.14 show the results obtained (for cycling at 5mA/cm²). As it can be seen, up to 180 cycles the sample PANI_MMT_200-1-1 shows the lowest average overpotential (22 mV) and highest stability indicating that in fact there is a performance improvement of lithium plating and stripping when compared to the cell with the separator without coating that was stable just up to 80 cycles with an average overpotential of 33 mV. This means that the clay/polymer composite coating improves Li⁺ conduction probably because the regular structured configuration of intercalated polymer chains in the interlayer space provides a good 2D channel for Li⁺ transition and propitiates a more uniform current distribution on metallic lithium surface reducing dendrite formation. Presence of montmorillonite can also act as a mechanical barrier impeding dendrite growth. Sample PANI_MMT_2-100-1 has a higher average overpotential in comparison to the separator without coating, meaning that it is more resistive to lithium plating and stripping. The porosity of the separator determines effective Li⁺ conductivity. In the coating layer, the porosity is derived from the gaps between the particles, where both the particle shape and size affect its porosity. Taking this into account, probably different porosities and particle shape of the coated layers could explain why even though the sample PANI_MMT_2-100-1 has the highest electrolyte uptake, it shows the highest overpotential for lithium conduction. This could be confirmed by porosity measurements and/or micrographs in future work.

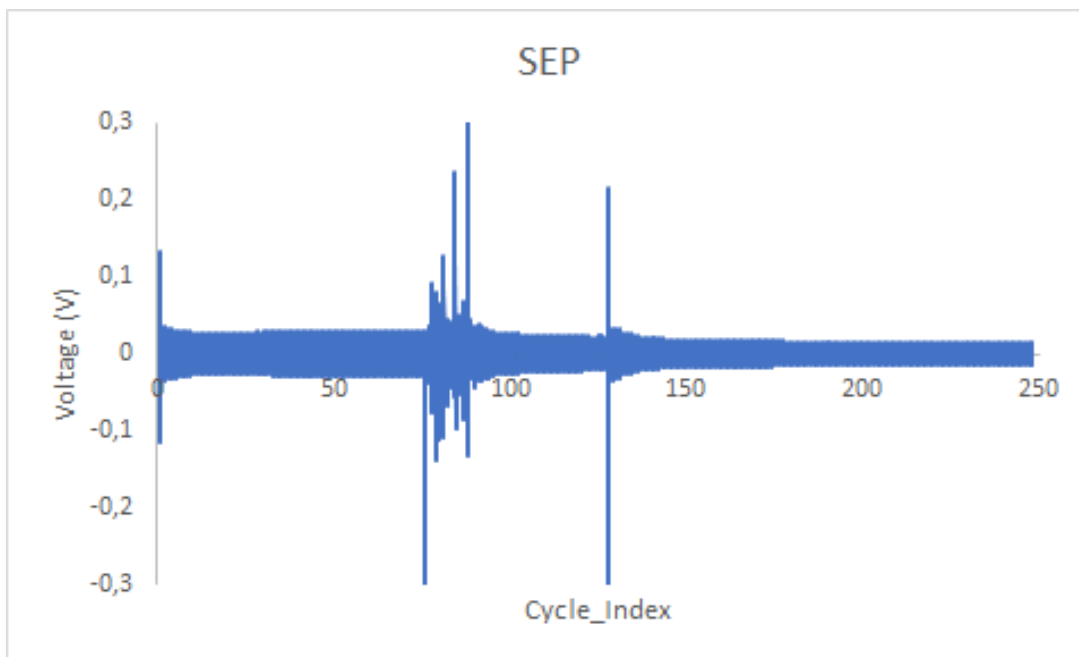


Figure 4.5

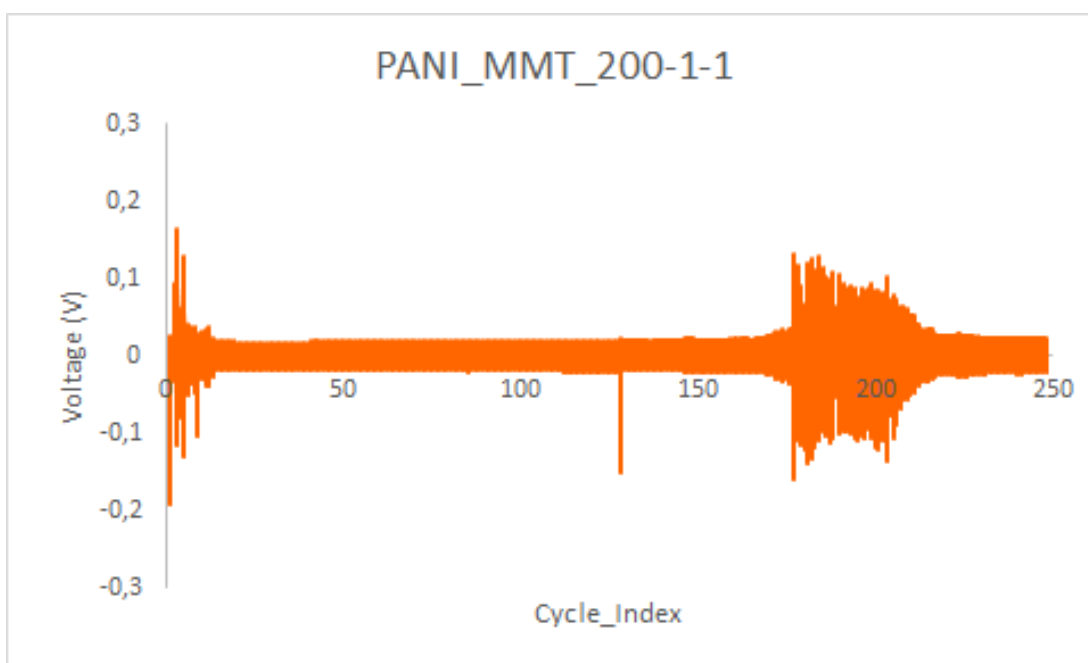


Figure 4.6.

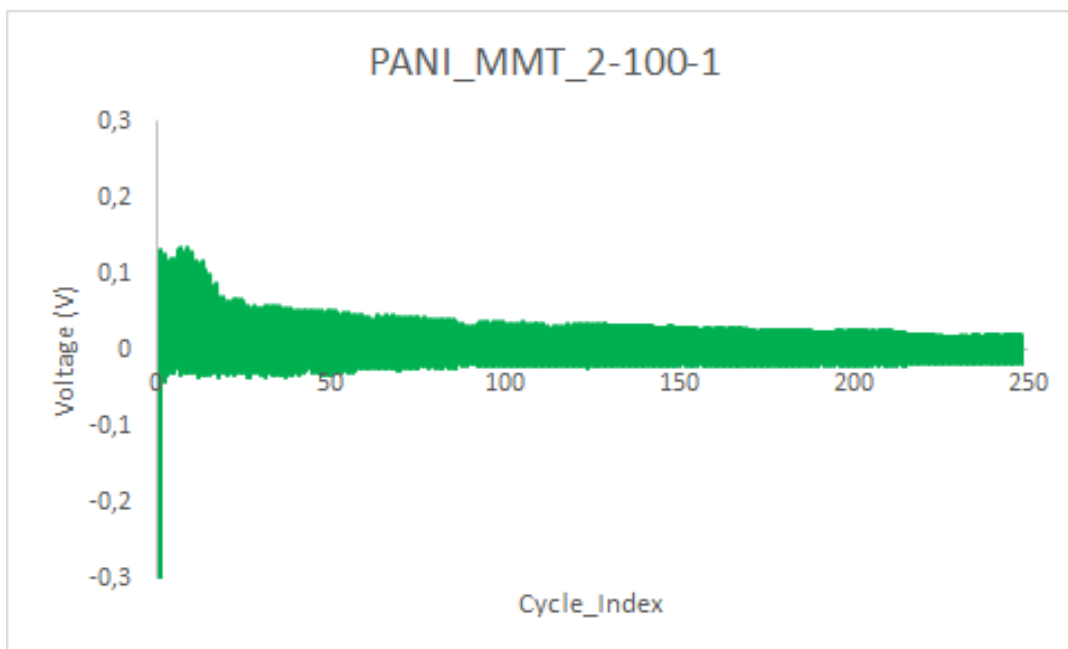


Figure 4.7.

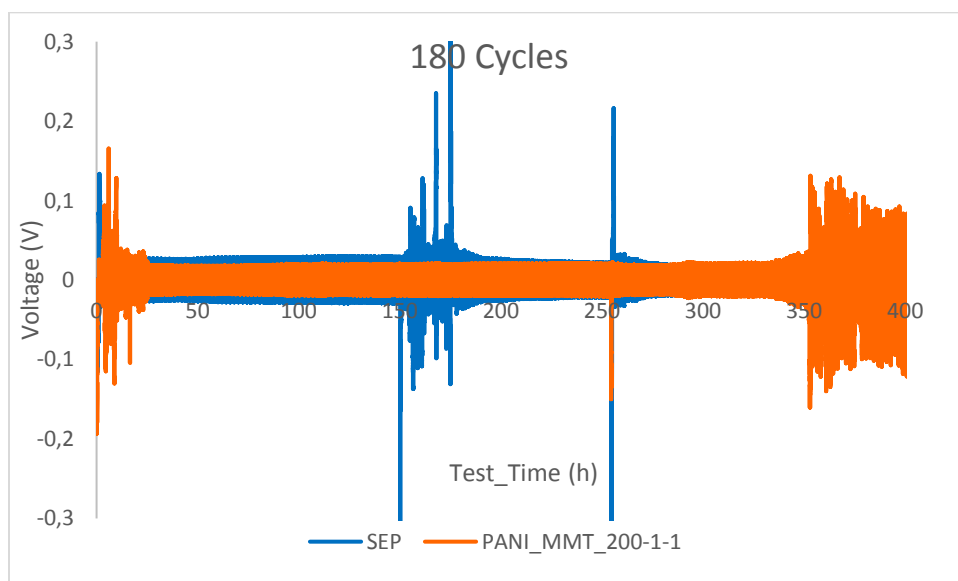


Figure 4.8.

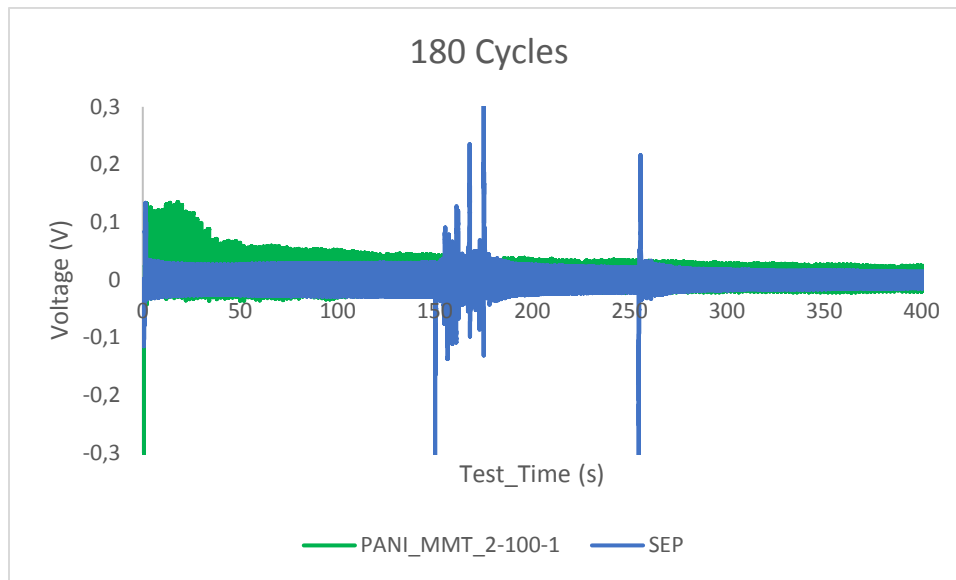


Figure 4.9.

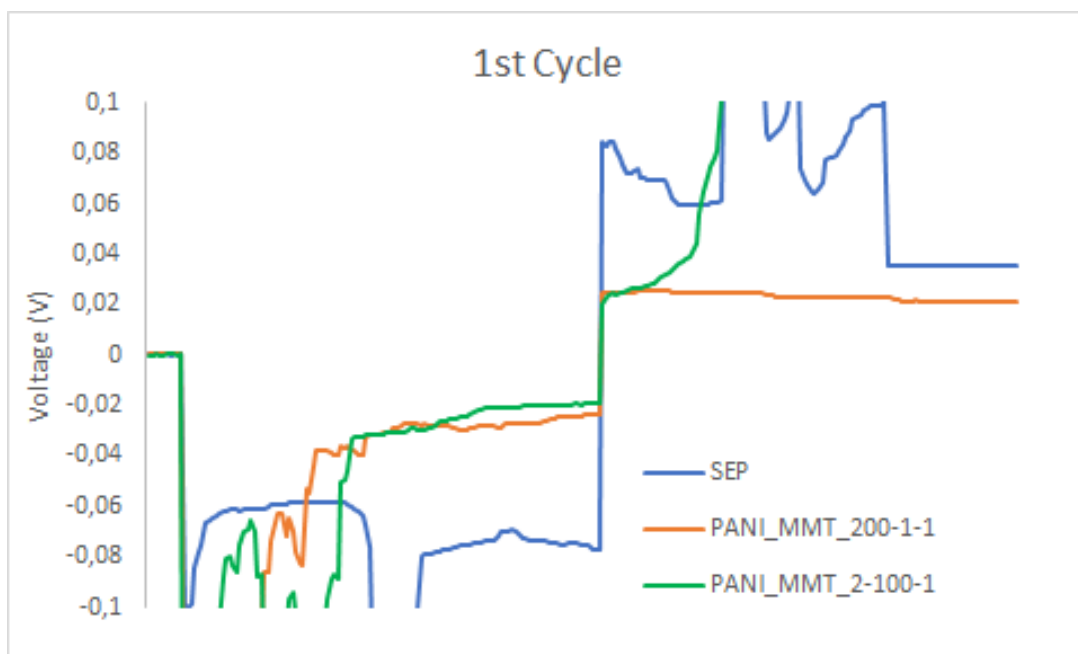


Figure 4.10.

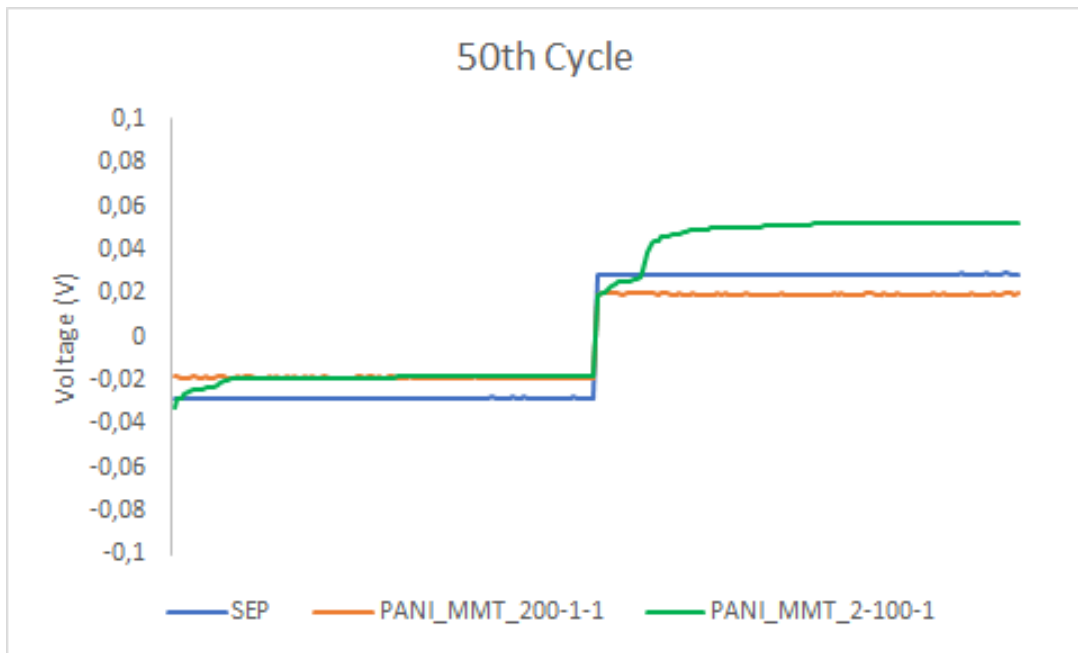


Figure 4.11.

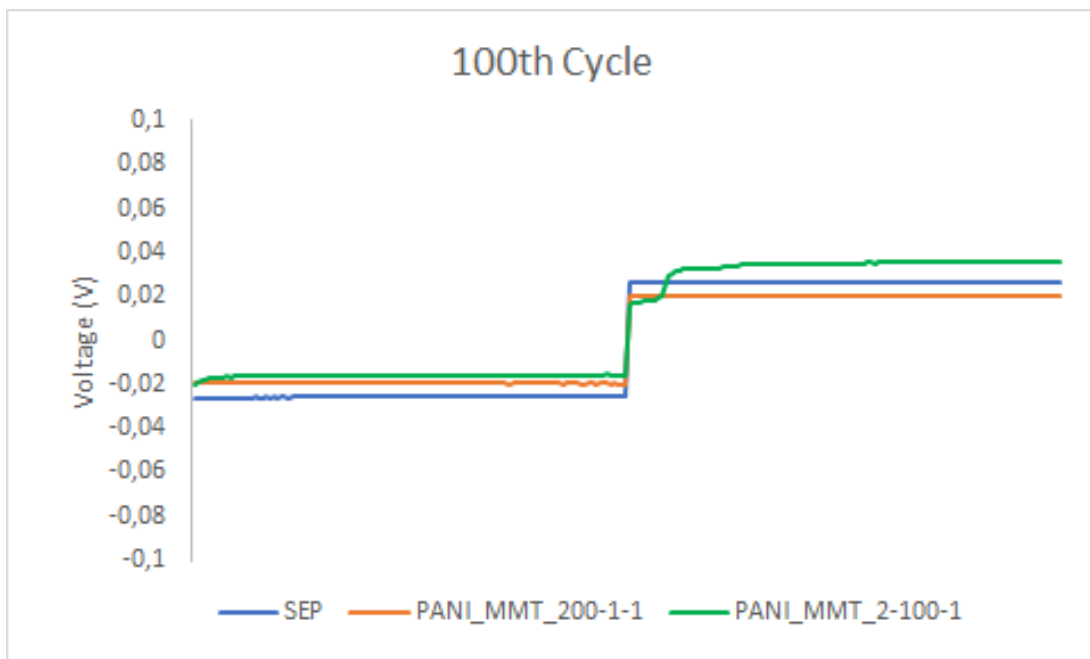


Figure 4.12.

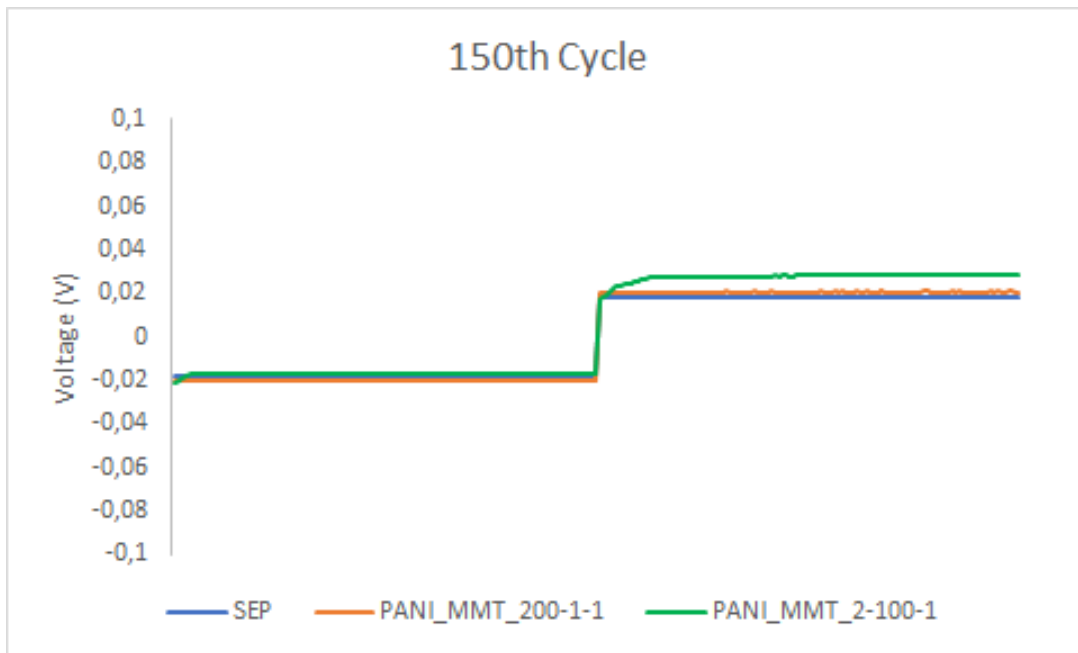


Figure 4.13.

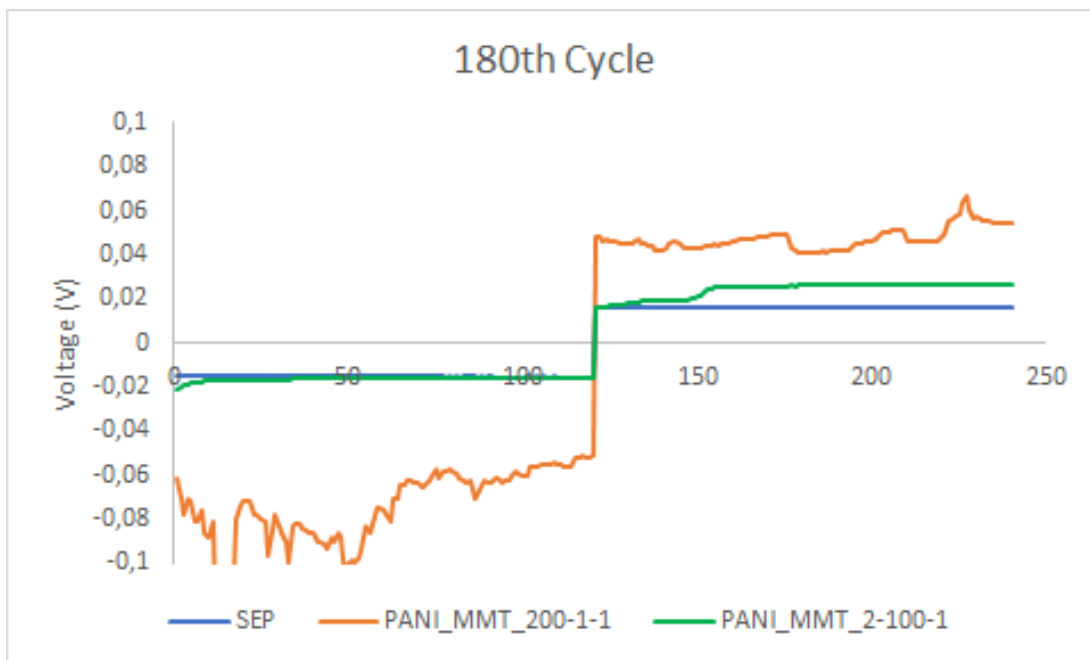


Figure 4.14.

Figures 4.15 to 4.23 show the results obtained (for cycling at $10\text{mA}/\text{cm}^2$). Although in this case, sample PANI_MMT_200-1-1 shows the lowest overpotential and stability only up to 50 cycles after which it becomes unstable. This could be attributed to the deposition of solids on the separator (due to electrolyte decomposition reactions), which increase the resistance towards lithium passage. It is worth to highlight the fact that the current used was significantly higher than the current usually used in this kind of test in most of research studies. According to the reactions showed in Figure 1.9 (section 1.5) electrolyte decomposition is favoured at high currents. These parasitic reactions are more important in the samples with coating probably as a result of a change in the chemical affinity of the separator surface, it goes from being non-polar to being polar. In the case of the sample with more MMT, in addition, it is even more hydrophilic, so it is logical that the products that are formed (alcohols, alkoxides, and salts with carboxylic groups) join the OH groups of the Montmorillonite, constituting sites where lithium can be trapped.

The coating of sample PANI_MMT_2-100-1 does not seem to improve the separator performance at this current density.

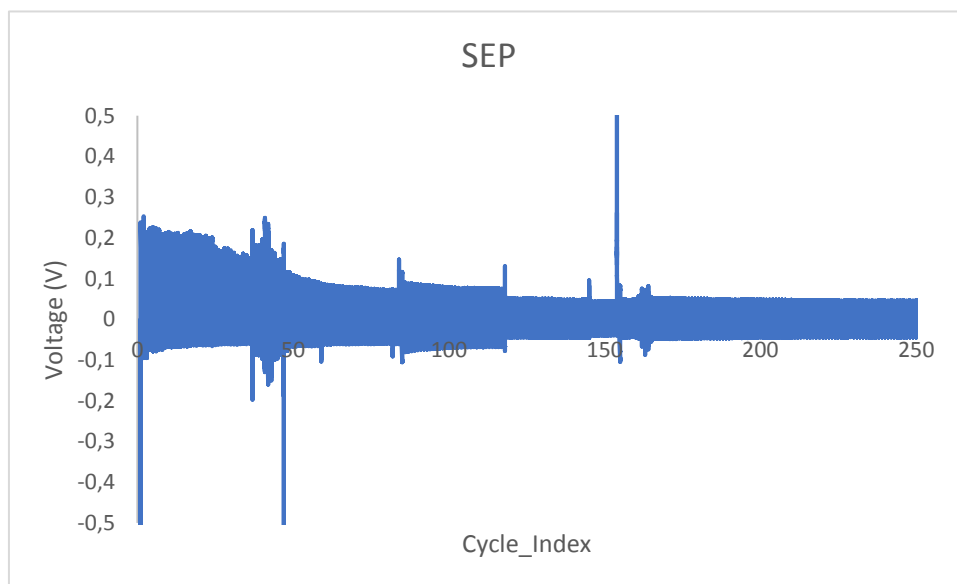


Figure 4.15.

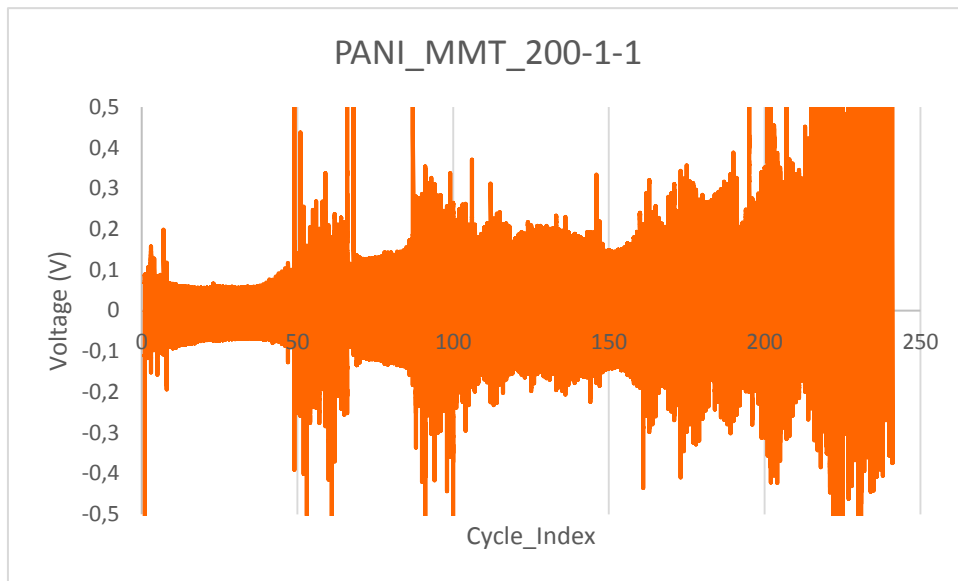


Figure 4.16.

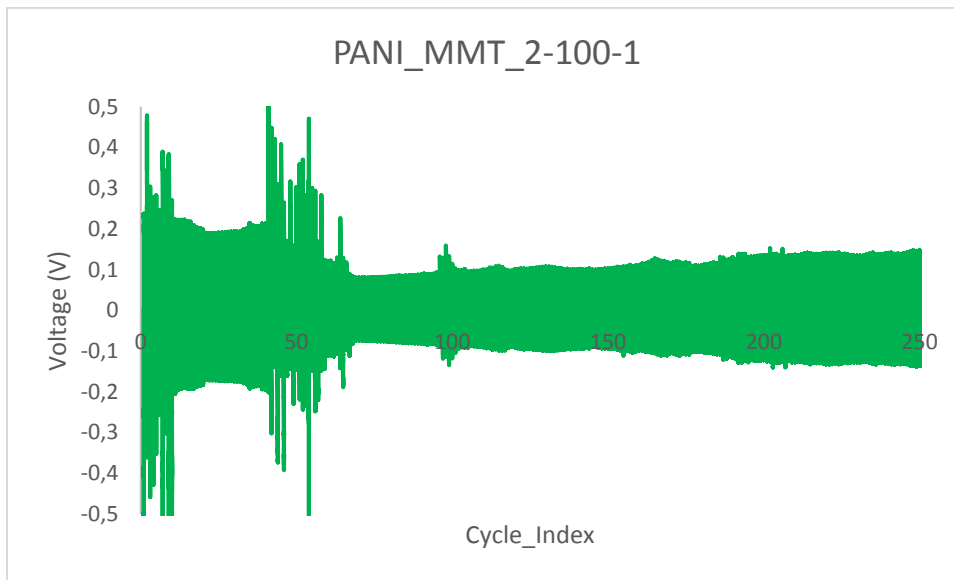


Figure 4.17.

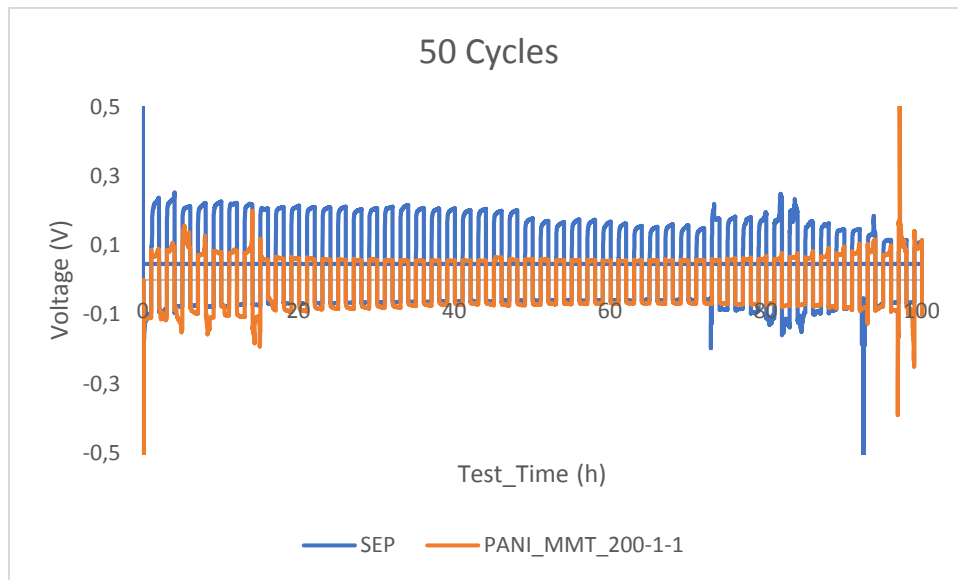


Figure 4.18.

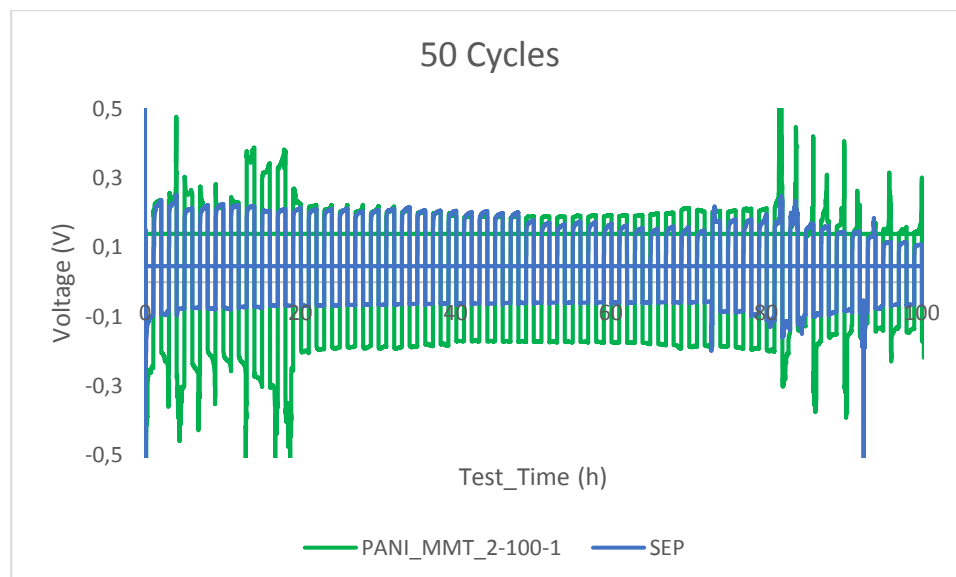


Figure 4.19.

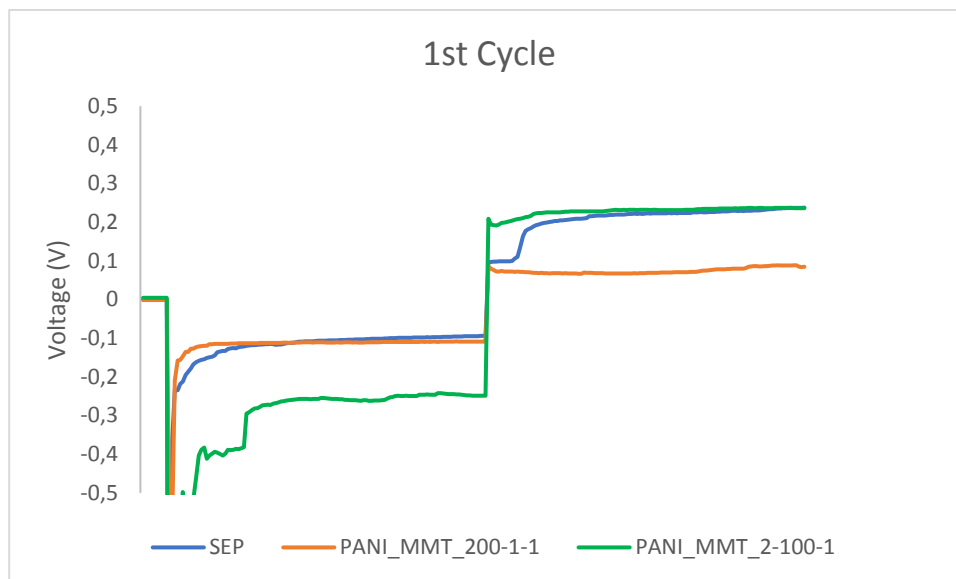


Figure 4.20.

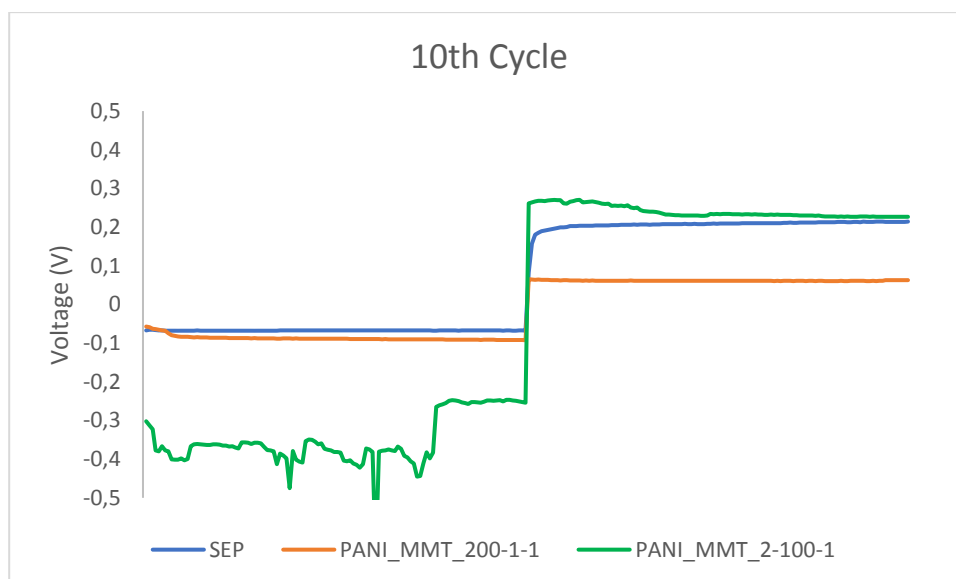


Figure 4.21.

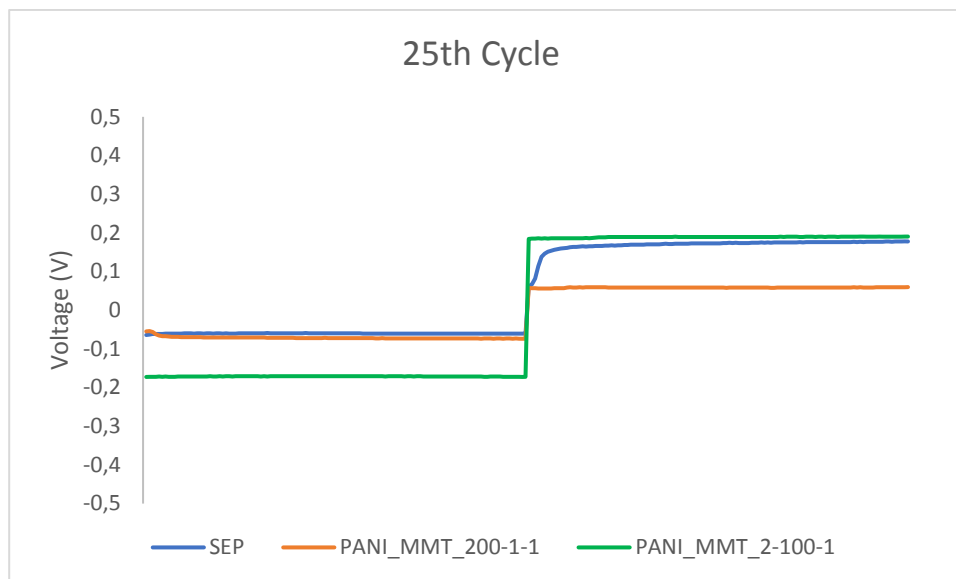


Figure 4.22.

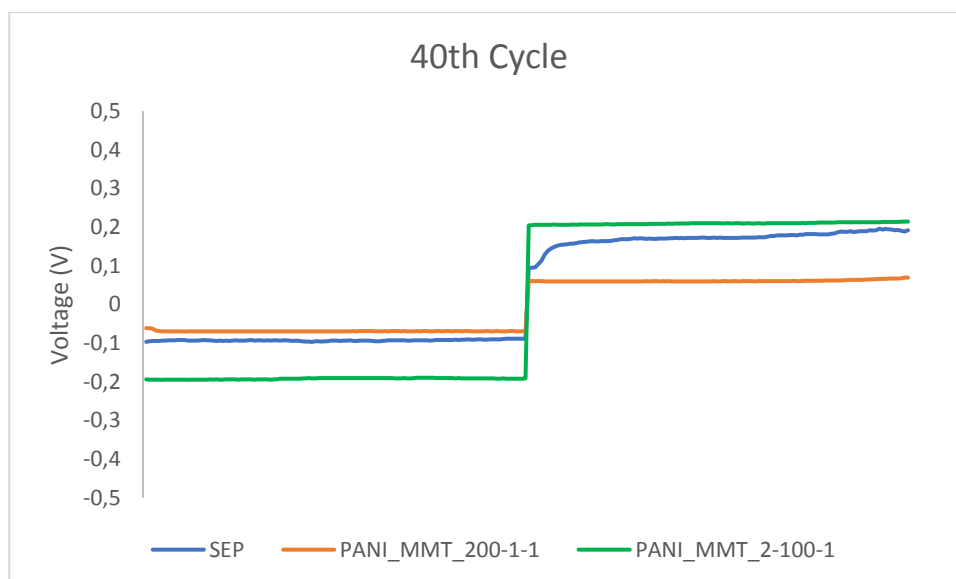


Figure 4.23.

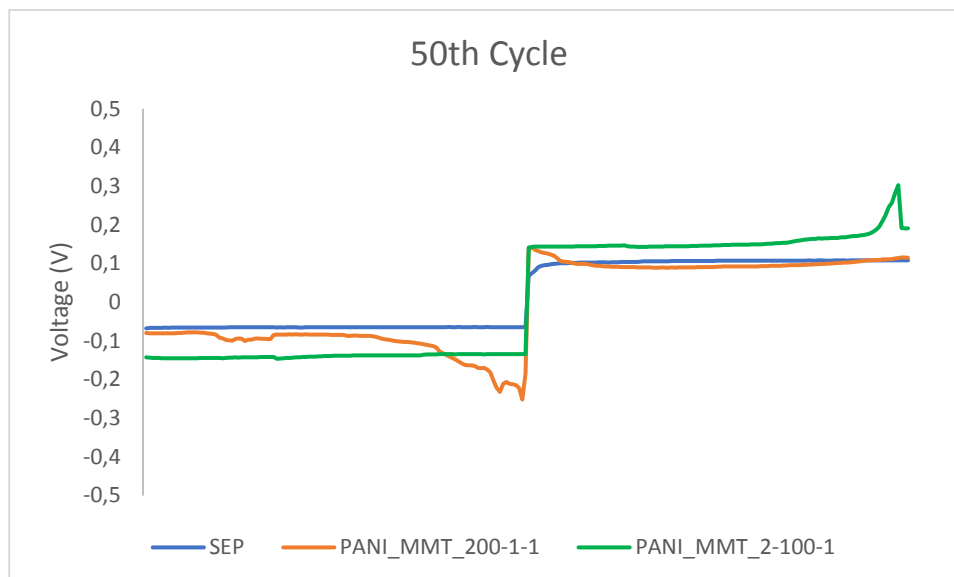


Figure 4.24.

4.5.2 CYCLING PERFORMANCE USING A HIGH VOLTAGE CATHODE (LiNi_{0.5}Mn_{1.5}O₄)

As it has been developed in section 1.4.2, the spinel LiNi_{0.5}Mn_{1.5}O₄ is a promising high-voltage cathode material for the development of high-energy Li-ion batteries, but the major drawback of this material is a disproportionation reaction, where Mn⁺³ forms Mn⁺² which is dissolved into the electrolyte, and moves towards the anode where it catalyses undesired reactions that cause a capacity fade in the battery.

In the second part of this work, the coated separators were tested towards a LiNi_{0.5}Mn_{1.5}O₄ cathode provided by Lithops S.r.l. Firstly, galvanostatic charge/discharge cycles were performed for half cells, using metallic lithium and LNMO. Electrochemical cycling was conducted in 2032-type coin cells with 15mm diameter electrodes. The cells were operated between 3.5 and 4.9 V at ambient temperature. In the next step, full cells were assembled using the same LNMO cathode and a graphite anode (both provided by Lithops S.r.l.). Coin 2032-type cells were used following the same procedure as it has been described before. Electrochemical cycling tests were performed at constant current between 3.5 and 4.9 V at ambient temperature.

4.5.2.1 RESULTS

I) Cycling performance of half cells (Li vs LNMO)

Figures 4.25, 4.26 and 4.27 show the first 5 cycles at a current equal to C/10. As it can be seen, there is a significant difference between the cells that contained the coated separators and the one with the bare Celgard®2500. In fact, the cell with the separator without coating was not able to cycle at all, even at a low current (C/10) probably because of the poor affinity of polypropylene separators with carbonate-based electrolytes like the one used in this work (1M LiPF₆ in EC and DMC). This is in correspondence with the results obtained by electrolyte uptake and retention measures (section 4.3). The poor wettability of the separator with the electrolyte can increase the electrolyte filling time during assembly process and impact the ability to retain the electrolyte solution, thereby affecting the performance of the battery.

The cells with the PANI/MMT coated separators were submitted to 100 cycles at a current of 1C and another 100 cycles at C/5. Figures 4.28 and 4.29 show the cycling performance. At C/5 the specific capacity is similar for both samples and is around 120 mAh/g whereas at a high current (1C) the sample PANI_MMT_200-1-1 is unstable, which is in accordance to the behaviour seen for the lithium plating and stripping test at high current density (section 4.5.1) and could be related to solid depositions on the coating due to parasitic reactions of the electrolyte favoured in presence of the clay.

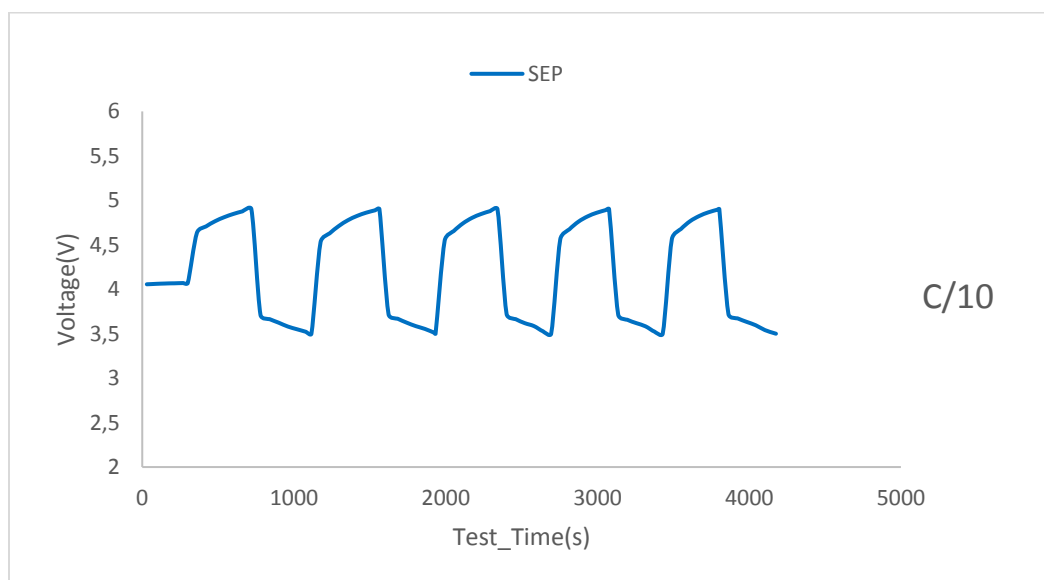


Figure 4.25

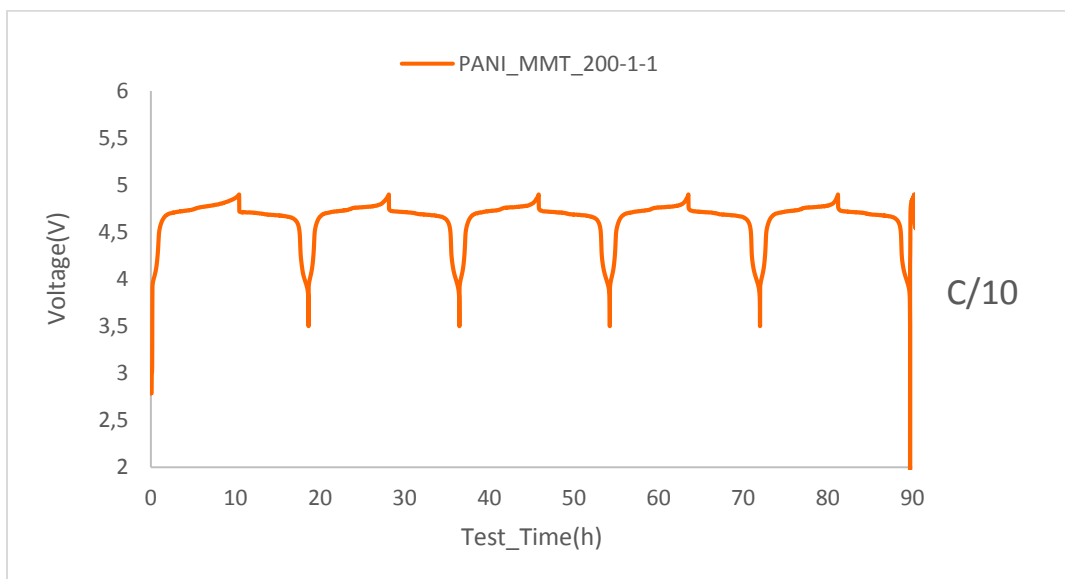


Figure 4.26

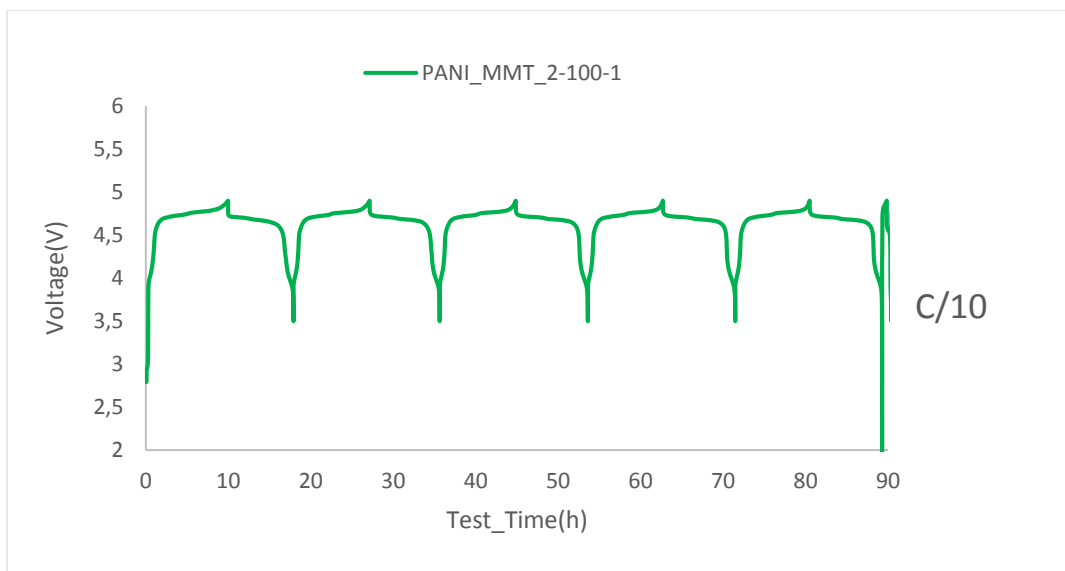


Figure 4.27

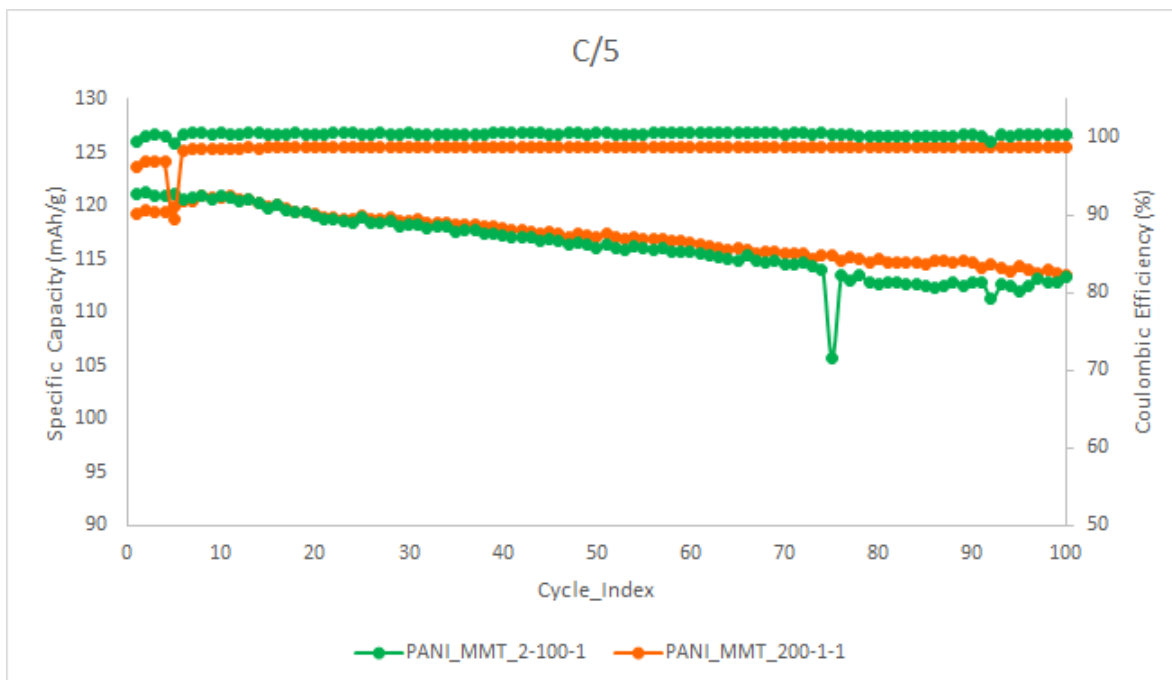


Figure 4.28

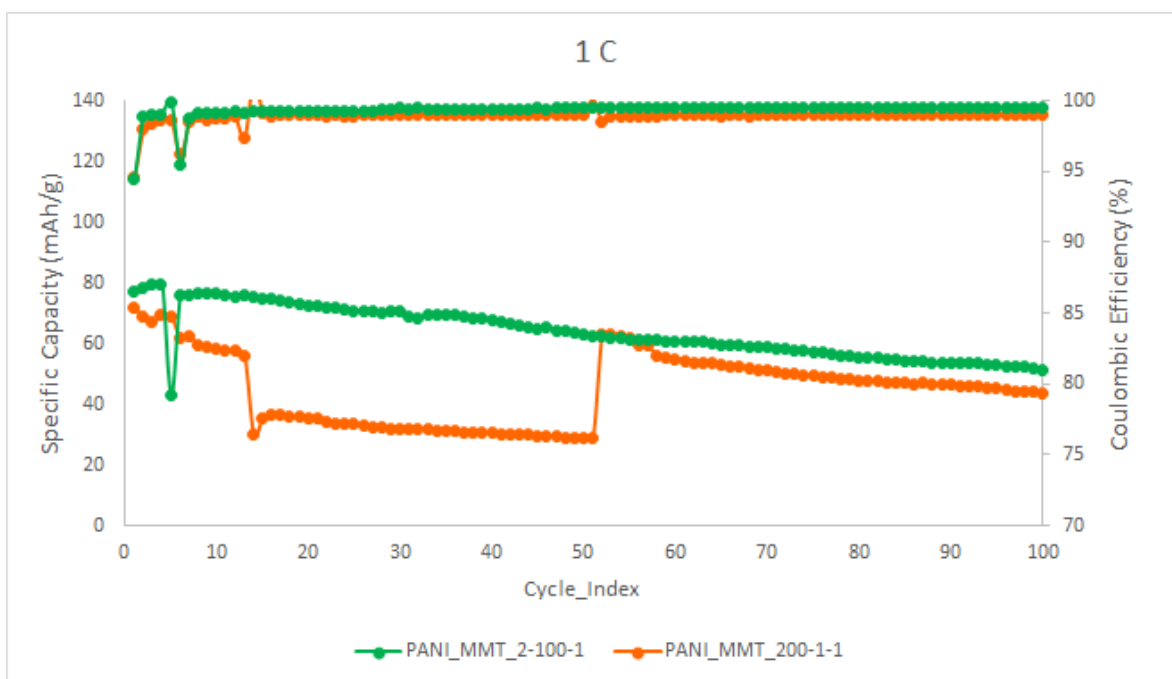


Figure 4.29

II) Cycling performance of full cells (Graphite vs LNMO)

Figures 4.30, 4.31 and 4.32 show the first 5 cycles at C/10 for all the samples and once again it can be corroborated the poor behaviour of the cell with the separator without coating in contrast with the performance of the cells with the PANI/MMT coated separators. The cycling enhancement by the coatings was also corroborated when compared to galvanostatic cycling tests (in the same conditions) using another separator (glass microfiber Whatman®) usually used for Li-ion batteries, where it was seen a similar behaviour between the glass microfiber separator and the PANI/MMT coated modified PP separator. (See Appendix A)

For the bare Celgard®2500 cell, it was decided to diminish the current until cycling was achieved (Figure 4.33). Finally, it was decided to use for this sample a current of C/25 for which the cycling performance (for 20 cycles) can be seen in Figure 4.34. Soaking the separator into the electrolyte for two days before assembling the cells was also tried without getting positive results. The cycling poor behaviour attributed to this separator, in particular, was also verified when identical cells cycled at the same conditions but using another polyolefin separator (Celgard®2325) with different porosity were tried. (See Appendix B)

For the PANI/MMT coated separator cells, galvanostatic cycling was performed for 130 cycles (Figure 4.35) at a current of C/5 between 3.5 and 4.9 V at ambient temperature. It can be appreciated that the sample PANI_MMT_200-1-1 starts with a higher specific capacity than the sample PANI_MMT_2-100-1, probably because the coating thickness was less in the first case being less resistive to cycling (this will be verified after duplicating the cells and repeating the tests, which is work in progress currently being carried out). Nevertheless, it is evident that in the first case the cell rapidly losses capacity (steepest slope) while in the case of the coating of the clay/polymer composite with the higher percentage of polyaniline, the capacity loss is much more gradual. As it can be seen from Table 4.5, capacity fade was calculated considering the specific capacity at the 1st cycle and the one at the 130th cycle. It is corroborated that the capacity fade for the sample PANI_MMT_2-100-1 (32.72%) is less than that for the sample PANI_MMT_200-1-1 (46.83%). This could be related to a better capacity of this coating to impede migration of manganese ion to the graphite anode.

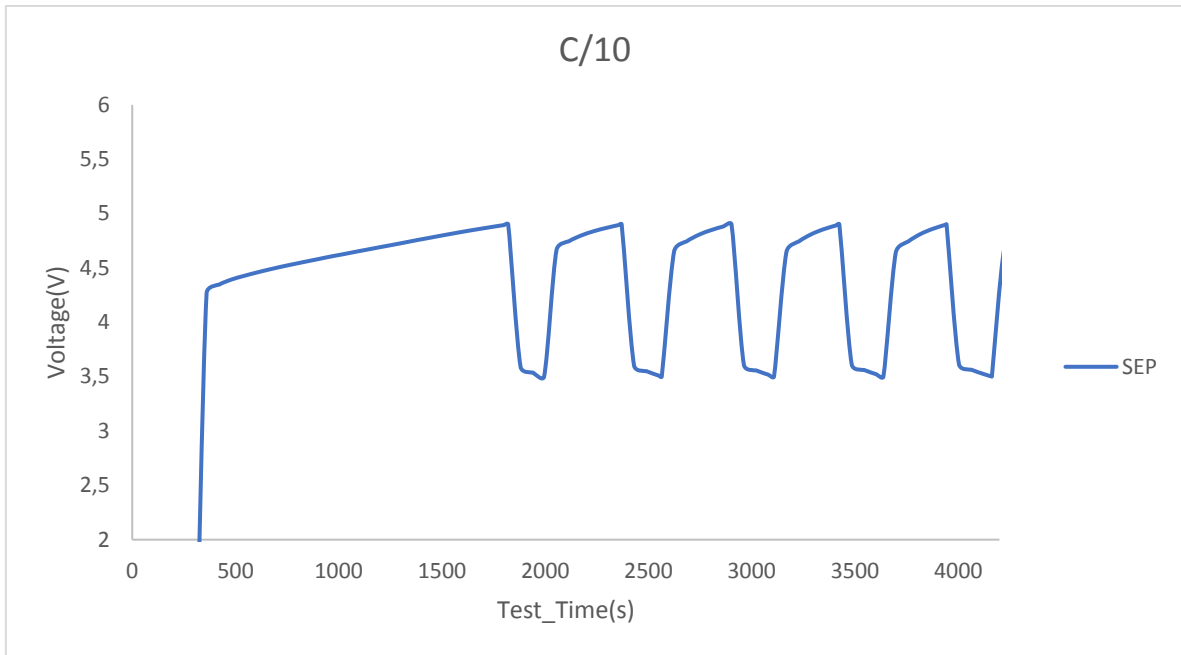


Figure 4.30

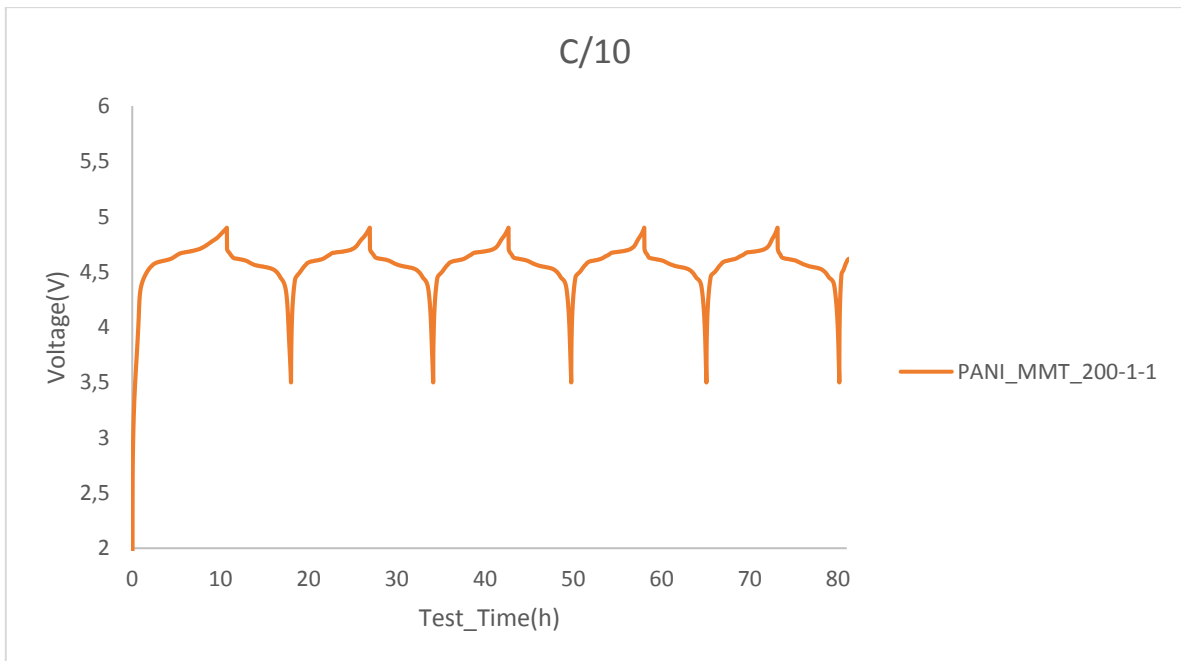


Figure 4.31

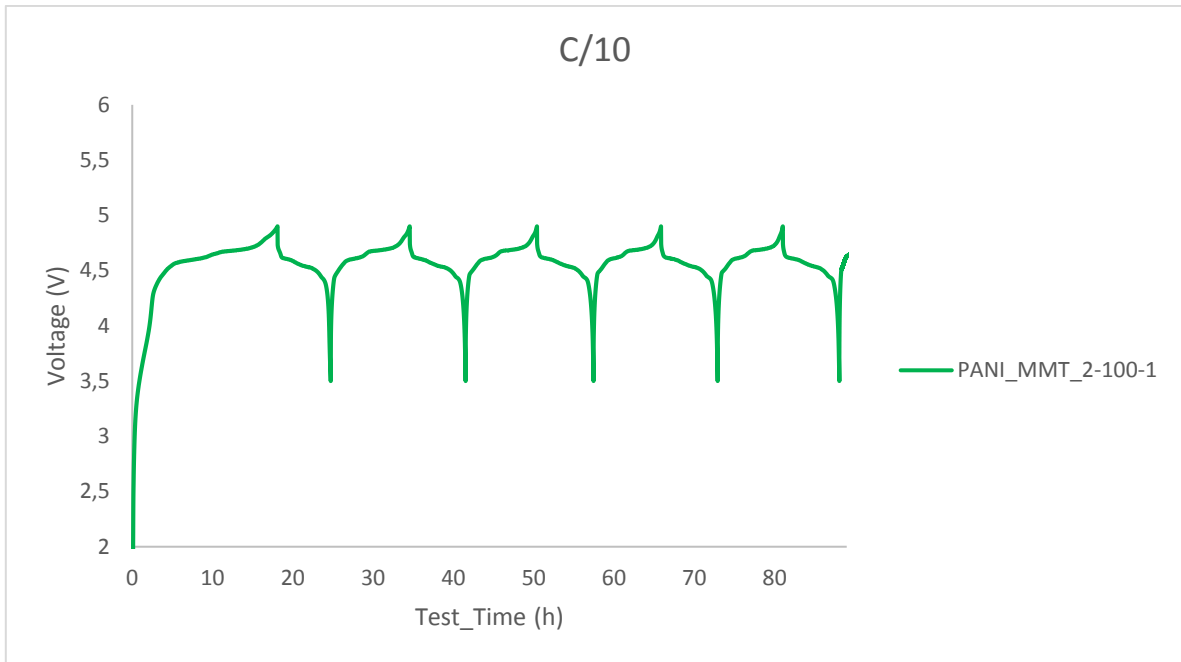


Figure 4.32

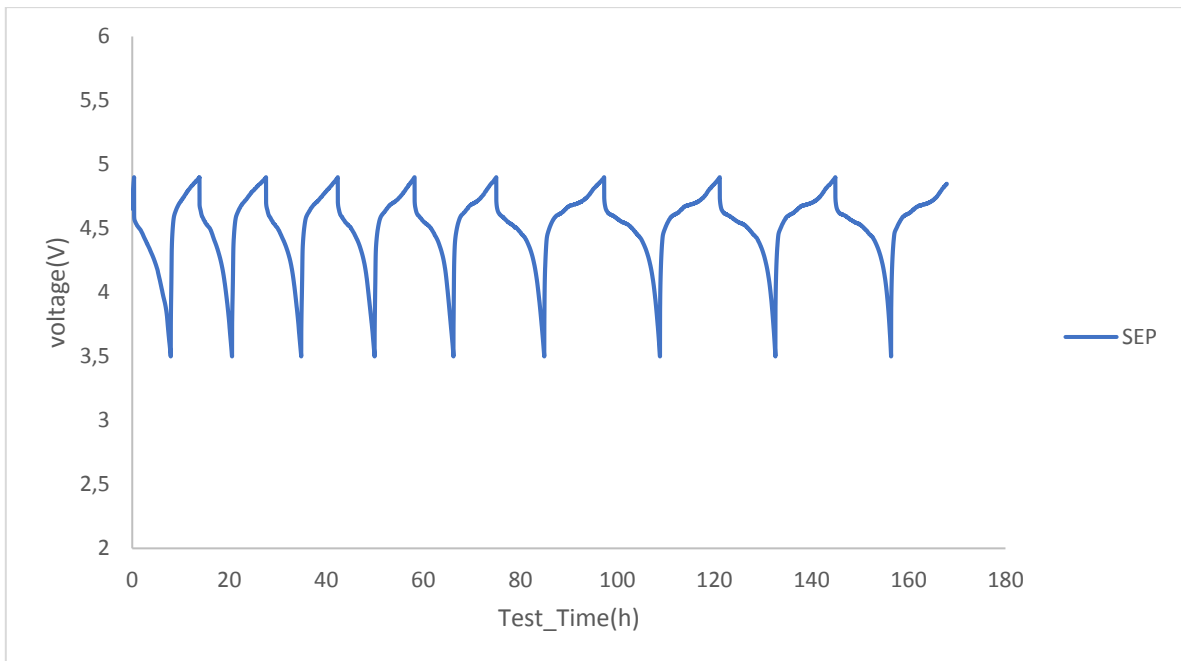


Figure 4.33

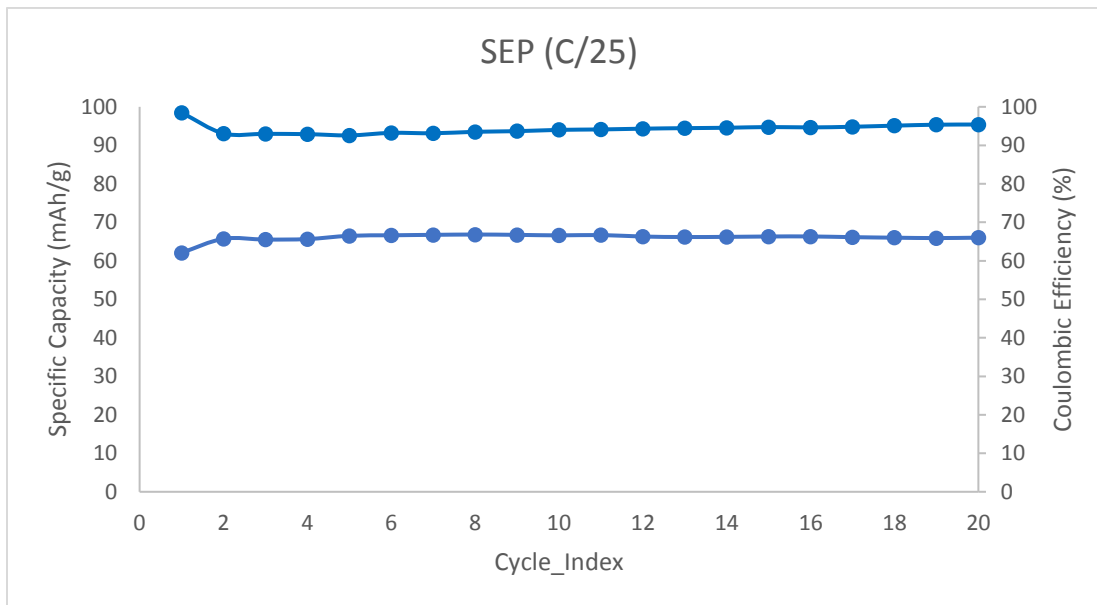


Figure 4.34

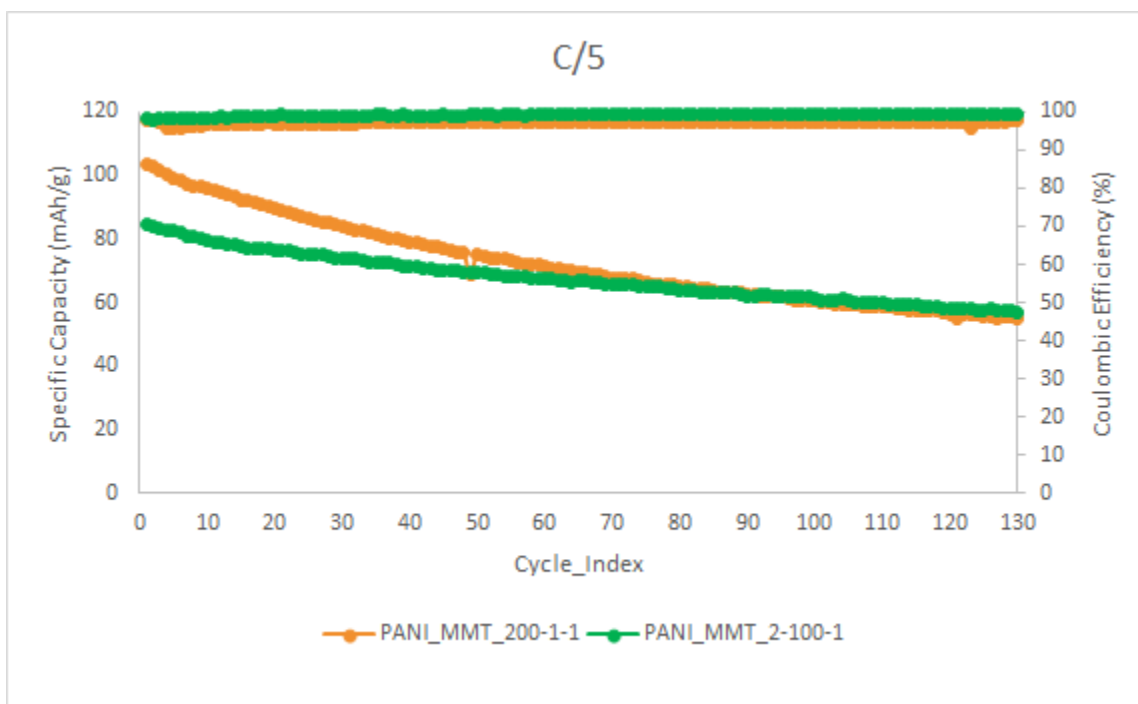


Figure 4.35

Table 4.5

Sample	Specific Capacity (1st Cycle)	Specific Capacity (130th Cycle)	Capacity Fade (%)
PANI_MMT_200-1-1	103.54	55.06	46.83
PANI_MMT_2-100-1	84.73	57.01	32.72

4.6 FURTHER CHEMICAL CHARACTERIZATION

After performing the galvanostatic electrochemical test described in the previous section, the cells (Graphite vs LNMO) were opened inside an argon filled glovebox and the components were separated. To corroborate the best performance of sample PANI_MMT_2-100-1 coating towards manganese passage impediment, X-ray photoelectron spectroscopy XPS was performed for the graphite anodes at the Department of Applied Science and Technology (DISAT) - Politecnico di Torino. Additionally, Fourier transform infrared spectroscopy (FTIR) was done and compared for the separators before and after cycling in order to study further the chemical environment.

4.6.1 XPS RESULTS

The Manganese (2p₃) atomic content was determined by XPS technique for the graphite anodes of both samples that had cycled with the coated separators, as well as for a reference graphite electrode (used as purchased). Figures 4.36, 4.37 and 4.38 show the obtained spectrums.

The graphite electrode already contains a 0.2 atomic percentage of manganese. When compared to the electrodes after cycling, it is seen that for the sample PANI_MMT_200-1-1 the atomic percentage of manganese increased to 1% while for the sample PANI_MMT_2-100-1 it remained in the same order of magnitude (0.1 %). This means that the sample of the coating that contains the higher percentage of polyaniline acts as an effective barrier to impede manganese ions migration to the anode, which could be explained by the fact that in this case the positive charges of doped PANI may have an electrostatic repulsion effect towards Mn⁺², not allowing its transference. On the other hand, in the other composite sample which contains mostly montmorillonite superficial charges are negative (as determined by zeta potential analysis) and this could have a retention effect by electrostatic interaction (attraction) with manganese cations which are retained in the separator but after saturation could be able to migrate and deposit on the graphite surface.

The mentioned results are in correspondence with the better electrochemical performance of the coated separator of sample PANI_MMT_2-100-1.

GRAPHITE

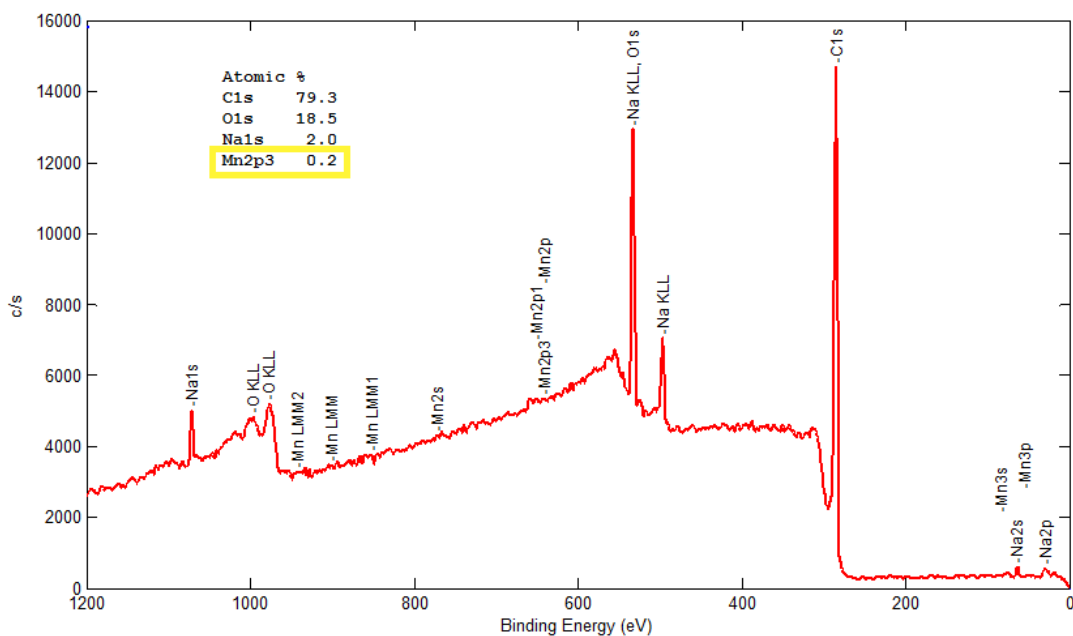


Figure 4.36

PANI_MMT_200-1-1

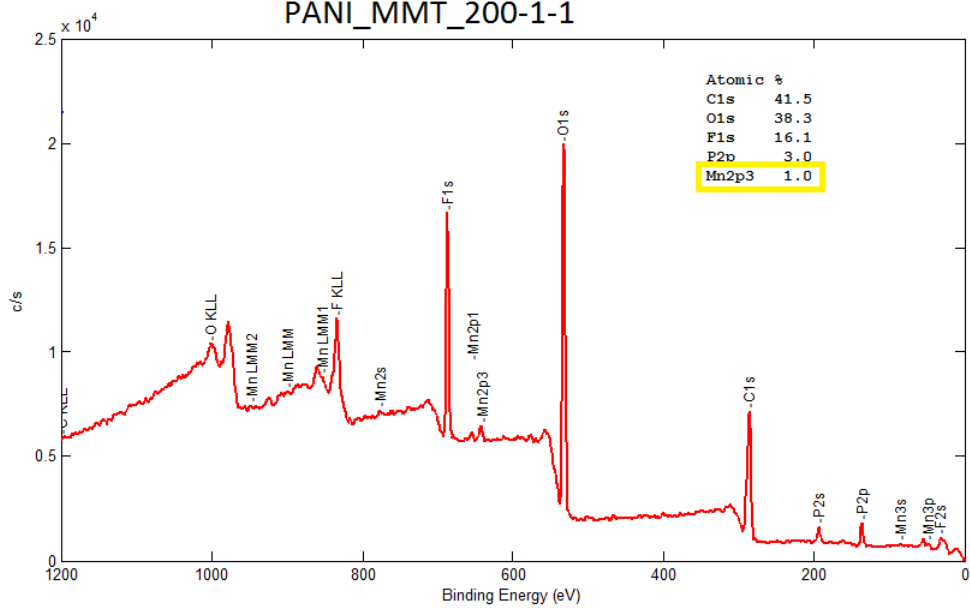


Figure 4.37

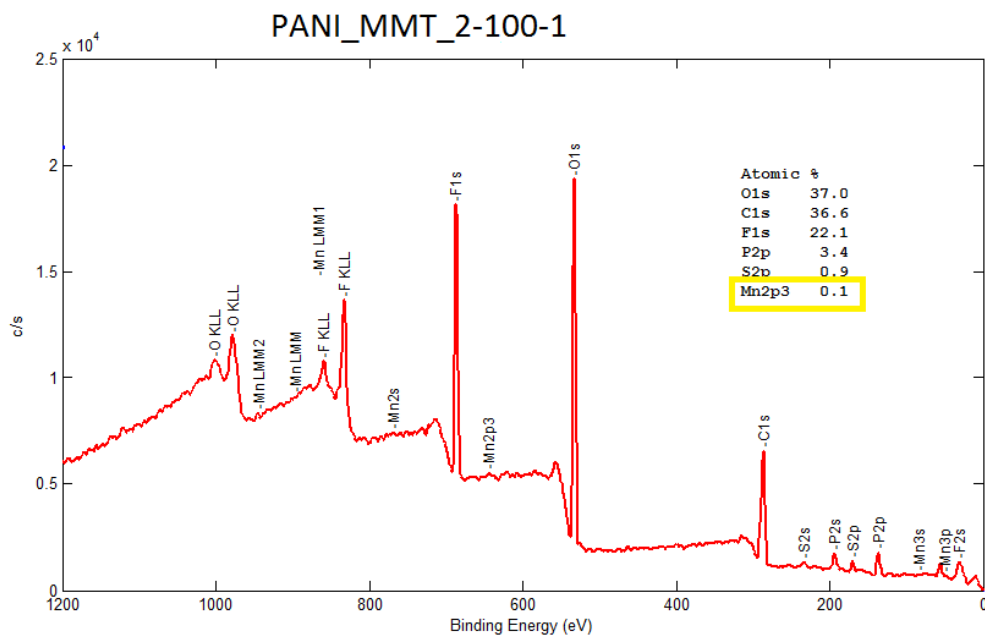


Figure 4.38

4.6.2 FTIR RESULTS

Figures 4.39 and 4.40 display the IR spectra of the coated separators samples PANI_MMT_200-1-1 and PANI_MMT_2-100-1, before cycling (soaked in electrolyte) and after cycling in the full cells (graphite vs LNMO).

For both coating samples peaks of the band 2800 – 3000 cm^{-1} , that correspond to the carbon-hydrogen sp^3 bond of polypropylene of the separator, diminish in intensity or disappear after cycling. This could be attributed to the deposition of solids on the surface which can be corroborated from Figure 4.41 where a picture of the separators after opening the cells can be seen. This effect is more evident for sample PANI_MMT_200-1-1.

In both cases some bands attributed to products of electrolyte decomposition can be distinguished: [52]

- Weak absorbance peaks at 1560 – 1740 cm^{-1} come from the alkyl carbonate salt $\text{ROCO}_2\text{-M}^+$ and carboxylate salt $\text{RCO}_2\text{-M}^+$ ($\text{M} = \text{Li}/\text{Ni}/\text{Mn}$).
- New peaks at 1015 – 1273 cm^{-1} can be attributed to species of the type $\text{Li}_x\text{PF}_y\text{O}_z$.

- Band 1467 – 1489 cm^{-1} comes from $\nu(\text{CO}_3)_{\text{sym}}$ of Li_2CO_3 formation.
- For sample PANI_MMT_200-1-1 the new peak at 2321 cm^{-1} could be assigned to H_3PO_4 formed by reaction of LiPF_6 with H_2O . As it was developed in section 3.2.3.1, from the FTIR results for this composite it was seen that some of the inorganic cations of the interlayer in montmorillonite had not been exchanged. This means, that there could be traces of water coming from the hydration spheres of this cations.

In both samples, peaks at 620 – 621 cm^{-1} correspond to the manganese – oxygen bond. These could be originated by manganese oxide produced from oxidation of Mn^{+2} (by atmospheric air) after dissolution from the LNMO cathode and retention in the separator. The peak seems to be more intense for sample PANI_MMT_200-1-1.

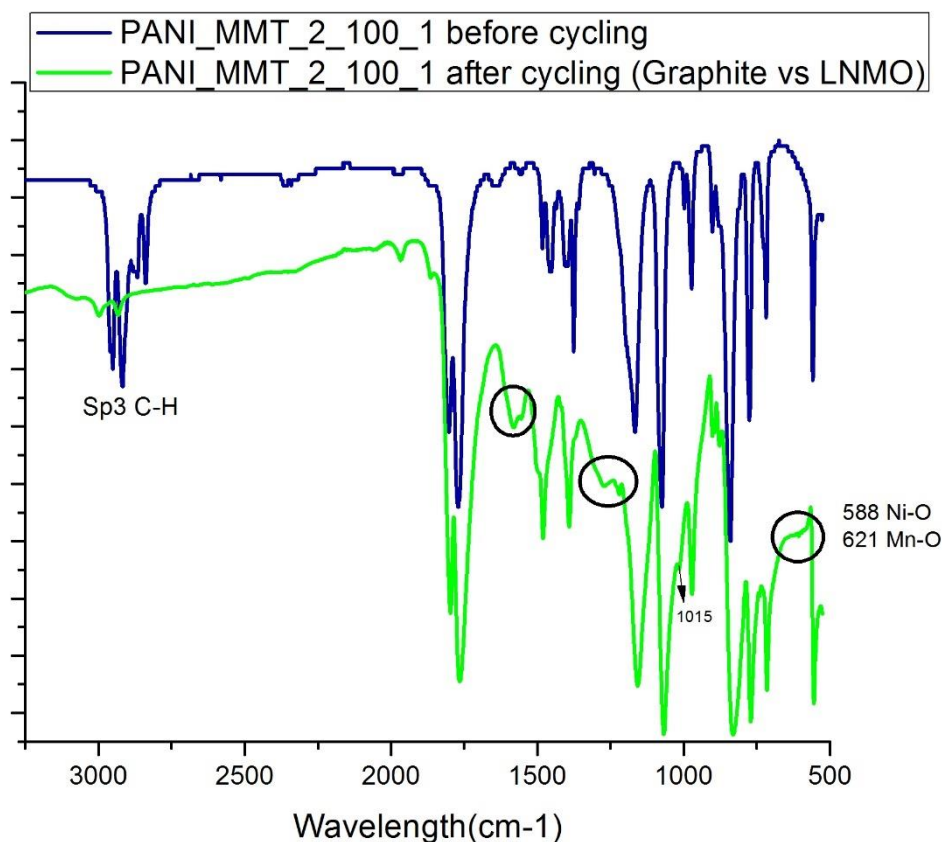


Figure 4.39

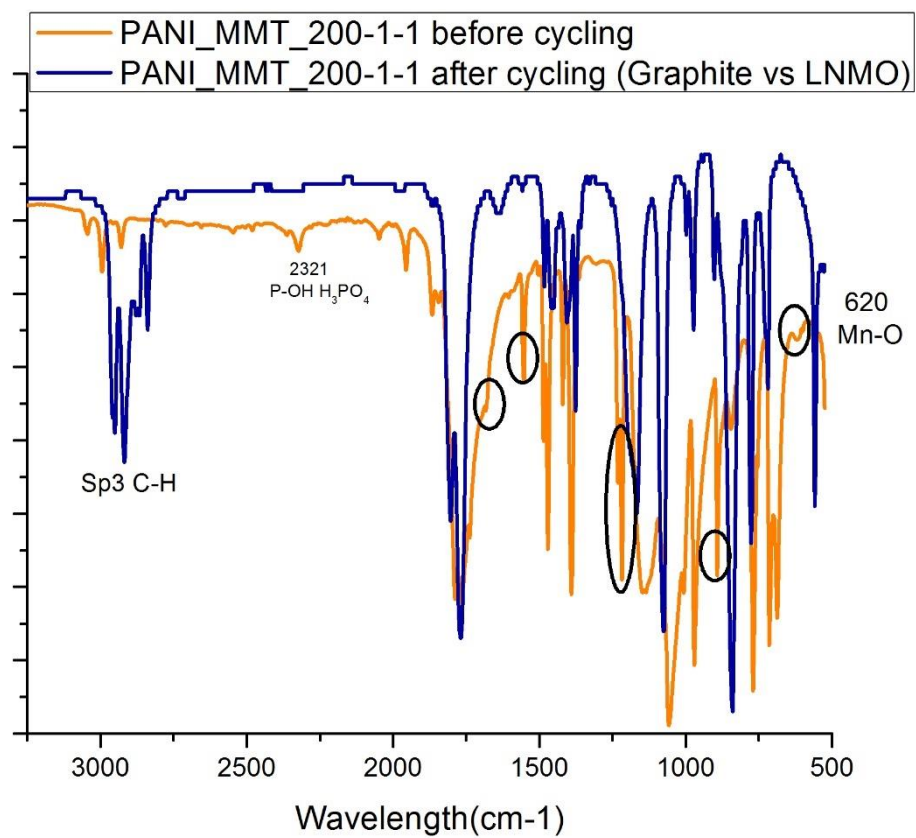


Figure 4.40

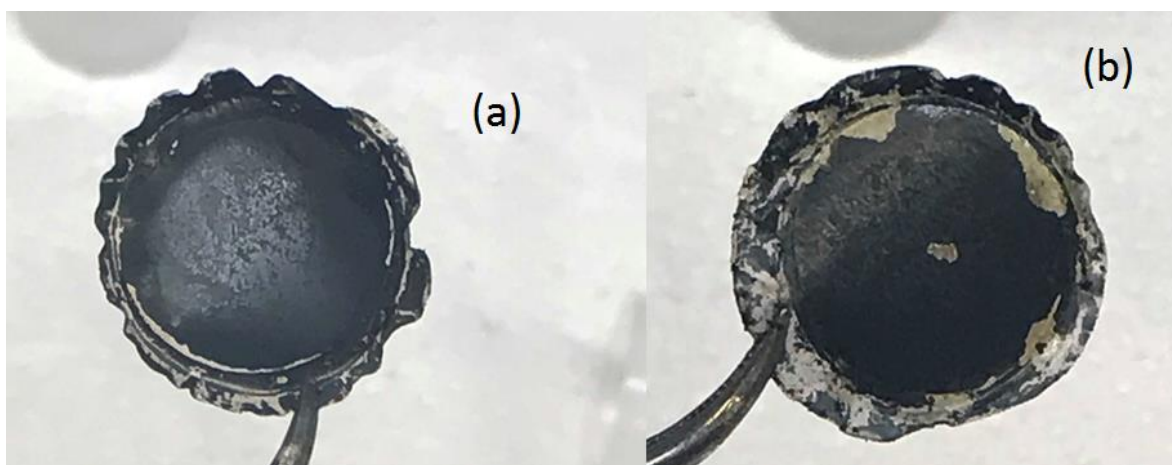
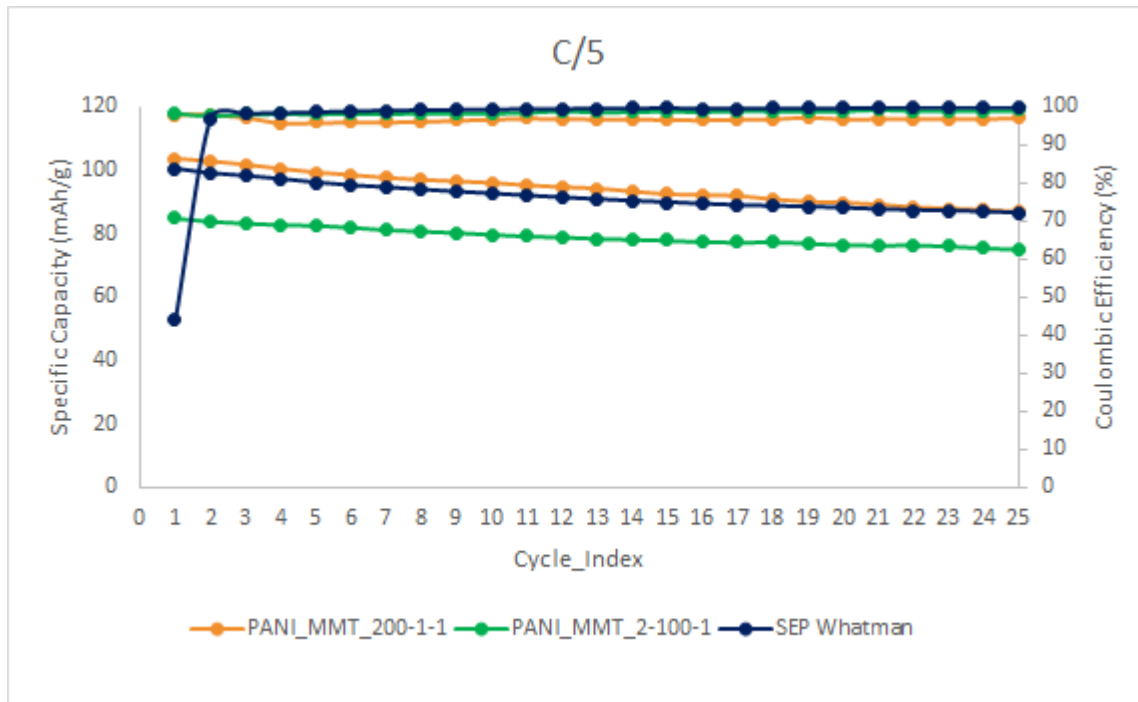


Figure 4.41. Coated separators after galvanostatic cycling in full cells (Graphite vs LNMO), of samples: (a) PANI_MMT_200-1-1 and (b) PANI_MMT_2-100-1.

APPENDIX A

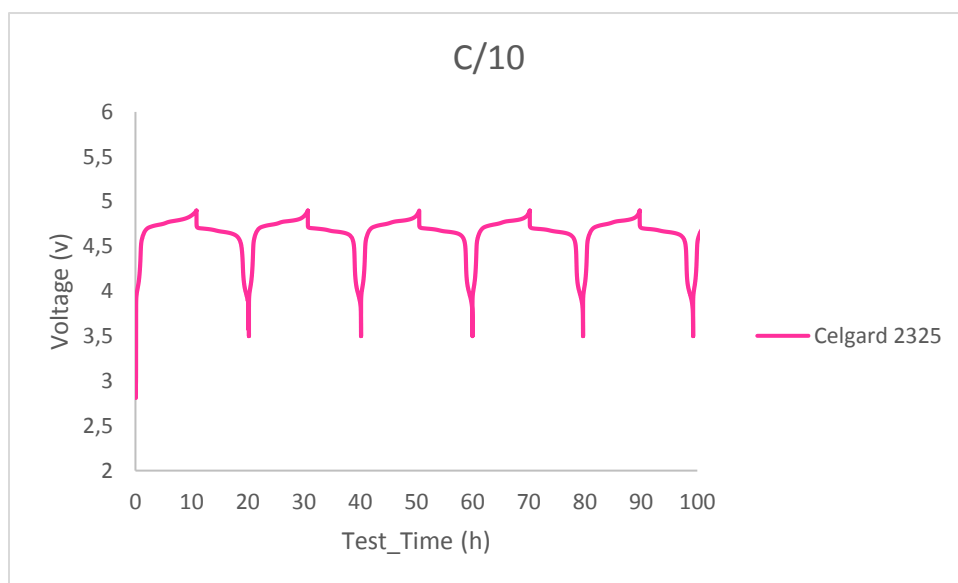
25 galvanostatic cycles (performed in the same conditions as described in the previous section) at a current of C/5 were compared between the two samples of coated separators, and a commercial glass microfiber separator (Whatman®). It can be seen from the figure below, that the cycling performance is comparative for all the cases. This confirms the outstanding improvement achieved by coating the Celgard®2500 polypropylene separator with the synthesized MMT/PANI nanocomposites. Using this polypropylene separator without coating it was not possible to achieve cycling (it was necessary to decrease 20 times the current). Furthermore, for this PP separator it was not possible to achieve cycling even after soaking into the electrolyte for 48 hours.



APPENDIX B

Galvanostatic cycling was tried for half cells (metallic lithium vs LNMO) in the same conditions as described in this work (between 3.5 and 4.9 volts, at ambient temperature) using a different polyolefin separator Celgard®2325. It was necessary to leave the separator soaking into the electrolyte for two days in order to achieve cycling. The same strategy was tried using the separator Celgard®2500 without having positive results (cycling was still not achieved). The figure bellow shows the first 5 cycling voltage curves. It shows that the cell is working properly.

This mentioned electrochemical test is still being performed. In the future more results will be available.



Conclusions

- Two clay/polymer nanocomposite materials were successfully synthesised from polyaniline and an Argentinian montmorillonite. The mass ratios used were adequate to obtain the two possibilities of configurations that were expected. From XRD analysis it could be verified the presence of polyaniline inside the interlaminar space of montmorillonite. From FTIR analysis it could be verified the presence of polyaniline in its conductive form (emeraldine salt), and it was seen, for the sample PANI_MMT_PSA_200-1-1 (higher content of MMT) the presence of inorganic cations, with their hydration spheres, in the basal space indicating that not all of these cations were exchanged with anilinium ions during the synthesis. From TGA analysis it could be calculated the respective mass content of polymer and clay in the composite samples and observed that the presence of montmorillonite increases the degradation temperature of polyaniline conferring thermal resistance to the composites. With XPS analysis the Si/N ratio was calculated which was in agreement with the TGA results, and the oxidation state and doping stage of polyaniline present in the surface and/or edges of MMT slabs of each sample, was determined. It was observed that for sample PANI_MMT_200-1-1 the oxidation state of PANI was mostly 50% (in agreement with the conductive form PANI-ES), whereas for the other sample polyaniline presented an intermediate oxidation state between the fully reduced (leucoemeraldine) and the partially reduced (emeraldine). Finally, zeta potential calculated by microelectrophoresis permitted to estimate the superficial charges of the composites. It was seen that for the sample PANI_MMT_PSA_200-1-1 superficial charges were negative, indicating that polyaniline was preferentially located in between the clay slabs. For sample PANI_MMT_PSA_2-100-1 superficial charges were positive, corresponding to a configuration where montmorillonite slabs are exfoliated and dispersed in a polyaniline matrix.
- The MMT/PANI composites synthesized were applied as a coating film onto a commercial polypropylene separator (Celgard®2500) used in lithium batteries. The coatings permitted to enhance significantly the electrolyte uptake, retention and wettability properties. Ionic conductivity was also improved.
- Metallic lithium symmetrical cells were assembled and electrochemically tested for lithium plating and stripping and dendrite growth suppression. Sample with the highest content of montmorillonite shows the best performance. However, at high current parasitic decomposition reactions of the electrolyte seem to be favoured by the presence of clay.
- Half cells (metallic lithium vs LNMO) and full cells (Graphite vs LNMO) were assembled and electrochemically tested for galvanostatic cycling. In both cases, in order to achieve cycling for the sample containing the separator without coating, it was necessary to use an extremely low current and still a low specific capacity was obtained. On the contrary, for the samples of the coated separators cycling was perfectly carried out and it was comparable to the performance obtained using the same materials but another kind of separator (glass fiber). This showed that the clay/polymer coatings provided an outstanding improvement of commercial Celgard®2500 separator. Sample with the highest content of polyaniline showed the best cycling performance. Furthermore, from XPS analysis it could be seen that in this case the coated separator effectively blocks the passage of manganese

ions towards the graphite anode, decreasing the capacity fade of the cell. Additional information of the electrochemical environment of the separators after cycling, could be obtained by FTIR analysis.

- Work in progress: the same strategy but using a different polyolefin separator is currently being tried. Celgard®2325 was coated following the same procedure described in this work. Cells of bare separator as well as for coated separators with the clay/polymer samples are being electrochemically tested. For bare Celgard®2325 cells, cycling was achieved (after soaking into the electrolyte for 48 hours). In the future the resulting data will be available for further study.

Bibliography

- [1] BAMFORD, C.H., COMPTON, R. G. "Electrode Kinetics: Principles and Methodology," in *Comprehensive Chemical Kinetics, Volumen 26*, Nueva York: Elsevier Science Publishing B.V, 1986, p. 450.
- [2] VALENZUELA, C.A.A. (2015). *Estudio y Caracterización de Ánodos de Litio Metálico* (tesis para optar al grado de magíster en ciencias de la ingeniería, mención química). Universidad de Chile, Santiago de Chile, Chile.
- [3] Linden, David & B Reddy, Thomas. (2001). *Handbook of Batteries*, 3rd Edition.
- [4] W. T. S. Lenntech. "Chemical properties of lithium." [Online]. Available: <https://www.lenntech.com/periodic/elements/li.htm>.
- [5] Argus White Paper. "The lithium market-the future is electric." [Online]. Available: <https://www.argusmedia.com/-/.../white-papers/the-lithium-market>.
- [6] JULIEN, C.M., MAUGER, A., ZAGHIB K., GROULT, H. "Comparative Issues of Cathode Materials for Li-Ion Batteries," in *Inorganics* **2014**, 2, 132-154; doi:10.3390/inorganics2020132.
- [7] DE GIORGIO, F. (2016). *High-voltage lithium-ion batteries for a sustainable transport* (dottorato di ricerca in chimica, esame finale). Università di Bologna, Bologna, Italy.
- [8] SHKROB, I.A., KROPF, A.J., MARIN, T.W., LI, Y., POLUEKTOV, O.G., NIKLAS, J., ABRAHAM, D.P. "Manganese in Graphite Anode and Capacity Fade in Li Ion Batteries," in *The Journal of Physical Chemistry*, 2014, dx.doi.org/10.1021/jp507833u | J. Phys. Chem. C 2014, 118, 24335–24348.
- [9] LIU, H., BANERJEE, A., ZIV, B., HARRIS K.J., PIECZONKA, N.P.W., LUSKI, S., BOTTON, G.A., GOWARD, G.R., AURBACH, D., HALALAY, I.C. "Elucidating the Li-Ion Battery Performance Benefits Enabled by Multifunctional Separators," in *Applied Energy Materials*, ACS Appl. Energy Mater. 2018, 1, 1878–1882.
- [10] ZHANG, H., WANG, X., LIANG, Y. "Preparation and characterization of a Lithium-ion battery separator from cellulose nanofibers," in *Heliyon*. 2015, e00032, open access article under the CC BY-NC-ND license (<http://creativecommons.org/licenses/by-nc-nd/4.0/>).
- [11] SHI C., DAI, J., LI, C., SHEN, X., PENG, L., ZHANG, P., WU, D., SUN, D., ZHAO, J. "A Modified Ceramic-Coating Separator with High-Temperature Stability for Lithium-Ion Battery," in *Polymers* 2017, 9, 159; doi:10.3390/polym9050159
- [12] YU L., MIAO J., JIN, Y., LIN, J.Y.S. "A comparative study on polypropylene separators coated with different inorganic materials for lithium-ion batteries," in *Front. Chem. Sci. Eng.* 2017, 11(3): 346–352

- [13] BALBUENA, P., WANG, Y. *Lithium-Ion Batteries. Solid-Electrolyte Interphase*. Londres: Imperial College Press, 2004, p. 407.
- [14] AURBACH, D., MARKOVSKY, B., SCHECHTER, A., EIN-ELI, Y., COHEN, H. "A comparative study of synthetic graphite and Li electrodes in electrolyte solutions based on ethylene carbonate-dimethyl carbonate mixtures," *J. Electrochem. Soc.*, vol. 143, no. 12, pp. 3809–3820, 1996.
- [15] AURBACH, D., MOSHKOVICH, M. "A study of lithium deposition-dissolution processes in a few selected electrolyte solutions by Electrochemical Quartz Crystal Microbalance," *J. Electrochem. Soc.*, vol. 145, no. 8, pp. 2629–2639, 1998.
- [16] NOVAK, P., JOHO, F., LANZ, M., RYKART, B., PANITX, J.-C., ALLIATA, D., KÖTZ, R., HAAS, O. "The complex electrochemistry of graphite electrodes in lithium-ion batteries," *J. Power Sources*, vol. 97–98, pp. 39–46, 2001.
- [17] AURBACH, D., COHEN, Y. "Micromorphological studies of lithium electrodes in alkyl carbonate solutions using in situ Atomic Force Microscopy," *J. Phys. Chem. B*, vol. 104, no. 51, pp. 12282–12291, 2000.
- [18] AURBACH, D., ZINIGRAD, E., COHEN, Y., TELLER, H. "A short review of failure mechanisms of lithium metal and lithiated graphite anodes in liquid electrolyte solutions," *Solid State Ionics*, vol. 148, no. 3, pp. 405–416, 2002.
- [19] YANG, H., GUO, C., NAVEED, A., LEI, J., YANG, J., NULI, Y., WANG, J. "Recent progress and perspective on lithium metal anode protection," in *Storage Materials* 14 (2018) 199–221.
- [20] RAWLINS, J., HIHARA, L., TIWARI, A. (2014). *Intelligent Coatings for Corrosion Control*, Ch.14. ISBN: 9780124114678.
- [21] SCOTTO, J. (2016). *Fisicoquímica de polímeros electroquímicamente activos. Estudio de la conmutación redox de la polianilina* (tesis doctoral). Universidad Nacional de La Plata, La Plata, Argentina.
- [22] MANERE, P.J. (2011). *Materiales nanoestructurados basados en polianilina, nanotubos de carbono y grafeno* (tesis doctoral). Universidad de Zaragoza, Zaragoza, Spain.
- [23] GENIES, E. M.; LAPKOWSKI, M., "Electrochemical in situ epr evidence of two polaron-bipolaron states in polyaniline". *Journal of Electroanalytical Chemistry* 1987, 236 (1-2), 199-208.
- [24] STAFSTRÖM, S.; BRÉDAS, J. L.; EPSTEIN, A. J.; WOO, H. S.; TANNER, D. B.; HUANG, W. S.; MACDIARMID, A. G., "Polaron lattice in highly conducting polyaniline: Theoretical and optical studies". *Physical Review Letters* (1987), 59 (13), 1464-1467.
- [25] MONKMAN, A. P.; BLOOR, D.; STEVENS, G. C.; STEVENS, J. C. H.; WILSON, P., "Electronic structure and charge transport mechanisms in polyaniline". *Synthetic Metals* (1989), 29 (1), 277-284.

- [26] TIGELAAR, D. M.; LEE, W.; BATES, K. A.; SAPRIGIN, A.; PRIGODIN, V. N.; CAO, X.; NAFIE, L. A.; PLATZ, M. S.; EPSTEIN, A. J., "Role of solvent and secondary doping in polyaniline films doped with chiral camphorsulfonic acid: Preparation of a chiral metal". *Chemistry of Materials* (2002), 14 (3), 1430-1438.
- [27] LEE, K.; HEEGER, A. J.; CAO, Y., "Reflectance of polyaniline protonated with camphor sulfonic acid: Disordered metal on the metal-insulator boundary". *Physical Review B* (1993), 48 (20), 14884-14891.
- [28] ŁUZNY W K, E., "Relations between the structure and electric conductivity of polyaniline protonated with camphorsulfonic acid". *Macromolecules* (2000), 33 (2), 425-429.
- [29] JOZEFOWICZ, M. E.; EPSTEIN, A. J.; POUGET, J. P.; MASTERS, J. G.; RAY, A.; SUN, Y.; TANG, X.; MACDIARMID, A. G., "X-ray structure of polyanilines". *Synthetic Metals* (1991), 41 (1-2), 723-726.
- [30] POUGET, J. P.; JOZEFOWICZ, M. E.; EPSTEIN, A. J.; TANG, X.; MACDIARMID, A. G., "X-ray structure of polyaniline". *Macromolecules* (1991), 24 (3), 779-789.
- [31] LUX, F. "Properties of electronically conductive polyaniline: a comparison between well-known literature data and some recent experimental findings", in *Polymer* (1994), vol 35, P. 2915-2936.
- [32] YOO, J. E.; KREKELBERG, W. P.; SUN, Y.; TARVER, J. D.; TRUSKETT, T. M.; LOO, Y. L., "Polymer conductivity through particle connectivity". *Chemistry of Materials* (2009), 21 (9), 1948-1954.
- [33]. ZUO, F.; ANGELOPOULOS, M.; MACDIARMID, A. G.; EPSTEIN, A. J., "AC conductivity of emeraldine polymer". *Physical Review B* (1989), 39 (6), 3570-3578.
- [34] ANGELOPOULOS, M.; DIPIETRO, R.; ZHENG, W. G.; MACDIARMID, A. G.; EPSTEIN, A. J. J., "Effect of selected processing parameters on solution properties and morphology of polyaniline and impact on conductivity". *Synthetic Metals* (1997), 84 (1-3), 35-39.
- [35] GAMBA, M. (2017). *Montmorillonitas modificadas para la retención de pesticidas poscosecha, imazalil y tiabendazol* (tesis doctoral). Universidad Nacional de La Plata, La Plata, Argentina.
- [36] MORARU, V.N. "Structure formation of alkylammonium montmorillonites in organic media", in *Applied Clay Science* 19 (2001) 11–26.
- [37] JONES, T.R. "The properties and uses of clays which swell in organic solvents", in *Minerals* (1983) 18, 399---410.
- [38] YANG, G., HOU, W., FENG, X., XU, L., LIU, Y., WANG, G., DING, W. "Nanocomposites of Polyaniline and a Layered Inorganic Acid Host: Polymerization of Aniline in the Layers, Conformation, and Electrochemical Studies", in *Adv. Funct. Mater.* (2007) 17, 401–412. DOI: 10.1002/adfm.200500941.
- [39] DO NASCIMENTO, G.M., CONSTANTINO, V.R.L., LANDERS, R., TEMPERINI, M.L.A. "Spectroscopic characterization of polyaniline formed in the presence of montmorillonite clay", in *Polymer* 47 (2006) 6131e6139.

- [40] HAMEED, A.S. "Phosphate Based Cathodes and Reduced Graphene Oxide Composite Anodes for Energy Storage Applications", Ch 2, in *Springer Theses*, DOI 10.1007/978-981-10-2302-6_2.
- [41] PHYSICAL ELECTRONICS, INC. [Online]. Available: <https://www.phl.com/surface-analysis-techniques/xps-esca.html>
- [42] GOLCZAK, S., KANCIURZEWSKA, A., FAHLMAN, M., LANGER, K., LANGER, J.J., MICKIEWICZ, A. "Comparative XPS surface study of polyaniline thin films", in *Solid State Ionics* 179 (2008) 2234–2239.
- [43] KANG, E.T., NEOH, K.G., TAN, K.L. "Polyaniline: a polymer with many interesting intrinsic redox states", in *Prog. Polym. Sci.*, Vol. 23, 211-324, 1998.
- [44] YANG, S., QIN, H., LI, X., LI, H., YAO, P. "Enhancement of Thermal Stability and Cycling Performance of Lithium-Ion Battery at High Temperature by Nano-ppy/OMMT-Coated Separator", in *Journal of Nanomaterials* (2017), Article ID 6948183, <https://doi.org/10.1155/2017/6948183>.
- [45] RTI Laboratories. *FTIR Analysis*. [Online]. Available: <http://rtilab.com/techniques/ftir-analysis/>
- [46] BARRIOS, V.A.E., MENDEZ, J.R.R., AGUILAR, N.V.P., ESPINOSA, G.A., RODRIGUEZ, J.L.D. "FTIR- An Essential Characterization Technique for Polymeric Materials", Chapter in *InTech* (2012), DOI: 10.5772/36044.
- [47] BEKRI-ABBES, I., SRASRA, E. "Characterization and AC conductivity of polyaniline-montmorillonite nanocomposites synthesized by mechanical/chemical reaction", in *Reactive & Functional Polymers* 70 (2010) 11-18.
- [48] KIM, B-H, JUNG, J-H., HONG, S-H., JOO, J., EPSTEIN, A.J., MIZOGUCHI, K., KIM, J.W., CHOI, H.J. "Nanocomposite of Polyaniline and Na⁺-Montmorillonite Clay", in *Macromolecules* (2002) 3541419-1423.
- [49] MARINS, J.A., SOARES, B.G. "A facile and inexpensive method for the preparation of conducting polyaniline-clay composite nanofibers" in *Synthetic Metals* (2012), <https://doi.org/10.1016/j.synthmet.2012.10.015>.
- [50] PERKINELMER, INC. *Thermogravimetric Analysis (TGA)*. [Online]. Available: https://www.perkinelmer.com/lab-solutions/resources/docs/faq_beginners-guide-to-thermogravimetric-analysis_009380c_01.pdf
- [51] OKAMOTO, H., KOTAKA, T. "Effect of counter ions in electrochemical polymerization media on the structure and responses of the product polyaniline films III. Structure and properties of polyaniline films prepared via electrochemical polymerization", in *Polymer* 40 (1999) 407-417.
- [52] ZHOU, H., LIU, B., XIAO, D., YIN, C., LI, J. "Fluoroethylene carbonate as the additive of lithium difluoro(oxalate)borate-sulfolane electrolytes to improve the electrochemical performance of LiNi_{0.5}Mn_{1.5}O₄ cathode", in *J Mater Sci: Mater Electron* (2019) 30: 5098. <https://doi.org/10.1007/s10854-019-00808-0>

- [53] AHMED, S. M., "Mechanistic investigation of the oxidative polymerization of aniline hydrochloride in different media". *Polymer Degradation and Stability* (2004), 85 (1), 605-614.
- [54] CIRIC-MARJANOVIC, G.; TRCHOVA, M.; STEJSKAL, J. J., "Theoretical study of the oxidative polymerization of aniline with peroxydisulfate: Tetramer formation". *International Journal of Quantum Chemistry* (2008), 108 (2), 318-333.
- [55] CAO, Y.; ANDREATTA, A.; HEEGER, A. J.; SMITH, P. J., "Influence of chemical polymerization conditions on the properties of polyaniline". *Polymer* (1989), 30 (12), 2305-2311.
- [56] TZOU, K.; GREGORY, R. V., "Kinetic study of the chemical polymerization of aniline in aqueous solutions". *Synthetic Metals* (1992), 47 (3), 267-277.
- [57] FU, Y.; ELSENBÄUMER, R. L., "Thermochemistry and kinetics of chemical polymerization of aniline determined by solution calorimetry". *Chemistry of Materials* (1994), 6 (5), 671-677.
- [58] SAPURINA, I.; STEJSKAL, J., "The mechanism of the oxidative polymerization of aniline and the formation of supramolecular polyaniline structures". *Polymer International* (2008), 57 (12), 1295-1325.
- [59] PLESU, N.; KELLENBERGER, A.; MIHALI, M.; VASZILCSIN, N., "Effect of temperature on the electrochemical synthesis and properties of polyaniline films". *Journal of Non-Crystalline Solids* (2010), 356 (20-22), 1081-1088.
- [60] GHOLAMIAN, M.; CONTRACTOR, A. Q., "Effect of the temperature of synthesis on the conductivity and electrochemical behaviour of polyaniline". *Journal of Electroanalytical Chemistry* (1988), 252 (2), 291-301.
- [61] KONYUSHENKO, E. N.; STEJSKAL, J.; TRCHOVA, M.; BLINOVA, N. V.; HOLLER, P. J., "Polymerization of aniline in ice". *Synthetic Metals* (2008), 158 (21-24), 927-933.
- [62] STEJSKAL, J.; RIEDE, A.; HLAVATA, D.; PROKES, J.; HELMSTEDT, M.; HOLLER, P., "The effect of polymerization temperature on molecular weight, crystallinity, and electrical conductivity of polyaniline". *Synthetic Metals* (1998), 96 (1), 55-61.
- [63] STEJSKAL, J.; HLAVATA, D.; HOLLER, P.; TRCHOVA, M.; PROKES, J.; SAPURINA, I., "Polyaniline prepared in the presence of various acids: a conductivity study". *Polymer International* (2004), 53 (3), 294-300.
- [64] FURUKAWA, Y.; HARA, T.; HYODO, Y.; HARADA, I., "Vibrational spectra of polyaniline and its 15N- and 2H-substituted derivatives in as-polymerized, alkali-treated and reduced states". *Synthetic Metals* (1986), 16 (2), 189-198.
- [65] FARMER, V.C., MORTLAND, M.M., (1966). "An infrared study of the coordination of pyridine and water to exchangeable cations in montmorillonite and saponite". *Journal of the Chemical Society A*, 344-351.

[66] KARICKHOFF, S.W., BAILEY, G.W., (1976). "Protonation of organic bases in clay–water systems". *Clays and Clay Minerals* 24, 170–176.

[67] FELDKAMP, J.R., WHITE, J.L., (1979). " Acid-base equilibria in clay suspension". *Journal of Colloid and Interface Science* 69, 97–106.

[68] POUGET, J.P. "X-ray Structure of Polyaniline", in *Macromolecules* (1991), 24, 779-789 779.

[69] MARINS, J.A., SOARES, B.G. "A facile and inexpensive method for the preparation of conducting polyaniline-clay composite nanofibers", in *Synthetic Metals* 162 (2012) 2087-2094.